Stress Granule-mediated Mechanism of the Cellular Death Pathway Necroptosis Induced Through Oxidative Stress and Viral Infection

by

Mateusz Bartlomiej Szczerba

A Dissertation Presented in Partial Fulfillment
of the Requirements for the Degree
Doctor of Philosophy

Approved February 2021 by the
Graduate Supervisory Committee:

Bertram Lewis Jacobs, Chair
Jeffrey Langland
Qiang Chen
Douglas Lake

ARIZONA STATE UNIVERSITY

May 2021

ABSTRACT

Environmental stressors can perturb cellular homeostasis. Cells activate an integrated stress response that will alleviate the effects of the ongoing stress. Stress-activated protein kinases function to phosphorylate the eukaryotic translation initiation factor, eIF2α, which results in inhibition of translation of house-keeping genes. Following these events, formation of cytoplasmic messenger ribonucleoprotein complexes, known as stress granules, will take place. Stress granules typically have a pro-survival function. These studies demonstrate that assembly of stress granules can also lead to necroptosis. Necroptosis is a caspase-independent, receptor-interacting protein kinase 3 (RIPK3)-dependent cell death pathway executed by mixed lineage kinase domain-like (MLKL) protein. Cellular stress is induced using arsenite (oxidative stress) or by infection with vaccinia virus (VACV) E3 protein Z-DNA-binding domain mutant, VACV-E3LΔ83N. In both cases, RIPK3-dependent death was observed in interferon (IFN)-primed L929 cells. This death led to phosphorylation and trimerization of MLKL, indicative of necroptosis. Necroptosis induced by oxidative stress and VACV-E3LΔ83N infection was dependent on the host Z-form nucleic acid sensor, DNA-dependent activator of IFN-regulatory factors (DAI), as it was inhibited in DAI-deficient L929 cells. Under both cellular stresses, DAI associated with RIPK3 and formed high-molecular-weight complexes, consistent with formation of the necrosomes. DAI localized into stress granules during necroptosis induced by arsenite and the mutant virus, and the necrosomes formed only in presence of stress granule assembly. The significance of stress granules for cellular stress-induced necroptosis was demonstrated using knock-out (KO) cell lines

unable to form granules: T cell-restricted intracellular antigen 1 (TIA-1) KO MEF cells and Ras GTPase-activating protein-binding proteins 1 and 2 (G3BP1/2) KO U2OS cells. Necroptosis was inhibited in absence of stress granule formation as no cell death or activation of MLKL was observed in the knock-out cell lines following arsenite treatment or VACV-E3LΔ83N infection. Furthermore, wild-type VACV was able to inhibit stress granule assembly, which coincided with the virus ability to inhibit necroptosis. These studies have led to a model of Z-form nucleic acids being involved in activation of the stress granule-mediated necroptosis following induction by environmental stressors. These results have significance for understanding the etiology of human diseases and the antiviral innate immunity.

This dissertation is dedicated to my family.

To my parents, thank you for your unconditional love and support throughout my life.

You taught me to reach out for my dreams and always strive to be a better person.

To my husband, thank you for always standing by my side and believing in me.

Your patience and understanding mean the world to me.

ACKNOWLEDGEMENTS

I would like to express special gratitude for my advisor, Dr. Bert Jacobs. Everything that I have accomplished in this dissertation stemmed from your excellent mentorship. Your enthusiasm for science and creativity have been a great motivation to do exciting discoveries. I also appreciate how caring you are. Ph.D. studies were the most challenging time in my professional career. And I know that I could not have done it without your guidance and understanding.

Thank you to my committee members, Dr. Jeff Langland, Dr. Doug Lake, and Dr. Shawn Chen. It has been a pleasure to be your mentee and I appreciate the invaluable feedback that I have received from you over the years. Your assistance in shaping the trajectory of my projects was indispensable.

Dr. Karen Kibler, I would like to thank you for all the years of guidance and collaborations on exciting experiments. Thank you also for many friendly chatters. Your knowledge and expertise are admirable. It has been a privilege to work with you.

Thank you to all the Jacobs lab members, current and past. Sharing experiences, overcoming experimental hurdles, aiming for moving forward with our exciting research has been a driving force in our lab. I know that working environment is crucial in being productive. I consider myself lucky to have been part of this group. Sambhavi, Megan, and Jackie, special thanks to you for being more than lab colleagues.

I would like to acknowledge my undergraduate students: Carly Snyder, Azeez Usman, Wesley Hoyland, and Carolina Gogerty. You have given me a valuable lesson of how to be a mentor. You made me question my ways and taught me how to look at things

from many different perspectives. It was/has been fun working with you and I am proud to have contributed in some way to your career development.

Thank you to Dr. Maneesha Muralinath for invaluable lessons on how to teach science. Working in a lab and knowing your research does not automatically translate to being able to lecture on the same topic. Thank you for showing me how to work with students and teaching me a variety of approaches in academic instruction.

Thank you to my family: my sister Anna Majerska, my cousin Klaudia Patrzalek, and my auntie Sabina Patrzalek for being my devoted listeners and my everyday companions, even though thousands of miles separate us.

I would like to express special thanks to my best friend Magdalena Grzybowska. We have known each other since kindergarten, and our friendship has remained strong throughout all these years. You are this one friend of mine who understands me without words. You are my soulmate and I consider myself lucky to be able to call you my friend. Thank you for all the support throughout my life, and for making life a happy adventure.

I would like to acknowledge my funding sources: Graduate and Professional Student Association (GPSA) and School of Biological and Health Systems Engineering (SBHSE) at ASU. The funding allowed me to participate in a range of scientific meetings, including international conferences, which helped me in my development as a scientist.

Thank you to everyone who contributed to this work. Your assistance and support are deeply appreciated.

TABLE OF CONTENTS

LIST OF TABLES

LIST OF FIGURES

CHAPTER 1

INTRODUCTION

Cellular stress can be defined as any environmental factor or condition that perturbs cellular homeostasis. This phenomenon can be detrimental to the cell in that it can lead to damage of cellular macromolecules: proteins, DNA, RNA, and lipids. Cells have developed mechanisms to counteract the effects of a stress. One of them is switching gene expression patterns to conserve resources and remediate cellular damage. The aim is to reduce global translation, in that resources are no longer utilized to express house-keeping genes. Instead, stress-induced gene expression can take place. This intracellular stress response is known as the integrated stress response (IRS) and has a function to counteract the effects of the ongoing stress (1, 2).

Cells are subjected to a variety of environmental stresses. Depending on the type of the stress acting upon a cell, a different member of the stress-induced serine/threonine protein kinase family will become activated (Fig. 1) (reviewed in (3)):

a) haem-regulated inhibitor (HRI) (or eIF2α kinase 1, EIF2AK1) is activated during oxidative stress, heat shock, or heme deprivation (4, 5)
b) protein kinase dependent on RNA (PKR) (eIF2α kinase 2, EIF2AK2), inducible by interferon (IFN) becomes activated during viral infection upon binding to double-stranded RNA (dsRNA) (6, 7)
c) PKR-like endoplasmic reticulum kinase (PERK) (also known as eIF2α kinase 3, or EIF2AK3) is activated by presence of misfolded protein in the ER (ER stress) (8, 9)

d) general control non-derepressible 2 (GCN2) (also known as eIF2α kinase 4, or EIF2AK4) is activated in response to nutrient limitation (amino acid starvation), UV irradiation, or proteasome inhibition (10, 11)

Regardless of the type of the protein kinase responding to the stress, all of them perform their function via phosphorylation of the eukaryotic translation initiation factor, eIF2α (Fig. 1). In eukaryotes, regulation of translation occurs predominantly at the level of initiation. This important step in protein synthesis requires a multitude of eukaryotic initiation factors, one of which is eIF2. eIF2 is indispensable for translation of the majority of cellular mRNAs. eIF2 functions as a binding mediator between the initiator tRNA ($tRNAi^{Met}$) and the 40S ribosomal subunit (Fig. 2). This reaction is dependent on GTP and produces eIF2-GDP, which is afterwards recycled back into eIF2-GTP by the guanine nucleotide-exchange factor, eIF2B (Fig. 1). eIF2-GTP, $tRNAi^{Met}$, the 40S ribosomal subunit, and additional initiation factors form the 43S translation preinitiation complex, which will bind and scan the mRNA in search for the start codon (Fig. 2). Once an AUG is found, GTP bound to eIF2 is hydrolyzed, eIF2-GDP is released, and the large ribosomal subunit (60S) will bind, completing the formation of the translation initiation complex (12, 13).

eIF2 is a heterotrimer comprised of α, β, and γ subunits. The activity of eIF2 is regulated via phosphorylation of its α subunit at Ser51. When eIF2α is phosphorylated, eIF2 changes from a substrate to an inhibitor of eIF2B, making it impossible to recycle eIF2-GDP to eIF2-GTP (14). Therefore, the four eIF2α kinases inhibit global translation by reducing the levels of eIF2-GTP, minimizing energy and nutrient consumption for the

sake of cell survival. This will allow cells to enhance eIF2α-independent translation of genes specifically acting to remediate the ongoing stress.

Accumulation in the cytoplasm of the stalled 48S translation preinitiation complexes (PICs), comprising of mRNA, 40S ribosomal subunit, and translation initiation factors, lacking the eIF2-GTP-tRNAi^{Met} ternary complex and therefore unable to recruit the 60S ribosomal subunit, leads to formation of stress granules (Fig. 2) (15). As translation elongation is not affected by phosphorylation of eIF2α, ribosomes already involved in translation continue translation elongation and finally "run off" the mRNA, leading to polysome disassembly. This results in accumulation of messenger ribonucleoprotein particles (mRNPs), with long stretches of exposed non-translating mRNAs. These free stretches of mRNA become engaged in RNA-RNA interactions as well as are targeted by RNA-binding proteins (RBPs), like Ras GTPase-activating protein-binding protein 1 (G3BP1), T cell-restricted intracellular antigen 1 (TIA-1), and TIA-1-related protein (TIAR) (16-18). These RBPs contain low-complexity and intrinsically disordered regions (IDRs) that interact with each other and facilitate a phase separation, concentrating these proteins and bound mRNAs into distinct subcellular structures, stress granules (Fig. 2) (19-22). This process is referred to as biomolecular condensation, and it has been shown to be concentration dependent as overexpression of the SG nucleating proteins TIA-1 and G3BP1 is sufficient to induce SG formation without an ongoing cellular stress (23, 24).

Although eIF2α kinase-mediated phosphorylation of eIF2α is a major trigger of SG assembly, two other mechanisms have been described leading to formation of SGs. The first mechanism is independent of eIF2α phosphorylation. It involves blocking of the

cap-binding eIF4F complex formation. eIF4F complex forms by association of translational initiation factors eIF4A and eIF4E with another translational initiation factor, eIF4G. Binding of the eIF4F complex to the 5' end of mRNA allows interaction between eIF4G and the poly(A)-binding protein (PABP) at the 3' end of mRNA, leading to mRNA circularization (25, 26). eIF4F complex assembly is regulated by the mechanistic target of rapamycin (mTOR) serine/threonine kinase. Under optimal growth conditions, mTOR constitutively phosphorylates eIF4E-binding protein (4E-BP), allowing eIF4E complex formation. During cellular stress, inactivation of mTOR leads to accumulation of hypophosphorylated 4E-BP and its association with eIF4E, resulting in inhibition of the eIF4F complex assembly. This in turn leads to inhibition of translation initiation, accumulation of the non-canonical 48S PICs and induction of SG assembly (27, 28). The second mechanism relates to the ubiquitin-dependent proteasome system (UPS), the main cellular protein degradation pathway. The UPS plays a role in sustaining protein synthesis by supplying amino acids to the translational machinery. It has been shown that inhibition of the UPS reduces general translation initiation, which results in induction of SG assembly. SG formation induced by proteasome inhibition still required phosphorylation of eIF2α, which was performed by GCN2 activated due to the amino acid starvation (29, 30).

Stress granules are one of many non-membraneous organelles found in eukaryotic cells (31). Direct RNA-protein and protein-protein interactions stabilize the more stable SG inner core, whereas low affinity protein-RNA interactions characterize the more dynamic outer shell-like layer (32). Stress granules assemble rapidly under stress conditions and serve as mRNA storage sites during the cellular stress. SGs remain in a

dynamic equilibrium with the surrounding cytoplasm. After the stress has ceased and the level of free mRNAs has decreased, within a few minutes the stalled ribosomal complexes in SGs can be returned to the cytoplasm allowing for the translation to resume. Furthermore, SGs are important for mRNA turnover as alternatively, they can direct mRNAs for degradation. SGs maintain a dynamic exchange with processing bodies (P-bodies, PBs) that are other types of RNA granules, containing RNA degrading enzymes and playing a role in RNA silencing (33, 34).

Aside from general inhibition of translation and stress granule formation, phosphorylation of eIF2α leads to enhanced translation of basic leucine zipper (bZIP) family of transcription factors, including activating transcription factor 4 (ATF4) and ATF5, which further induce expression of other bZIP transcriptional regulators, like ATF3 and CCAAT/enhancer-binding protein homologous protein (CHOP, also known as growth arrest and DNA-damage-inducible protein 153 or GADD153) (Fig. 1). Collectively, these transcriptional factors regulate expression of a large number of genes involved in metabolism and amino acid transport, the redox homeostasis, and apoptosis (35, 36). Furthermore, switching off the eIF2α-dependent translation will lead to a decreased level of IκBα – the inhibitor of nuclear factor kappa-light-chain-enhancer of activated B cells (NFκB). No longer part of the inhibitory complex, the transcription factor NFκB will translocate from the cytoplasm to the nucleus, where it will regulate expression of over 200 genes, mostly with pro-survival and inflammatory functions (37). Finally, another target of ATF4 is GADD34, which promotes dephosphorylation of eIF2α and resumption of eIF2α-dependent expression of house-keeping genes (Fig. 1) (38). Nonetheless, prolonged exposure of the cells to the ongoing stress leading to high levels

of eIF2α phosphorylation will shift the balance between the pro-survival and pro-apoptotic response towards apoptosis, which is an integral part of the IRS (Fig. 1) (2, 3).

Apoptosis is one of the major pathways of programmed cell death (PCD). Cellular death can be: a) accidental, resulting merely from a mechanical damage to the cell, or b) programmed, executed as a highly controlled signaling pathway. The idea of programmed cell death was first introduced in 1964 by Lockshin and Williams during their studies of apoptosis (39). Most commonly, PCD (especially apoptosis) occurs to delete unwanted, superfluous or potentially harmful cells, such as those undergoing transformation, and is normal part of eukaryotic development and physiology. Aside from morphological features and functional and immunological characteristics, PCD pathways can be generally divided into two classes: a) dependent on caspases, like apoptosis and pyroptosis, and b) independent of caspases, like necroptosis (40, 41).

Apoptosis is characterized by chromatin condensation and fragmentation, cell shrinkage, and membrane blebbing. It is a controlled cell suicide pathway resulting in production of apoptotic bodies, which are subsequently engulfed by surrounding cells and phagocytes (42, 43). Apoptosis is executed by two families of proteins: Bcl-2 protein family and cysteinyl aspartate-specific proteases or caspases. Caspases exist in the cell as inactive proenzymes (zymogens, procaspases). Caspases can be further divided into two groups: initiator caspases (caspase-2, -8, -9, and -10), which are activated in response to cellular signaling, and effector caspases (caspase-3, -6, and -7), activated by active initiator caspases (44-46). There are two known pathways leading to induction of apoptosis (Fig. 3):

a) the intrinsic pathway (mitochondria-dependent): induced by DNA damage and cytotoxic insults and manifested by loss of mitochondrial integrity and release of cytochrome c (cyt c) into the cytoplasm (47)
b) the extrinsic pathway (death receptor-dependent): induced via stimulation of death receptors of the tumor necrosis factor receptor (TNFR) family, like TNFR and FAS, executed by the death-inducing signaling complex (DISC) (48)

During cellular stress, the intrinsic-pathway pro-apoptotic Bcl-2-homology 3 (BH3)-only proteins, Bak and Bax, neutralize anti-apoptotic proteins Bcl-2, Bcl-xL, and Mcl-1, leading to mitochondrial outer membrane permeabilization (MOMP) (Fig. 3). MOMP results in efflux of apoptogenic factors, like cyt c, from the intermembrane space into the cytoplasm. Cyt c associates with the cytosolic apoptosis protease activating factor-1 (Apaf-1), which recruits procaspase-9 to form the apoptosome. Via its caspase activation and recruitment domain (CARD), procaspase-9 becomes activated, and in turn activates downstream executioner caspases-3, -6, and -7, leading to apoptotic death (Fig. 3) (47, 49).

Death receptors involved in the extrinsic pathway include: TNFR1 (ligand TNFα), FAS/CD95/APO-1 (ligand: FasL), TRAILR1/DR4 (ligand: TRAIL or TNF-related apoptosis-inducing ligand), TRAILR2/DR5 (ligand: TRAIL). Association of a death ligand with its receptor leads to receptor oligomerization and exposure of receptor intracellular death domain (DD). Homotypic interactions with adaptor proteins FADD (Fas-associated death domain) or TRADD (TNFR-associated death domain) lead to formation of DISC via recruitment and activation of procaspases-8 and -10. Caspases-8

and -10 will subsequently activate effector caspases-3, -6, and -7 (Fig. 3). Furthermore, caspase-8 will trigger the amplification loop, targeting BH3-only protein Bid, producing t-Bid, which contributes to MOMP-mediated death (42, 48, 50).

Pyroptosis, as opposed to immunologically silent apoptosis, is highly immunogenic as it leads to release of cytokines and intracellular content into the extracellular environment and induction of inflammation (51). Pyroptosis can be induced following detection of pathogen-associated molecular patterns (PAMPs) and damage-associated molecular patterns (DAMPs). Pyroptosis is dependent on caspase-1, also known as interleukin-1β (IL-1β)-converting enzyme (ICE). Like other caspases, caspase-1 exists in the cell as a zymogen and becomes activated as part of the inflammasome complex. Upon stimulation of NOD-like receptors (NLRs) by intracellular bacterial, viral, or host damage signals, several different inflammasomes can form, depending on the stimulated NLR: Nalp-1, Nalp-3, Ipaf, and AIM2. Activated caspase-1 acts mainly through formation of pores in the plasma membrane, leading to dissipation of cellular ionic gradient, allowing water influx, cell swelling and osmotic lysis. Furthermore, caspase-1 processes pro-forms of IL-1β and IL-18, which are also released during pyroptosis (Fig. 3) (42, 51, 52).

Another pro-inflammatory PCD pathway that results in osmotic rupture of the cell is necroptosis, also known as programmed necrosis. Necrosis has long been considered only an uncontrolled cell death pathway, lacking any underlying signaling mechanisms. Today, the term “necrosis” is indeed reserved for the accidental cell death (ACD), resulting from severe insults of physical (e.g., osmotic forces, high pressure and temperature), mechanical (e.g., shear forces), or chemical (e.g., extreme pH variations)

nature (53). Typically, necrosis is characterized by ATP depletion, elevated cytosolic calcium levels, and production of reactive oxygen species (ROS) and nitric oxide (NO). Elevated calcium levels lead to mitochondrial calcium overload and activation of proteases and phospholipases. Increased levels of ROS cause damage to proteins, lipids, and DNA and consequently lead to mitochondrial dysfunction, ion balance dysregulation, and loss of membrane integrity (54).

As opposed to accidental necrosis, programmed necrosis (or necroptosis) results from induction of a highly controlled signaling pathway (53). As mentioned before, necroptosis is a caspase-independent pathway. Instead, it is dependent on the receptor-interacting protein kinase 3 (RIPK3) (55). Canonically, necroptosis is induced by stimulation of the TNFR1 by its ligand, TNFα. Following the ligand binding, plasma membrane-bound complex I is formed: the TNFR1 cytoplasmic DD recruits TRADD, followed by recruitment of DD-containing serine/threonine kinase RIPK1, TNFR-associated factor 2 (TRAF2) and TRAF5, cytoplasmic inhibitor of apoptosis protein 1 (cIAP1) and cIAP2, and linear ubiquitin chain assembly complex (LUBAC) (56, 57). cIAP1/2 polyubiquitinate RIPK1 to form a docking platform for transforming growth factor-β-activated kinase 1 (TAK1) and the inhibitor of NFκB kinase (IKK) complex, NEMO-IKKa-IKKb (58). This activates the canonical NFκB signaling which collectively drives expression of pro-survival and inflammatory genes. Deubiquitination of RIPK1 by cylindromatosis (CYLD) will lead to dissociation of RIPK1 from TNFR1 (Fig. 3). RIPK1 DD is now available to interact with another DD-containing adaptor protein, FADD. FADD also contains death effector domain (DED), which recruits caspase 8 via homotypic interaction. Furthermore, RIPK1 contains a RIP homotypic interaction motif

(RHIM), just like RIPK3, leading to recruitment of RIPK3 and formation of complex II. Complex II will induce apoptosis as caspase 8 will cleave RIPK1-RIPK3 complex, which will inhibit necroptosis (56, 57, 59). When caspase 8 is inhibited, whether via chemical treatment or viral inhibitors, RIPK1 phosphorylates RIPK3, leading to its autophosphorylation and oligomerization (60). Subsequently, RIPK3 phosphorylates mixed lineage kinase domain-like (MLKL) protein, which is known to be the effector of necroptosis (Fig. 3) (61, 62). MLKL contains a C-terminal kinase domain (KD) and an N-terminal bundle and brace (NBB) region consisting of a four-helical bundle (4HB) domain and an auto-inhibitory brace (AIB) domain. RIPK3 phosphorylates serine 358 (S345 in mice) within the MLKL KD, leading to disruption of the interaction between the KD and the NBB region. Subsequently, highly phosphorylated inositol phosphates (IPs), like IP_6, produced via activity of IP kinases IPMK and ITPK1, will destabilize the inhibitory interaction between the components of the NBB region: the 4HB domain and the AIB domain. This will expose a patch of positively charged amino acids on the 4HB domain, allowing MLKL to interact with membrane-bound phosphatidylinositol phosphates (PIPs), effectively leading to MLKL integration into the plasma membrane. Finally, MLKL KD is phosphorylated at tyrosine 357 by TAM (Tyro3, Axl, and Mer) family of receptor tyrosine kinases, resulting in MLKL trimerization and pore formation (63-67). Water and sodium can enter the pores, resulting in cell swelling and eventual rupture, spilling DAMPs (63, 68-71).

The canonical death receptor-induced pathway is only one of a few known pathways leading to necroptotic death. Pathogen recognition receptors (PRRs), more specifically membrane-associated toll-like receptors (TLRs) have been demonstrated to

play a role as well. TIR-domain-containing adaptor-inducing interferon-β (TRIF) activated in TLR3 (dsRNA) and TLR4 (lipopolysaccharide) signaling pathway also contains the RHIM domain and has the ability to interact with and activate RIPK3 (Fig. 4) (72, 73). Furthermore, DNA-dependent activator of IFN-regulatory factors (DAI), also referred to as Z-DNA-binding protein 1 (ZBP-1) or tumor stroma and activated macrophage protein (DLM-1), has been shown to respond to DNA viruses, like murine cytomegalovirus (MCMV), herpes simplex virus 1 (HSV-1), and vaccinia virus (74-77) as well as RNA viruses, like influenza A virus (IAV) (78, 79), and activate the programmed necrosis via RHIM-mediated interaction with RIPK3 (Fig. 4).

DAI is a cellular protein whose gene was first identified as upregulated in host reactive stromal cells in response to ascites tumors (80). Furthermore, DAI was expressed in mouse macrophages stimulated with IFNγ or LPS. Initially, DAI was described as IFN-induced sensor of cytosolic DNA (81). Although identified as a cytosolic receptor, DAI was shown to shuttle between the cytoplasm and the nucleus. DAI contains two Z-DNA-binding domains (ZBDs), named Zα and Zβ, and three RHIM-like domains. As a Z-DNA-binding protein, DAI has been shown to localize to stress granules (82, 83). However, its function in stress granules has remained enigmatic. ZBDs of DAI are homologous to those in another known Z-DNA-binding protein, ADAR, as well as the immune evasion protein of vaccinia virus, E3. In fact, swapping the ZBD of E3 for the one from DAI maintains the virus pathogenicity, which is otherwise lost when the domain is missing or mutated (82, 84). Maelfait (85) demonstrated importance of ZBDs of DAI in programmed necrosis. When DAI ZBDs were mutated, MCMV-M45mutRHIM virus was unable to induce necroptosis, which otherwise is induced in

presence of DAI with functional ZBDs. Moreover, knock-in mice expressing DAI with mutations in its ZBDs (Zbp1Za1a2/Za1a2) failed to efficiently clear MCMV-M45mutRHIM infection, unlike wild-type mice (85). Furthermore, DAI has been identified as a crucial component of the necroptosis pathway in cells infected with IAV where it was shown to induce death by recognizing RNA during virus infection (78, 79). These findings showed importance of DAI-mediated necroptosis induced by nucleic acid binding as innate defense mechanism against viral infections. More recently, a similar pathway was demonstrated to be induced following infection with vaccinia virus E3 protein mutant, VACV-E3LΔ83N (75).

Vaccinia virus belongs to the family of *Poxviridae*. Poxviruses are large (200 nm in diameter and 300 nm in length), brick-shaped, enveloped viruses that infect a wide variety of animals, both invertebrate and vertebrate. Poxvirus replication takes places entirely in the cytoplasm. Poxviral double-stranded DNA (dsDNA) genome (130-300 kbp) encodes a variety of proteins, including those involved in immunomodulation (86-88).

Vaccinia virus (VACV), a prototype member of the orthopoxvirus (OPXV) subfamily, encodes a conserved immune evasion protein E3 (gene E3L). This 190 amino-acid protein is comprised of two conserved domains (Fig. 5). The C-terminal domain, which contains a dsRNA-binding domain (dsRBD), is responsible for binding dsRNA that accumulates in the cells during VACV infection. Thereby, E3 protein masks viral presence from the cellular cytoplasmic receptors recognizing dsRNA: PKR and 2’-5’ oligoadenylate synthetase (2’-5’ OAS) (89-92). Recognition of dsRNA by PKR and 2’-5’ OAS leads to translational shutdown (see above) and degradation of RNA, respectively,

and thereby induction of an antiviral state (93). 2'-5' OAS introduces unusual 2'-5' bonds in newly synthesized RNA, which is thereby specifically recognized and degraded by RNase L. The E3 protein C terminus has been shown to be required for VACV IFN resistance and a broad host range as the viruses with mutations affecting dsRNA binding were unable to replicate in HeLa cells or in RK-13 cells treated with IFN (94). The function of the N terminus had remained less clear. It was shown that E3 N terminus is also required for IFN resistance and pathogenesis. VACV N-terminal mutant lacking the first 83 amino acids and hence the entire ZBD (VACV-E3LΔ83N) displayed 10,000-fold decrease in pathogenicity compared with the wild-type virus (89, 95). Furthermore, the N terminus has been shown to bind to Z-DNA and this ability correlated with the pathogenicity of the harboring virus (84). Recently, we demonstrated that N terminus is required for inhibition of necroptosis (75).

This work focuses on understanding in more detail the molecular patterns governing execution of necroptosis. We looked at two distinct manners of necroptosis induction: oxidative stress (Chapter 2) and viral infection (Chapter 3). As DAI turned out to be important for programmed necrosis in both induction scenarios, we investigated the significance of stress granules in necroptosis. Finally, techniques useful for investigation of necroptosis, including a novel crosslinking technique to identify protein aggregation, are described (Chapter 4).

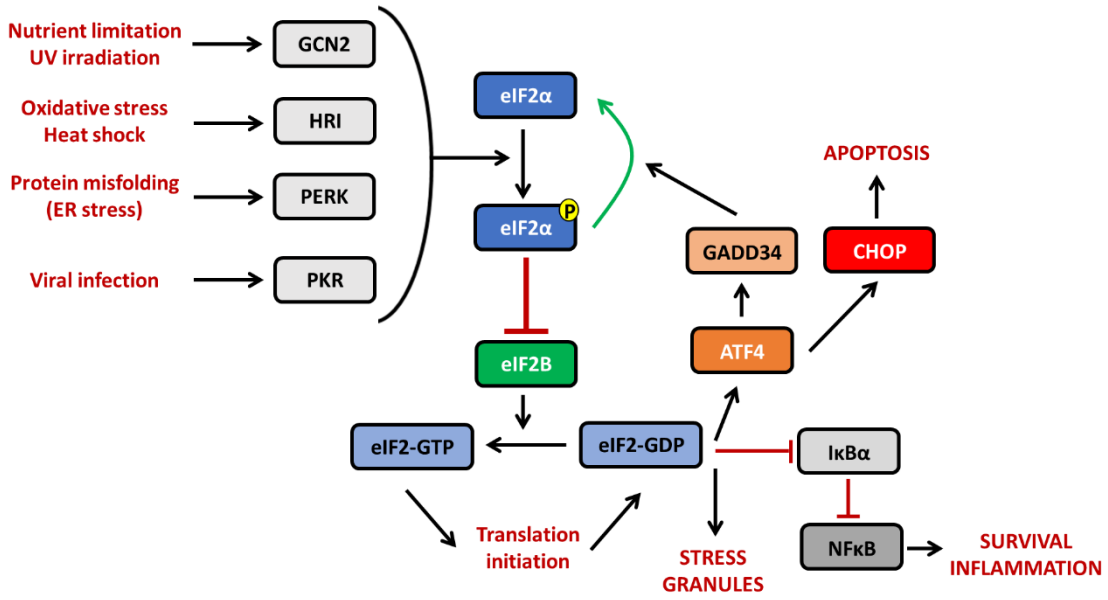

Figure 1. Schematic diagram of the integrated stress response. Different types of cellular stressors will induce a different stress-activated protein kinase: GCN2, HRI, PERK, or PKR. Each kinase functions to phosphorylate the α subunit of eIF2, which results in blocking eIF2B ability to replenish the pool of eIF2-GTP and inhibition of translation initiation. Low levels of eIF2-GTP lead to expression of ATF4 transcription factor, which in turn upregulates GADD34 responsible for dephosphorylation of eIF2α as well as CHOP, which can induce apoptosis. Furthermore, low levels of eIF2-GTP release IκBα-mediated inhibition of NFκB, leading to pro-survival and inflammatory signaling. Finally, low levels of eIF2-GTP lead to formation of stalled translation pre-initiation complexes, resulting in formation of stress granules (see Figure 2).

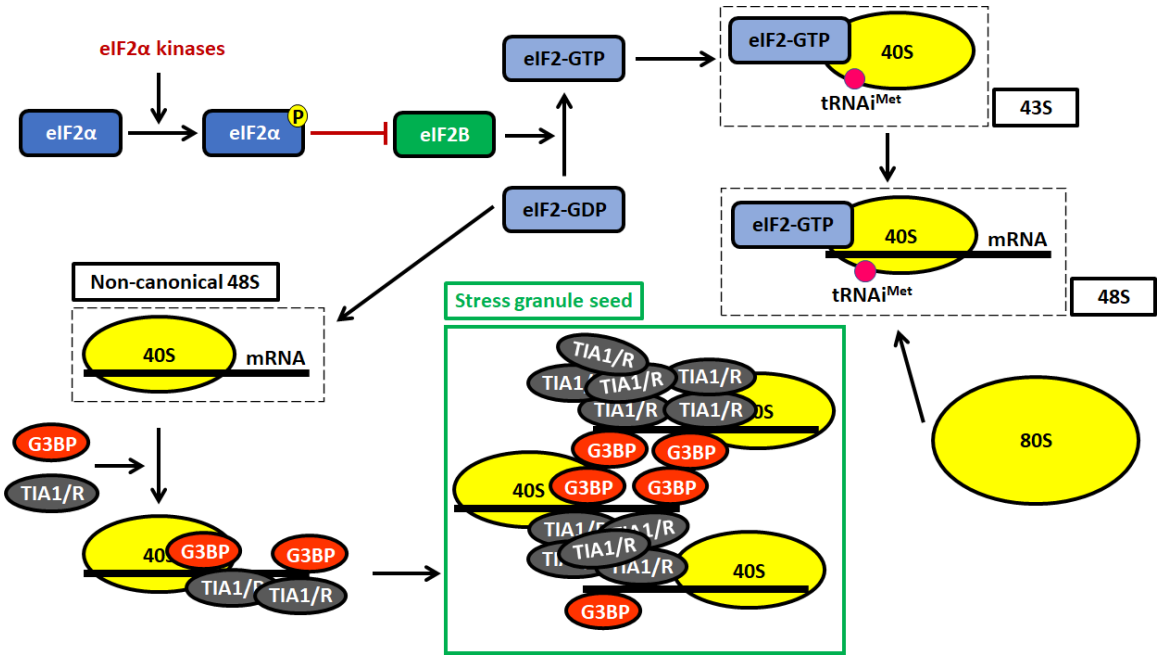

Figure 2. eIF2α kinase-induced formation of stress granules. Phosphorylation of eIF2α by eIF2α kinases results in decreased levels of eIF2-GTP (explained in Figure 1). eIF2-GTP forms the canonical 43S (with ribosomal 40S subunit and $tRNAi^{Met}$) and 48S (43S plus mRNA) translation pre-initiation complexes and is required for recruitment of the ribosomal large (60S) subunit. Decreased levels of eIF2-GTP lead to formation of non-canonical 48S translation pre-initiation complexes unable to recruit the ribosomal large subunit. Exposed mRNA becomes a binding target for RBPs and the stress granule nucleating proteins, TIA1/R and G3BP. G3BP dimerization and TIA1/R aggregation commences the stress granule formation process by bringing many 48S complexes together.
Drawing was not done to scale. Additional transcription factors participating in regulation of translation initiation are not shown.

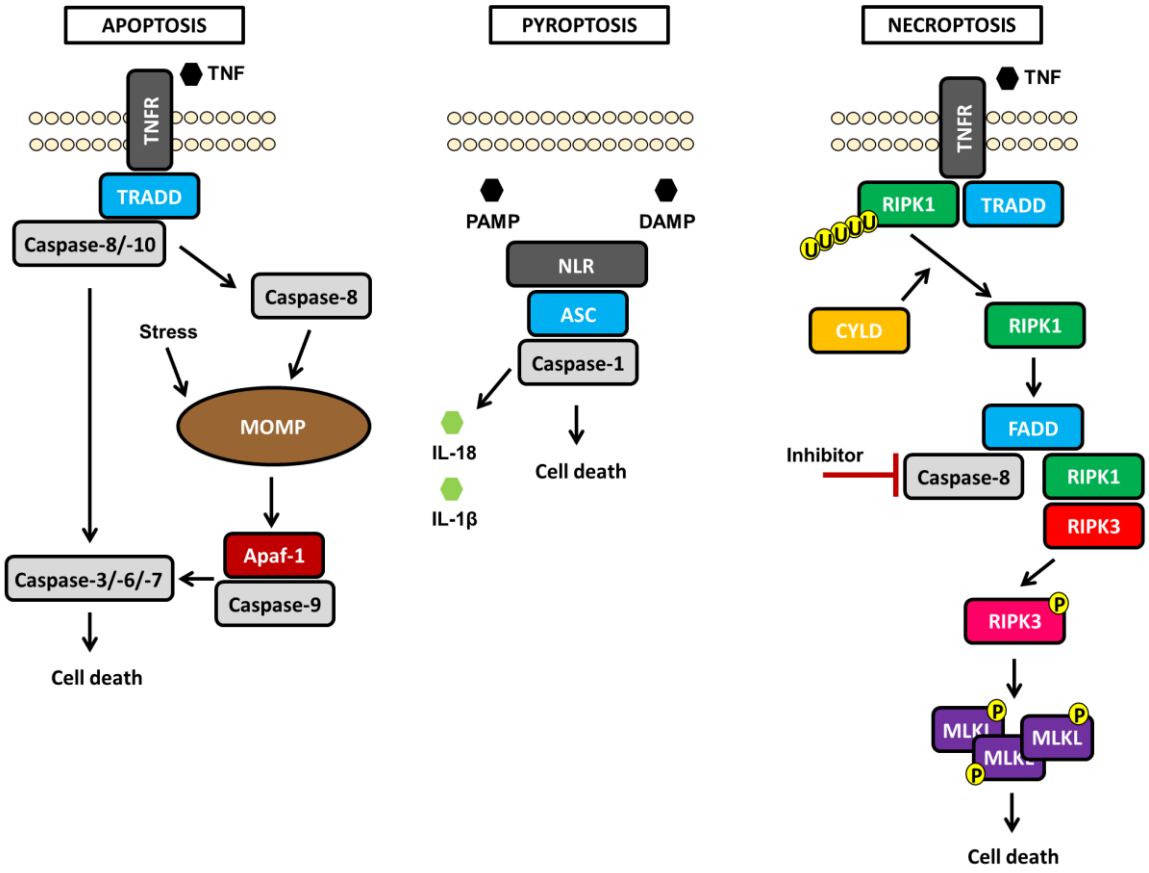

Figure 3. Major programmed cell death pathways. Apoptosis, pyroptosis, and necroptosis are the major PCD pathways. Apoptosis and pyroptosis are caspase-dependent, whereas necroptosis is dependent on RIPK3. Apoptosis is induced either via intracellular stress, which leads to mitochondrial permeabilization and activation of initiator caspase-9, or via stimulation of a membrane-bound death receptor, which activates initiator caspases-8 and -10. Initiator caspases activate effector caspases-3, -6, and -7, which execute the apoptotic death. Pyroptosis is induced by NLR-mediated recognition of PAMPs and DAMPs, which leads to activation of caspase-1 and execution of cell death. Necroptosis is canonically induced via stimulation of a membrane-bound death-receptor. This leads to activation of RIPK1, which forms a complex with RIPK3. If caspase-8 is inhibited, this complex activates MLKL, leading to necroptotic death.

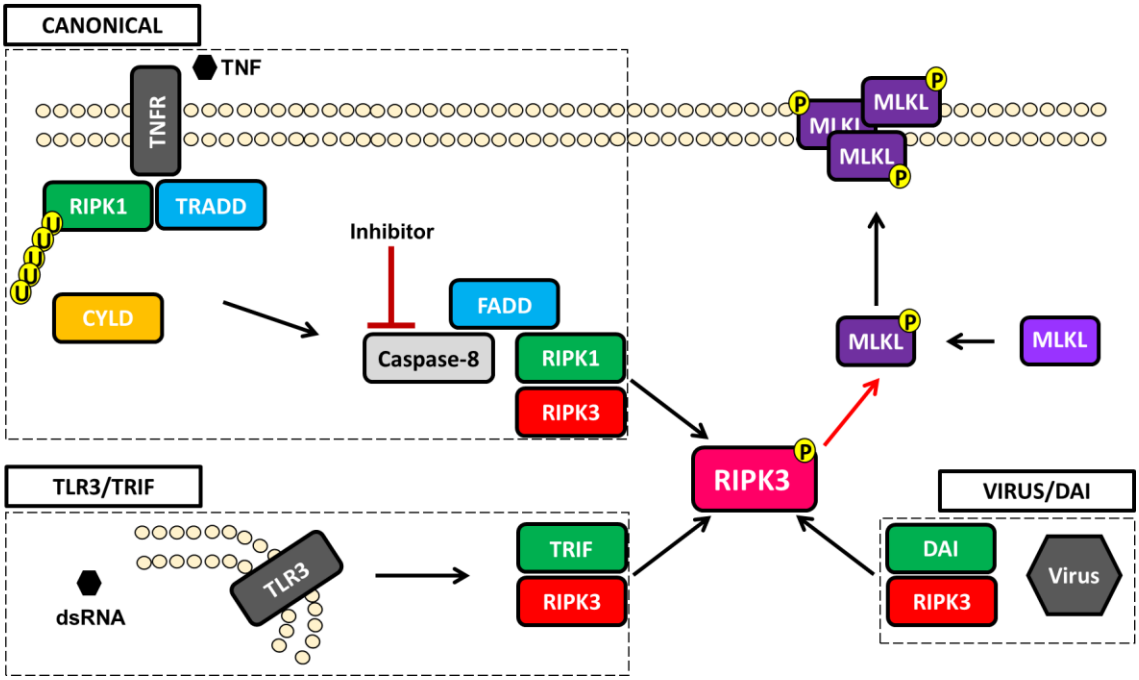

Figure 4. A simplified schematic of RIPK3 activation pathways leading to necroptosis. RIPK3, the crucial mediator of necroptosis, is indicated in red or in pink (when activated). RIPK3 can become activated by interaction with any of the other RHIM domain-containing proteins (indicated in green): DAI, RIPK1, and TRIF. The canonical pathway is induced via a death receptor and mediated by RIPK1. dsRNA can induce TLR3 and activate necroptosis mediated by TRIF. Viruses have been shown to be detected by DAI, which can then induce necroptosis.

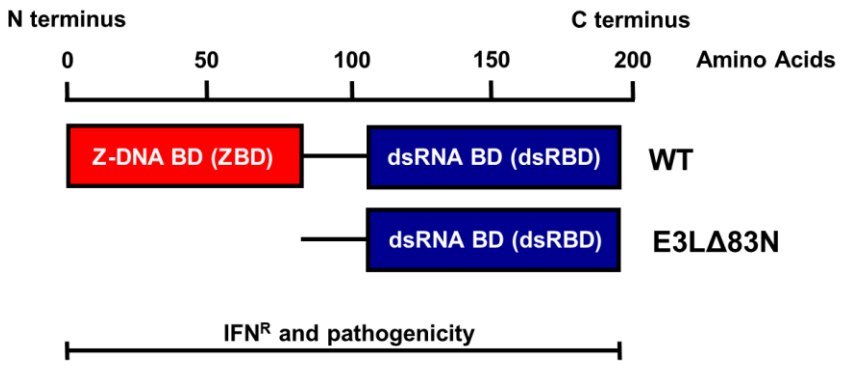

Fig. 5. A schematic of the vaccinia virus immune evasion protein E3. E3 protein is a 25-kDa protein consisting of 190 amino acids. The protein contains two conserved domains: the N-terminal domain is a Z-DNA-binding domain (ZBD), whereas the C-terminal domain is a double-stranded RNA (dsRNA)-binding domain (dsRBD). Both E3 domains are required for complete IFN resistance of the virus and pathogenicity in mice. Depicted are the full-length wild-type E3 protein (WT) and the N-terminal deletion mutant, lacking the first 83 amino acids (the entire ZBD) (E3LΔ83N).

CHAPTER 2

OXIDATIVE STRESS INDUCES DAI-MEDIATED NECROPTOSIS DEPENDENT ON FORMATION OF STRESS GRANULES

ABSTRACT

Oxidative stress has been implicated in aging and neurodegenerative diseases. Cellular death has progressively gained recognition as a significant player in human diseases, including neurodegeneration. In this work we show that oxidative stress induces the RIPK3-dependent cell death pathway, necroptosis. This pathway is mediated by the cellular protein DAI, which localizes to arsenite-induced stress granules. RIPK3 localizes to stress granules in the presence of DAI, which leads to a DAI-RIPK3 necrosome formation, phosphorylation of MLKL and execution of necroptosis. Inability of cells to form granules results in lack of necroptosis induction during oxidative stress. Altogether, oxidative stress induces DAI-mediated necroptosis dependent on stress granule formation. Since oxidative stress has been implicated in neurodegenerative diseases, this work suggests that necroptotic death may play a role in age-related degenerative diseases.

INTRODUCTION

Various environmental stressors perturb cellular homeostasis (2). Upon the cell being subjected to a stressor, an intracellular adaptive response becomes activated, leading to expression of stress-induced genes, directing cellular metabolism to counteract the effects of the ongoing stress (1). This integrated stress response (ISR) results from activation of one of the four stress-activated protein kinases: GCN2, HRI, PERK, or PKR (7, 96-98). Each of these kinases phosphorylates the eukaryotic translation initiation factor, eIF2 on its α subunit, resulting in inhibition of the translation of housekeeping genes. Phosphorylation of eIF2α leads to formation of stalled translation pre-initiation complexes containing the 40 S ribosomal subunit and untranslated mRNA (2). The exposed mRNA becomes bound by any of several RNA-binding proteins, including TIAR, TIA-1, and G3BP, which organize the stalled complexes into stress granules (SGs): cytoplasmic microdomains that store the stalled translational complexes until the stress ceases (99-101). SGs can then release the untranslated mRNA back into the cytoplasm, allowing the cell to regain homeostasis. Alternatively, the mRNA can also be directed for degradation (102, 103). If the cellular stress persists, it can result in programmed apoptotic cell death (104). In contrast to accidental cell death caused by mere mechanical damage to the cell, programmed cell death (PCD) pathways are highly regulated pathways, controlled by a plethora of cellular regulatory proteins (39, 105). The most common PCD pathways include caspase-dependent apoptosis and pyroptosis, and caspase-independent necroptosis [reviewed in (106-108)].

Necroptosis is a receptor-interacting protein kinase 3 (RIPK3)-dependent PCD (109, 110). Canonically, necroptosis is activated via stimulation of one of the death receptors, including the tumor necrosis factor receptor (TNFR) or Fas/CD95 (111-113). Upon stimulation, the receptor recruits the protein kinase RIPK1, which can interact with RIPK3 via their mutual RIP homotypic interaction motif (RHIM) domains (60, 114). Activated RIPK3 undergoes autophosphorylation and phosphorylates the mixed lineage kinase-like (MLKL) protein (61, 62). Subsequently, phosphorylated MLKL (pMLKL) trimerizes and forms pores in the plasma membrane, leading to swelling of the cell and subsequent rupture, which are key characteristics of necroptotic death (63, 70). The explosive rupture of cells during necroptotic cell death can release damage-associated molecular patterns, DAMPs, that can act in a pro-inflammatory manner [reviewed in (115)].

Aside from the canonical death receptor-mediated stimulation, necroptosis has been shown to be induced following RIPK3 activation by the cellular DNA-dependent activator of IFN-regulatory factors, DAI (also known as DLM and ZBP-1) (116). Murine cytomegalovirus (mCMV) and vaccinia virus (VACV) inhibit DAI-mediated necroptosis using their vIRA (M45) and E3 proteins, respectively (75, 77). When missing these necroptosis inhibitors, mutant viruses induce necroptosis that is dependent on DAI. Furthermore, infection with influenza A virus (IAV) results in activation of DAI-mediated necroptosis (78, 79). DAI, similar to RIPK1, contains a RHIM domain, allowing it to interact with and activate RIPK3, leading to necroptosis (83, 117). The exact mechanism of DAI-mediated necroptosis activation has remained enigmatic. In addition to activating RIPK3, DAI has been shown to be recruited to arsenite-induced

stress granules (82). The consensus Zα1 domain of DAI was sufficient to recruit DAI to stress granules (118). However, the physiological relevance of recruitment of DAI to stress granules has been unclear, especially since the cells previously used to show recruitment of DAI to stress granules do not express RIPK3, the key mediator of necroptotic cell death. Therefore, it has remained undetermined whether stress granules play a role in necroptosis.

In this manuscript, we investigated cell death induced by an oxidative stressor, sodium arsenite. We show that arsenite induces necroptosis that is dependent on the protein DAI. As arsenite induces SGs (97), we evaluated their significance for the necroptosis pathway. Our data shows that DAI and RIPK3 localize to SGs under conditions of arsenite-induced necroptosis. As DAI is a Z-DNA-binding protein and all proteins containing the Z-DNA-binding domain (ZBD) localize to stress granules (118), we asked whether RIPK3 becomes localized to SGs specifically in conditions of necroptosis. RIPK3 localizes into SGs only in the presence of DAI, suggesting that DAI recruits RIPK3 to SGs, leading to RIPK3 activation. Furthermore, inability of cells to form granules (TIA-1 KO and G3BP1/2 KO) significantly reduced arsenite-induced DAI-mediated necroptosis. Thus, oxidative stress leads to recruitment of RIPK3 to stress granules, in a DAI-dependent manner, leading to RIPK3 activation and necroptotic cell death. Since oxidative stress and accumulation of stress granules have both recently been implicated in age-related degenerative diseases (119-121), this work suggests a role for DAI sensing of stress granules in PCD associated with age-related degeneration.

MATERIALS AND METHODS

Cells. All cells were grown at 37^{o}C in atmosphere supplemented with 5% CO_2. Murine fibroblast L929 cells, DAI KO L929 cells, and MLKL KO L929 cells were maintained in the Minimum Essential Media (MEM) (Corning) supplemented with 5% fetal bovine serum (FBS). Mouse embryonic fibroblasts (MEF), TIA-1 KO MEF, human bone osteosarcoma epithelial cells (U2OS), and G3BP1/2 KO U2OS cells were a kind gift from Dr. Nancy Kedersha (Brigham and Women's Hospital, Inc., Boston) (*8*). These cells were maintained in Dulbecco's Modification of MEM media (DMEM) (Corning) supplemented with 10% FBS and 2 µM L-Glutamine.

Cell treatments. To determine the requirement for activity of RIP proteins, cells were pretreated with N-(6-(isopropylsulfonyl)quinolin-4-yl)benzo[d]thiazol-5-amine (GSK'872, RIPK3 inhibitor; GlaxoSmithKline) at 3 µM and 2,2-dimethyl-1-(5(S)-phenyl-4,5-dihydro-pyrazol1-yl)-propan-1-one (GSK'963, RIPK1 inhibitor; GlaxoSmithKline) at 5 µM, one hour prior to treatment with sodium arsenite, and continuously treated thereafter. For induction of the canonical necroptosis pathway, cells were pretreated with carbobenzoxy-valyl-alanyl-aspartyl-[O-methyl]-fluoromethylketone (Z-VAD-FMK, pan-caspase inhibitor, ApexBio) at 100 µM, one hour prior to treatment with 20 ng/mL mouse tumor necrosis factor alpha (TNF-α, Sigma), and continuously treated thereafter.

SYTOX nuclear stain exclusion assay. To assess viability of L929 cells, the cells were seeded in 12-well CytoOne tissue culture-treated plates (USA Scientific) and pretreated with 100 U/mL of mouse alpha-interferon (IFN-α, Calbiochem) for 18 h before

they were treated with 500 μM sodium arsenite. Hoechst 33342 (H3570, Thermo Fisher) and SYTOX Green Nucleic Acid Stain (S7020, ThermoScientific) were applied for 15 min. before the arsenite treatment and throughout the time following the arsenite treatment. Cells were incubated at 37 °C with 5% CO_2-supplemented air on an EVOS FL auto imaging system (Invitrogen) with onstage incubator system and an image was taken every 30 min. for 12 h.

Protein extraction and Western immunoblot analysis. For analysis of protein levels, cells were routinely scraped, pelleted, and lysed in RIPA lysis buffer (150 mM NaCl, 1% Nonidet P-40, 0.5% sodium deoxycholate, 0.1% SDS, 25 mM Tris pH 7.4) by 10-min. incubation on ice. Standard protocol for SDS-PAGE was followed. Proteins were transferred on a nitrocellulose membrane in 10 mM 3-(cyclohexylamino)-1-propane sulfonic acid (CAPS), 20% v/v methanol, pH 11. Antibodies used for immunoblotting were specific for ZBP1/DAI (mAb, Zippy-1, AG-20B-0010-C100, Adipogen), RIP3 (D4G2A, mAb, #95702, Cell Signaling Technology), G3BP1 (pAb, 13057-2-AP, Proteintech). Secondary antibodies used were goat anti-rabbit IgG or goat anti-mouse IgG, both HRP-linked (Cell Signaling Technology). Antibodies specific for β-actin were HRP-linked (sc-47778, Santa Cruz Biotechnology). Immunoreactive bands were visualized by chemiluminescence with SuperSignal West Pico PLUS or Dura Extended Duration substrate (ThermoFisher).

MLKL phosphorylation assay. L929 or MEF cells were seeded in a 6-well tissue culture-treated dish (VWR) and pretreated with 100 U/mL (L929) or 1000 U/mL (MEF) of mouse IFNα (Calbiochem) for 18 h before they were treated with 500 μM (L929) or 50 μM (MEF) sodium arsenite. Following 5 hours of arsenite treatment, the

cells were scraped and pelleted and subsequently lysed in RIPA lysis buffer as described above. Next, lysates were centrifuged in QIAshredder columns (79654, Qiagen) to aid MLKL extraction from the membrane-bound trimer. Western immunoblot analysis (described above) followed using primary antibodies specific for phosphorylated MLKL (mAb, S345, ab196436, abcam) and total MLKL (mAb, D6W1K, Cell Signaling Technology).

MLKL trimerization assay. L929 or MEF cells were seeded, treated, and lysed in RIPA lysis buffer like described for MLKL phosphorylation assay. Western immunoblot analysis was performed like described above with the following exceptions: SDS-PAGE was run in non-reducing conditions and proteins were transferred overnight onto a nitrocellulose membrane at low voltage (20 V). To detect MLKL trimers, primary antibodies specific for total MLKL (mAb, D6W1K, Cell Signaling Technology) were used.

DSP crosslinking. L929 cells were seeded in a 6-well tissue culture-treated dish (VWR) and pretreated with 100 U/mL of mouse IFNα (Calbiochem) for 18 h before they were treated with 500 µM sodium arsenite. Following 2 hours of arsenite treatment, the cells were scraped, pelleted, and resuspended in phosphate-buffered saline (PBS). To crosslink proteins, dithiobis(succinimidyl propionate) (Lomant's Reagent, DSP) (22586, ThermoFisher Scientific) was added at 1 mM and the cell suspension was incubated at 25^{o}C for 30 min. Cells were pelleted, resuspended in RIPA lysis buffer (recipe above) and lysed for 10 min. on ice. Crosslinked protein complexes were subjected to a non-reducing SDS-PAGE, followed by an overnight (16-20 hour) transfer at 20V to a nitrocellulose membrane. Western immunoblot analysis followed the protocol described

above. To analyze protein monomers, DSP-crosslinked samples were reduced by addition of 1,4-dithiothreitol (DTT, Sigma-Aldrich) at 50 mM and incubation at 37ºC for 60 min. Samples were denatured at 95ºC for 15 min. prior to Western immunoblot analysis (described above).

Creation of DAI KO and MLKL KO L929 cells. L929 cells at 50% confluency were infected with Edit-R Lentiviral particles containing Cas9 sgRNA (#VCAS10133, Dharmacon) at MOI 0.3 and incubated at 37°C for 4 hours, after which L929 growth medium was added. Following 24-hour incubation, the medium was replaced with L929 growth medium containing 8 µg/mL blasticidin. Following selection, expression of Cas9 in cells was confirmed via Western immunoblot (#NBP2-36440L, Novus Biologicals). In order to knock out the DAI gene, Cas9-expressing L929 cells at 50% confluency were infected with a mixture of three Edit-R Lentiviral DAI-specific sgRNAs (sgRNA1: VSGM10144-246664134, sgRNA2:-246664138, sgRNA3:-246664139, Dharmacon) at an MOI of 0.3 and incubated at 37°C for 4 hours, after which L929 growth medium was added. After 24 hours, the medium was replaced with L929 growth medium containing 10 µg/mL puromycin. Following selection, surviving cells were seeded into a 96-well dish with one cell per well and were clonally expanded. The successful knock-out of the DAI gene was confirmed via Western immunoblot analysis (mAb, Zippy-1, AG-20B-0010-C100, Adipogen).

To create MLKL KO L929 cells, the same protocol was followed, except a single Edit-R Lentiviral MLKL-specific sgRNA was used (VSGM10144-246701514, Dharmacon). The successful knock-out of the MLKL gene was confirmed via Western immunoblot analysis (mAb, D6W1K, Cell Signaling Technology).

Co-immunoprecipitation. L929 cells were seeded in a 6-well tissue culture-treated dish (VWR) and pretreated with 100 U/mL of mouse IFNα (Calbiochem) for 18 h before they were treated with 500 μM sodium arsenite. Following 2 hours of arsenite treatment, the cells were scraped, pelleted, resuspended in a non-denaturing lysis buffer [10 mM Tris-HCl, pH 7.5, 1 mM DTT, 2 mM $MgCl_2$, 50 mM KCl, 1% Triton X-100, 1X HALT Protease/ Phosphatase Inhibitor Cocktail (78446, ThermoFisher)] and lysed by incubation for 10 min. on ice. Equal volume of Buffer I (20 mM Tris-HCl, pH 7.5, 0.4 mM NaCl, 1 mM DTT, 1 mM EDTA, 1% Triton X-100, 20% glycerol, 2 mM Na_3VO_4) was added. Lysates were precleared by incubation with Protein A/G PLUS-Agarose (sc-2003, Santa Cruz) for 30 min. at 4°C with rotation. To capture protein complexes, the lysates were incubated with antibodies specific for ZBP1/DAI (mAb, Zippy-1, AG-20B-0010-C100, Adipogen) or G3BP1 (mAb, 66486-1-Ig, Proteintech) overnight at 4°C with rotation. Protein complexes were isolated by addition of Protein A/G PLUS-Agarose (sc-2003, Santa Cruz) and incubation for 90 min. at 4°C with rotation, followed by three 5-min. washes in Buffer I, and pelleting the beads with bound antibodies and protein complexes. The proteins were released by addition of 4x Laemmli (250 mM Tris, pH 6.8, 8% SDS, 50% glycerol, 0.04% bromophenol blue) with 50 mM DTT and boiling for 15 min. at 95°C. Western immunoblot analysis followed (described above) with the following exception: to detect DAI, antibody specific for ZBP1/DLM-1/DAI (NBP1-76854, Novus Biologicals) was used.

Immunofluorescence. L929 cells were seeded in a 48-well CytoOne tissue culture-treated plates (USA Scientific) and pretreated with 100 U/mL of mouse IFNα (Calbiochem) for 18 h before they were treated with 500 μM sodium arsenite. Following

2 hours of arsenite treatment, cells were fixed in 2% paraformaldehyde for 10 min. at room temperature, after which cells were washed with PBS. All following steps were performed at room temperature. Cells were permeabilized with 0.2% Triton X-100 (in PBS) for 5 min. and then washed again with PBS. To limit unspecific antibody binding, cells were blocked with 2% bovine serum albumin (BSA) (in PBS) for 10 minutes. Primary antibodies specific for G3BP1 (66486-1-Ig, Proteintech, 1:100) and DAI (ZBP1/DLM-1/DAI, NBP1-76854, Novus Biologicals, 1:250) were diluted in the blocking solution at the indicated dilutions and applied to cells for 1 hour, after which cells were washed with PBS. Secondary antibodies (Alexa Fluor 488, A-11001, Thermo Fisher, 1:1000, and Texas Red, T2767, Thermo Fisher, 1:250) were diluted in the blocking solution at the indicated dilutions and applied to cells for 1 hour in the dark, after which cells were washed with PBS. Cells were stained with DAPI (4′,6-diamidino-2-phenylindole) (in PBS) for 15 min. and washed with PBS. Cells were imaged using EVOS FL auto imaging system (Invitrogen).

Propidium iodide (PI) nuclear stain exclusion assay. To assess viability of MEF cells, the cells were seeded in 12-well CytoOne tissue culture-treated plates (USA Scientific) and pretreated with 1000 U/mL of mouse alpha-interferon (IFN-α, Calbiochem) for 18 h before they were treated with 50 μM sodium arsenite. Hoechst 33342 (H3570, Thermo Fisher) and propidium iodide (P1304MP, Thermo Fisher) were applied for 15 min. before imaging on an EVOS FL auto imaging system (Invitrogen) at 8 hours following arsenite treatment.

To assess viability of U2OS cells, the cells were seeded in 48-well CytoOne tissue culture-treated plates (USA Scientific) and transfected the following day with a total of

0.3 µg DNA using X-tremeGENE HP DNA Transfection Reagent (06 366 244 001, Roche) according to the manufacturer's recommendations. At 48 hours post-transfection, the cells were treated with 500 µM sodium arsenite and cell viability was assessed 14 hours later as described.

Statistical analysis. All data is a representation of at least three independently conducted experiments. Normal-based 95% confidence interval (CI): mean ± 2 SD was used as the basis for statistical analysis. Fisher-Snedecor distribution (F test) with the significance level (α) of 0.05 was used to compare variances between groups. Two-sided Student's t-test (α of 0.05, 0.01, or 0.001) was performed to assess statistical significance of the observed differences between samples. The t-distribution for equal or unequal variances was used based on the results of the F test.

RESULTS

IFN sensitizes L929 cells to arsenite-induced programmed cell death. Since DAI has been shown to be recruited to arsenite-induced stress granules, and DAI can bind to and activate RIPK3, leading to necroptotic cell death, we decided to ask if DAI can lead to necroptotic cell death in arsenite-treated cells (82, 116). All of our work has been done with murine L929 cells, which form stress granules in response to treatment with sodium arsenite and constitutively express RIPK3 (75, 122). Unlike RIPK3, DAI is not constitutively expressed in untreated cells, but is inducible by treatment with type I IFN (75).

In order to investigate whether we could induce cell death in conditions of oxidative stress, we treated L929 cells with arsenite. We were unable to observe significant amounts of death in L929 cells treated with arsenite alone (Fig. 6, blue square). Since DAI is IFN-inducible, we tested whether priming the cells with mouse IFNα would increase the death following the arsenite treatment. In fact, pretreating cells with IFN resulted in significant increase in cell death, with 50% of the cells dying at 7 hours post-arsenite treatment, and 75% of the cells at 11 hours (Fig. 6, red square) (t-test, p-values from 2.63×10^{-7} to 0.036). IFN treatment alone did not lead to significant cell death (Fig. 6, + sign). Necroptosis, unlike apoptosis, occurs within a rapid time frame. In fact, treatment of cells with TNFα and zVAD [inducers of the canonical necroptosis pathway (112)] resulted in a similar viability pattern as in IFN-primed L929 cells treated with arsenite (Fig. 6, green circle) (t-test, p-values from 2.5×10^{-9} to 0.02).

Arsenite induces a RIPK3-dependent necroptotic cell death. To ask if the cell death seen in cells treated with arsenite and IFN was necroptotic cell death, we utilized the RIPK3-specific inhibitor, GSK872, to test whether RIPK3 was involved in the arsenite-activated cell death. In fact, we observed a significant increase in L929 cell viability when the cells were treated with the RIPK3 inhibitor (Fig. 6, yellow square) (t-test, p-values from $5.5x10^{-5}$ to 0.022, compared with Arsenite+IFNα treatment). This data indicates that arsenite-induced cell death is a RIPK3-dependent pathway.

Necroptosis is characterized by activation of RIPK3 and subsequent phosphorylation of MLKL protein (61, 62). Phosphorylation of MLKL is specific for necroptosis as it has not been implicated in any other cellular death pathways. We investigated the status of MLKL in arsenite-treated L929 cells. As expected, treatment of cells with arsenite alone did not result in high levels of phosphorylated MLKL (pMLKL) (Fig. 7A, lane 2). When cells were pretreated with IFN, arsenite induced pMLKL (lane 5), confirming that the RIPK3-dependent pathway is indeed necroptosis. Levels of pMLKL were comparable to those resulting from induction of the canonical necroptosis pathway by treatment of cells with TNFα and zVAD (lane 3). Furthermore, pretreatment of cells with GSK872 inhibited phosphorylation of MLKL in cells treated with arsenite and IFN (lane 6), further confirming RIPK3-mediated phosphorylation of MLKL.

MLKL executes necroptosis via formation of a trimer by its phosphorylated form in the cellular plasma membrane (63, 70). Formation of pores leads to ionic imbalance and water flow into the cells, resulting in cellular swelling and final rupture of the plasma membrane. In order to confirm that arsenite leads to this phenomenon, we looked at the trimerization status of MLKL. We observed very low levels of trimerized MLKL in L929

cells treated with arsenite alone (Fig. 7B, lane 3), resulting most probably from low levels of IFN naturally present in L929 cell cultures. High levels of trimerized MLKL were present in IFN-primed L929 cells treated with arsenite (lane 4), confirming that phosphorylated MLKL forms a trimer and leads to necroptosis observed in these cells in Fig. 6. The positive control for the canonical necroptosis death (TNFα and zVAD treatment) yielded similar levels of trimerized MLKL (Fig. 7B, lane 5).

Finally, to confirm dependence of arsenite-activated death on MLKL, we generated MLKL knockout (KO) L929 cells by CRISPR/Cas-9 deletion. Treatment of MLKL-deficient L929 cells with arsenite did not lead to any death, even in IFN-primed cells (Fig. 8) (t-test, p=1.6E-05) as opposed to death seen in wild-type L929 cells (t-test, p=8.1E-04), demonstrating that arsenite-induced death is dependent on MLKL. Altogether, these results demonstrate that arsenite induces necroptosis in IFN-primed L929 cells.

Arsenite-induced cell death is DAI-dependent. Activation of RIPK3 is accomplished by its interaction with any of three other RHIM-containing proteins: TIR-domain-containing adapter-inducing interferon-β (TRIF), RIPK1, or DAI (72, 75, 112, 116). Upon interaction, RIPK3 autophosphorylates and subsequently phosphorylates the downstream regulator, MLKL (61, 62). Necroptosis can, therefore, be induced by interaction of RIPK3 with any of these three proteins.

We asked which of the known RIPK3 interaction partners becomes activated following arsenite treatment. TRIF-mediated necroptosis, resulting from activation of Toll-like receptor 3 (TLR3) or TLR4, has been most frequently associated with immune cells only, where TLR3 and TLR4 are primarily found (72, 123, 124). In order to test for

requirement for RIPK1, we utilized a RIPK1 inhibitor, GSK963. We did not observe viability rescue in cells pretreated with GSK963 (Fig. 6, purple square). In contrast, necroptosis induced by treatment with TNFα and zVAD, which has been known to progress through RIPK1, was completely inhibited by GSK963 (Fig. 6, gray circle). This data demonstrated that RIPK1 is not involved in arsenite-induced necroptosis.

We next tested whether arsenite-induced death is DAI dependent. DAI is a good candidate for the mediator of arsenite-induced necroptosis, as the arsenite-driven death was only observed in IFN-primed L929 cells and expression of DAI in L929 cells is IFN-dependent (75). To confirm our hypothesis, we generated DAI KO L929 cells. As shown in Fig. 9, little arsenite-inducible death occurred in DAI KO L929 cells, even when cells were primed with IFN. In contrast, DAI KO L929 cells were sensitive to death induced by TNFα and zVAD, which progresses through RIPK1 activation, but not through activation of DAI (t-test, p-values from $7.9x10^{-5}$ to 0.028). Additionally, MLKL phosphorylation (Fig. 10A) and trimerization (Fig. 10B) were inhibited in arsenite-treated DAI KO L929 cells, but not in cells treated with TNFα and zVAD. Collectively, this data demonstrated that arsenite-induced necroptosis is dependent on DAI.

DAI and RIPK3 form a macromolecular complex following arsenite treatment of IFN-primed L929 cells. Necroptosis is executed by a complex referred to as the necrosome (125). Necrosomes comprise RIPK3 and one of the other proteins containing the RHIM domain: RIPK1, TRIF, or DAI (72, 75, 112, 116). As arsenite-induced necroptosis is dependent on DAI, we asked whether we could detect necrosomes containing DAI and RIP3. To do this, we treated cells with a cell-permeant disulfide-containing chemical crosslinker, DSP. DSP was added to the cells at 2 hours following

arsenite treatment in order to covalently bind proteins which were in a complex with each other at the time of crosslinker addition. To visualize cross-linked proteins, cell lysates were run on a non-reducing gel. We were able to detect DAI and RIPK3 in macromolecular complexes in cells treated with arsenite and IFN (Fig. 11, lane 4), but not in cells treated with arsenite (lane 3) or IFN alone (lane 2). This data is consistent with previous findings demonstrating that RIPK1-activated RIPK3 polymerizes, forming a macromolecular complex (the necrosome) with multiple copies of RIPK3 molecules (60).

DAI interacts with RIPK3 during arsenite-induced necroptosis. Even though DAI and RIPK3 both formed a complex that localized in the same place on the immunoblot gel, we cannot confirm with that data whether DAI and RIPK3 physically interact with each other. As direct interaction between RIPK3 and another protein containing the RHIM domain is required for activation of RIPK3 (72, 75, 112, 116), we performed co-immunoprecipitation (co-IP) to identify direct interaction between DAI and RIPK3. To this purpose, IFN-primed L929 cells were lysed early following arsenite treatment (2 hours), and co-IP with antibody specific for DAI was performed.
As seen in Fig. 12A, we were able to detect RIPK3 in the DAI-immune precipitate only in IFN-primed cells treated with arsenite (lane 4), indicating direct DAI and RIPK3 interaction in arsenite-treated cells. As expected, when cells were treated with only arsenite (no IFN) or with only IFN (no arsenite), RIPK3 was not pulled down with the DAI-specific antibody (lanes 2 and 3). Altogether, this data demonstrated that DAI and RIPK3 interact in arsenite-treated cells undergoing necroptosis.

DAI localizes to stress granules during arsenite-induced necroptosis. When cells are subjected to arsenite, oxidative stress is induced, leading to activation of one of the four stress-activated protein kinases, the heme-regulated inhibitor, or HRI (97). HRI activation leads to phosphorylation of the eukaryotic translation initiation factor, eIF2α. This results in shutting off the translation of the housekeeping genes, and prevention of formation of pre-initiation complexes in the cytoplasm (2). Such complexes are organized into distinct cytoplasmic stress granules. Stress granules are formed by recruitment of the naked untranslated mRNAs by the RNA-binding proteins: TIAR, TIA-1, and G3BP1 (99-101).

To ask if DAI and RIPK3 are being recruited to arsenite-induced stress granules, we performed a co-immunoprecipitation experiment, pulling down with antibodies specific for DAI in order to isolate DAI and associated proteins in conditions of arsenite-induced necroptosis. After releasing the protein complexes from the resin, we performed an immunoblot for G3BP1, one of the canonical stress granule proteins. Induction of DAI alone, following treatment with IFN, did not result in substantial DAI-G3BP1 complex formation (Fig. 12A, lane 2). We observed G3BP1 being pulled down together with DAI only in conditions of arsenite-induced necroptosis (arsenite treatment of IFN-primed cells) (lane 4), demonstrating that DAI interacts with G3BP1 only during arsenite-induced necroptosis.

This data suggests that DAI localizes to stress granules during necroptosis following arsenite treatment. To further demonstrate this, we performed immunofluorescence experiments. Cells were treated with arsenite and immunofluorescence performed 1 hour later. G3BP1 was disbursed throughout the cell in

untreated cells (Fig. 3B, mock). IFN induced DAI expression that was distributed throughout the cytoplasm, with concentration in a perinuclear localization (Fig. 12B, IFN). Treatment of L929 cells with sodium arsenite led to G3BP1 being recruited into cytoplasmic punctate structures typical of stress granules (Fig. 12B, Arsenite). Finally, combined treatment of L929 cells with IFN and arsenite, and hence induction of necroptosis, resulted in DAI localizing into punctate structures that colocalized entirely with the stress granules (G3BP1 staining). These results indicate that during arsenite-induced necroptosis, DAI localizes into cytoplasmic stress granules.

RIPK3 localizes to stress granules only in the presence of DAI. The results presented so far have demonstrated that during arsenite-induced necroptosis: 1) DAI interacts with RIPK3, which is an established manner of RIPK3 activation (83, 117), and 2) DAI localizes to stress granules. Next, we wanted to ask whether a DAI-RIPK3 necrosome is assembled in stress granules.

We started testing our hypothesis by performing co-immunoprecipitation with antibody specific to G3BP1, the stress granule marker protein (99). DAI co-precipitated with G3BP only in IFN-primed L929 cells treated with arsenite (Fig. 13A, left panel, lane 4), consistent with the above data, demonstrating localization of DAI into stress granules during arsenite-induced necroptosis. Furthermore, RIPK3 was pulled down with G3BP1 antibody in IFN-primed L929 cells treated with arsenite (lane 4), but not in cells that had not been primed with IFN (lane 3). This data implies that DAI needs to be present in the stress granules prior to RIPK3 recruitment to stress granules.

To confirm our predictions of DAI recruiting RIPK3 to stress granules, we performed the same co-immunoprecipitation experiment in DAI KO L929 cells. The

results show that in the absence of DAI, RIPK3 does not migrate to stress granules, even in IFN-primed L929 cells following arsenite treatment (Fig. 13A, right panel, lane 8).

Necrosomes form only after DAI has localized to stress granules. To further demonstrate formation of DAI-RIPK3 necrosomes on stress granules, we performed DSP crosslinking, treating cells with DSP 2 hours following arsenite treatment. G3BP1 formed macromolecular complexes in cells treated with arsenite (Fig. 13B, left panel), regardless of whether the cells were primed with IFN (lane 4) or not (lane 3). As formation of granules requires only arsenite treatment and no IFN (Fig. 12B, Ars), we believe that these complexes represent stress granules. DAI and RIPK3 formed large complexes only under conditions of arsenite-induced necroptosis (Fig. 13B, left panel, lane 4). As IFN treatment is required for DAI expression in L929 cells (Fig. 12B, IFN), this data suggested that DAI recruits RIPK3 to stress granules where the DAI-RIPK3 necrosome is formed.

To confirm that formation of necrosomes is lost in the absence of DAI in stress granules, the same DSP crosslinking experiment was performed in DAI KO L929 cells. Similar to what was seen in wild-type L929 cells, G3BP1 formed macromolecular complexes (stress granules) in DAI-deficient cells following arsenite treatment (Fig. 13B, right panel, lanes 7 and 8). However, RIPK3 was not found in a macromolecular complex in IFN-primed cells treated with arsenite when DAI was absent (lane 8).

Altogether, our co-immunoprecipitation and DSP crosslinking data demonstrate that following arsenite treatment, necrosomes are assembled on G3BP1-containing stress granules via recruitment of RIPK3 to stress granules by DAI.

Arsenite-induced DAI-mediated death is inhibited in TIA-1 KO MEFs. We demonstrated that DAI and RIPK3 localize to stress granules where they form a necrosome (Figs. 12 and 13), which leads to execution of necroptosis (Figs. 6 through 8). Because stress granules appeared to play a role in arsenite-induced DAI-mediated necroptosis, we inquired whether stress granules are in fact required for necroptosis.

To investigate the importance of granules for necroptosis, we utilized MEF cells lacking one of the crucial stress granules proteins, TIA-1 (TIA-1 KO MEF cells). These cells have been shown to have a decreased ability to form stress granules following arsenite treatment compared to the wild-type MEF cells (100).

We performed a viability assay to investigate if deletion of TIA-1 would have an effect on death levels caused by arsenite. Arsenite treatment alone did not lead to significant loss of cell viability (Fig. 15), whether in wild-type or TIA-1-deficient MEF cells. Arsenite treatment of IFN-primed wild-type MEF cells (which induces expression of DAI, Fig. 14), led to a substantial amount of death (t-test, $p=0.0048$). This death was RIPK3-dependent as cell viability was rescued by the RIPK3 inhibitor, GSK872 (t-test, $p=4.3x10^{-4}$). Interestingly, when the same assay was performed in TIA-1 KO MEF cells, arsenite treatment of these cells did not cause death, even when the cells were primed with IFN (t-test, $p=4.2x10^{-4}$). Thus, DAI- and RIPK3-dependent cell death induced by arsenite was completely rescued in cells with reduced ability to form stress granules. This data demonstrates that stress granules are required for arsenite-induced death.

To further identify the arsenite-induced death in MEF cells, we looked at the phosphorylation levels of MLKL as well as MLKL trimerization. We detected phosphorylated MLKL (Fig. 16A, left panel) and trimerized MLKL (Fig. 16B, left panel)

in IFN-primed wild-type MEF cells following arsenite treatment, identifying the arsenite-induced death as necroptosis. However, there was little phosphorylated MLKL present in IFN-primed TIA-1-deficient MEF cells after arsenite treatment (Fig. 16A, right panel), further demonstrating arsenite-induced necroptosis is dependent on stress granules. Similarly, we did not detect any MLKL trimerization in TIA-1 KO MEF cells (Fig. 16B, right panel).

This data shows that formation of stress granules is required for arsenite-induced necroptosis.

Arsenite induces stress granule-dependent necroptosis in transfected U2OS cells. To confirm that dependence of necroptosis on stress granules is applicable to human cells, we utilized human bone osteosarcoma epithelial cell line, U2OS. These cells are DAI- and RIPK3-defficient and therefore unable to undergo necroptosis (77, 126, 127). We transfected U2OS cells with plasmids expressing human DAI and human RIPK3 to ask if we can activate arsenite-induced necroptosis by providing DAI and RIPK3 ectopically. When the cells were transfected with DAI alone or RIPK3 alone, little death was observed following arsenite treatment (Fig. 17). Transfection of U2OS cells with both DAI and RIPK3 rendered the cells susceptible to arsenite-induced death (t-test, $p=1.6x10^{-5}$).

Subsequently, we wanted to test whether this DAI- and RIPK3-mediated death was dependent on formation of stress granules. To this purpose, we performed the same viability assay in U2OS cells deficient in stress granule proteins G3BP1 and G3BP2. G3BP1/2 KO U2OS cells are unable to form granules under a wide range of conditions, including following arsenite treatment (99). Arsenite treatment of cells transfected with

DAI alone or RIPK3 alone did not result in significant death, consistent with what was observed in wild-type U2OS cells (Fig. 17). Nonetheless, in contrast to wild-type U2OS cells, G3BP1/2 KO U2OS cells were resistant to arsenite-induced death when transfected with both DAI and RIPK3 (t-test, $p=6.5x10^{-5}$), indicating that formation of stress granules is required for arsenite-induced necroptosis in human cells.

DISCUSSION

Oxygen free radicals are produced in the human body through physiological processes, primarily as result of aerobic metabolism (128-131). Antioxidant systems prevent oxidative damage to the body that results from activity of reactive oxygen species (ROS). Oxidative stress leads to overproduction of free radicals, which can damage biomolecules (lipids, proteins, nucleic acids), causing inflammation and tissue damage, and eventually leading to aging and many chronic diseases: Alzheimer's disease, Parkinson's disease, diabetes, cancer, cardiovascular diseases, stroke, septic shock, rheumatoid arthritis, and atherosclerosis [reviewed in (132)].

In this study, we investigated the effects of oxidative stress on the cell. It is known that cellular stress can result in apoptotic cell death (104). We induced oxidative stress with the canonical oxidative stress inducer, sodium arsenite (97), and investigated the activated cell death pathway. Arsenite treatment led to induction of rapid cell death in IFN-primed murine L929 cells (Fig. 6). The death was observed only in IFN-stimulated cells, indicating that an IFN-inducible protein is involved in the pathway. This death was characterized by dependence on the protein kinase RIPK3 as it was mitigated by the RIPK3 inhibitor, GSK872 (Fig. 6). Presence of the phosphorylated form of MLKL (Fig. 7A) as well as formation of MLKL trimers (Fig. 7B) was detected, identifying the arsenite-induced death as necroptosis.

Three RHIM-containing proteins can lead to activation of RIPK3: TRIF, acting downstream of TLR3 and 4; RIPK1, acting downstream of death receptors; and DAI, which can sense Z-form nucleic acid. Since TLR3 and 4 are primarily expressed in

immune cells, we thought it unlikely that TRIF was leading to activation of RIPK3 in response to arsenite treatment. Arsenite-induced cell death was not inhibited by treatment with GSK963 which effectively inhibits RIPK1-mediated cell death, and in fact inhibited cell death induced by treatment with TNFα+zVAD. This suggested that DAI might be responsible for activation of RIPK3 in response to treatment with arsenite, which is consistent with the IFN inducibility of DAI in L929 cells, and the need for IFN treatment to induce necroptotic cell death in response to treatment with arsenite. Using DAI KO L929 cells, we demonstrated that arsenite-induced necroptosis is in fact DAI dependent (Figs. 9 and 10). Furthermore, DAI localizes to G3BP1-containing stress granules (Fig. 12) where it forms a necrosome with RIPK3 (Fig. 13). In TIA-1 KO MEF cells, arsenite did not induce necroptosis (Fig. 15) and did not lead to MLKL phosphorylation and trimerization (Fig. 16), showing that stress granules are required for necroptosis. Lack of necroptosis following arsenite treatment was also observed in transfected human U2OS cells deficient in G3BP (Fig. 17). Altogether, our data shows that oxidative stress leads to DAI-dependent necroptosis, which is dependent on formation of stress granules, as depicted in the model in Figure 6.

Necroptosis has been implicated in a variety of diseases, including neurodegenerative diseases (e.g., multiple sclerosis) (119), cancer (133), cardiovascular diseases (134, 135), ethanol-induced liver damage (136), inflammaging (137) as well as viral and bacterial infections [reviewed in (138)]. We have recently shown that expression of pathogenic Tau leads to RIPK3-dependent MLKL phosphorylation and neuronal death (manuscript in preparation). Interestingly, an increased number of stress granules has been reported in brains of Alzheimer's patients (120, 121). Furthermore,

Alzheimer's disease is characterized by IFN-mediated inflammation of the brain (139). As seen in our studies, DAI is an IFN-induced protein. Additionally, we also demonstrated that DAI localizes into stress granules to activate necroptosis. Therefore, it would be interesting to inquire whether DAI might be involved in necroptosis that is responsible for neuron degradation in Alzheimer's disease.

Formation of large complexes by DAI and RIPK3 (Figs. 1D and 4B) is consistent with the fact that RIPK3 forms macromolecular complexes, previously shown upon activation by RIPK1 (60). Furthermore, RIPK1 and RIPK3 have been shown to assemble into filamentous structures exhibiting the characteristics of typical β-amyloids (140). Fibrillar peptide formations are a hallmark of Alzheimer's disease (141, 142), implicating additional potential for DAI-mediated necroptosis to play a role in neurodegenerative diseases.

Production of reactive oxygen species occurs during necroptosis (143) and production of mitochondrial ROS promotes necroptosis (144). Thus, oxidative stress may be the underlying pathway leading to necroptosis in our studies. Oxidation can have detrimental effects on the cellular macromolecules: proteins, lipids, and nucleic acids (128, 130, 131). Oxidation of RNA leads to formation of 8-oxoguanosine from guanosine (145). 8-oxoguanosine has a higher propensity to adapt an anti configuration, as opposed to the syn configuration found for most bases in nucleic acid. Since purines in Z form nucleic acid adopt an anti configuration, oxidation of RNA may sensitize it to flip into a Z configuration. 8-oxoguanosine has been detected following arsenite treatment of cells (146). Z-form nucleic acids (Z-NAs) in the cytoplasm are normally organized into cytoplasmic granules along with all known ZNA-binding proteins (118). In fact, the

presence of a ZBD is sufficient to localize a protein into stress granules. DAI contains two ZDB domains and has been previously shown to localize to stress granules (82). Our hypothesis is that oxidative stress leads to formation of 8-oxoguanosine, and hence Z-RNA, that localizes to stress granules where it is bound by the DAI Zα domain, leading to activation of RIPK3, phosphorylation of MLKL and necroptotic cell death (Fig. 6). Finally, it has been shown that 8-oxoguanosine accumulates in DNA and RNA with age (147), and elevated levels of RNA oxidation have been detected in Alzheimer's disease and related neurodegenerative disorders (148). These findings suggest a role for oxidation-induced necroptosis in age-related neurodegenerative diseases.

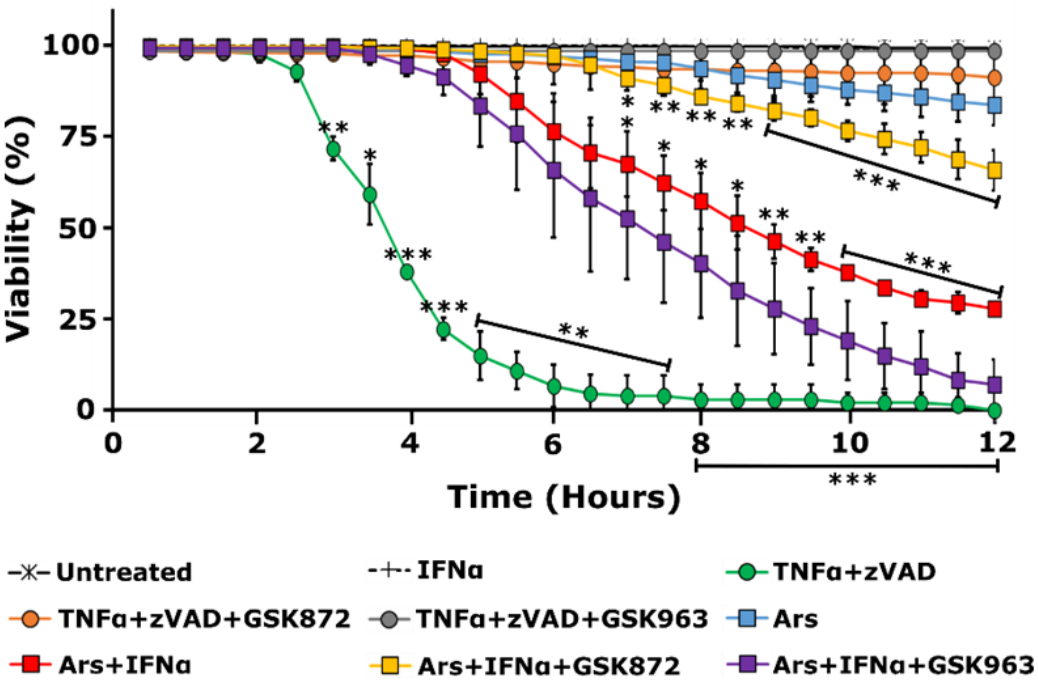

Figure 6. Arsenite induces RIPK3-dependent death in IFN-primed L929 cells.
Viability assay in L929 cells. Mock- or IFNα-primed cells were treated as indicated. Viability was measured in a SYTOX nuclear stain dye exclusion assay. Cellular death is reported as average cell viability (N > 300 cells) with error bars corresponding to ±1 standard deviation (SD). Student's t-test p-values (vs. Untreated): TNFα+zVAD: from $2.5x10^{-9}$ to 0.02; Ars+IFNα: from $2.63x10^{-7}$ to 0.036; (vs. Ars+IFNα): Ars+IFNα+GSK872: from $5.5x10^{-5}$ to 0.022. Complete list of p-values is included in the Appendix, in Table A1.
Ars: arsenite.

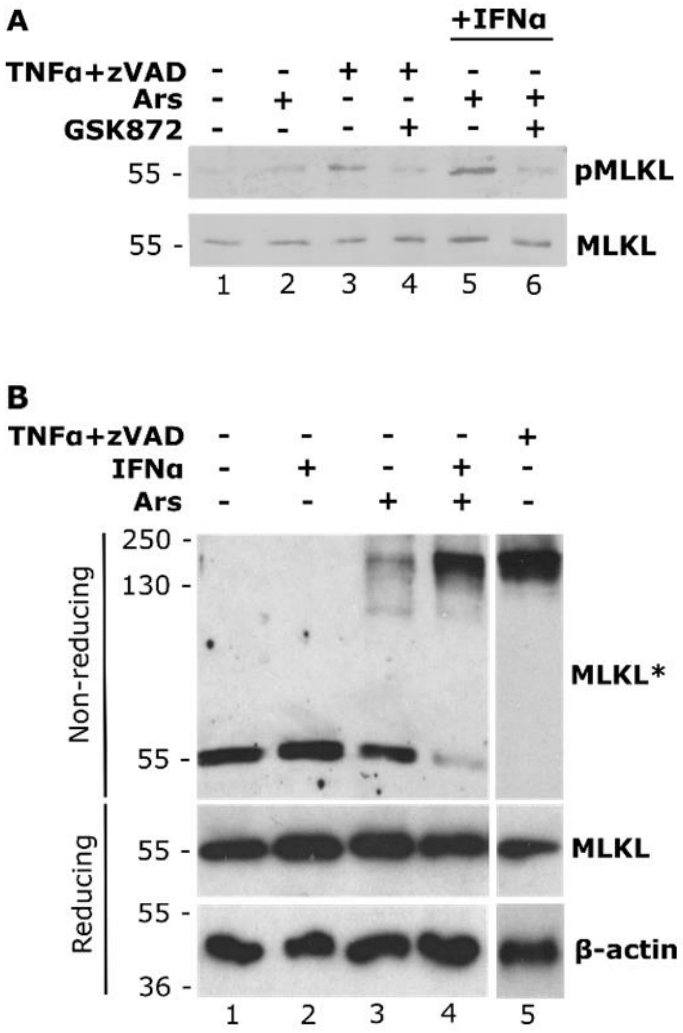

Figure 7. MLKL activation in arsenite-treated L929 cells. (A) Phosphorylation status of MLKL. L929 cells were mock- or IFNα-primed and subsequently treated as indicated. After 5 hours, cells were lysed and subjected to immunoblotting in reduced conditions. (B) Trimerization status of MLKL. Performed as in B, except immunoblotting was conducted in both non-reduced and reduced conditions. *Trimerized MLKL form is depicted (upper band).
Ars: arsenite.

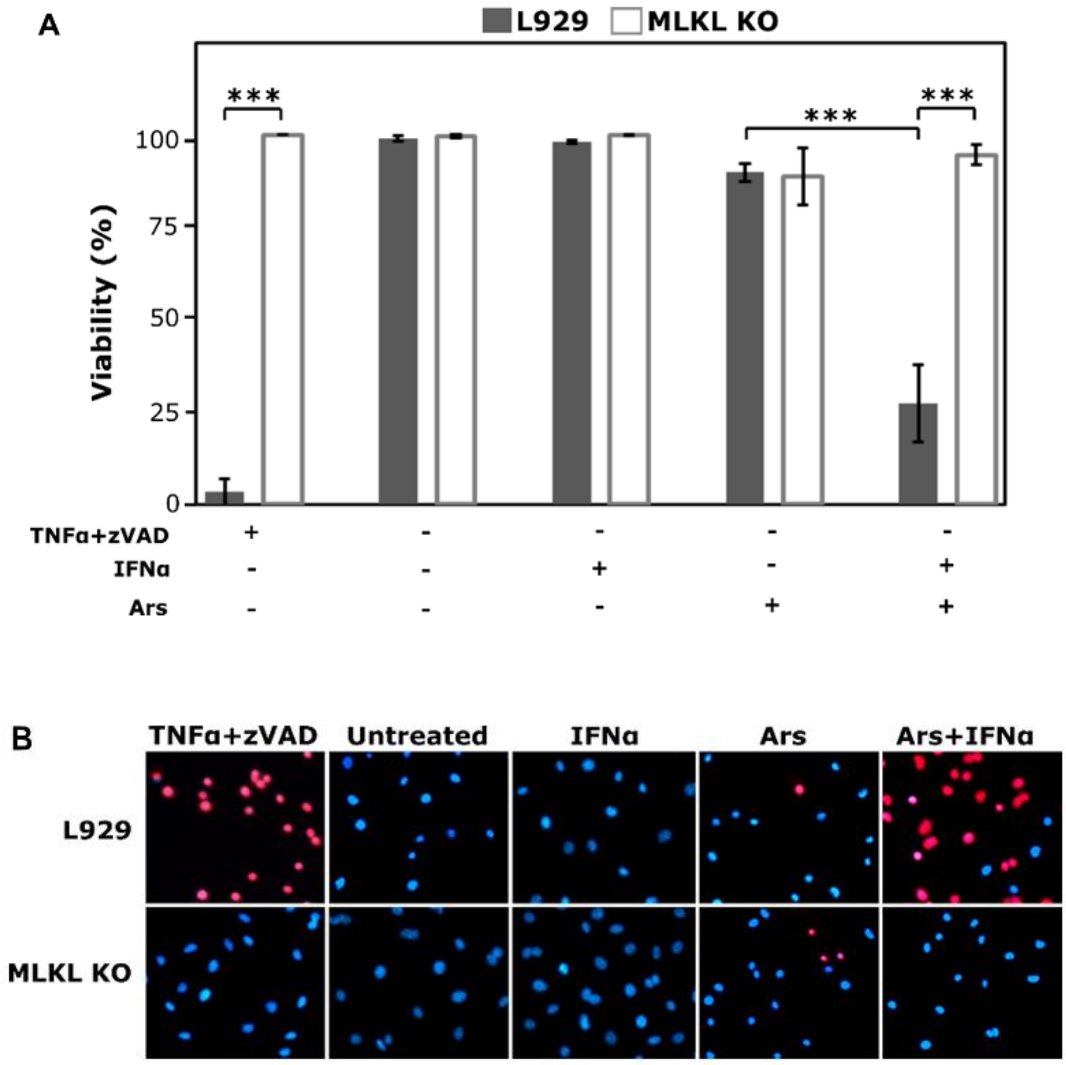

Figure 8. Lack of arsenite-induced death in MLKL-deficient L929 cells (A) Viability assay in L929 cells and MLKL-deficient L929 cells. Mock- or IFNα-primed cells were treated as indicated. Viability was measured in propidium iodide nuclear stain dye exclusion assay. Cellular death is illustrated as mean cell viability (N > 500 cells) ±1 SD. Student's t-test p-values (L929 vs. MLKL KO): TNFα+zVAD: $p=3.5x10^{-4}$, Ars+IFNα: $p=1.6x10^{-5}$; (Ars vs. Ars+IFNα in L929): $p=8.1x10^{-4}$. (B) Microscopy images of the viability assay in (A).
Ars: arsenite.

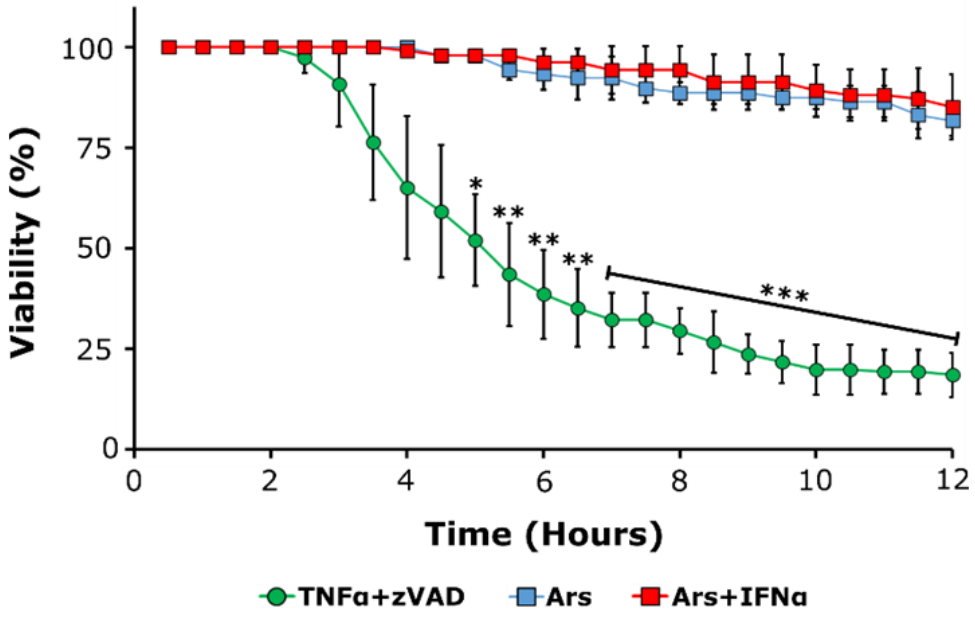

Figure 9. Arsenite does not induce death in DAI-deficient L929 cells. Viability assay in DAI-deficient L929 cells. Cells were treated with TNFα and zVAD, arsenite, or primed with IFN and treated with arsenite. Viability was measured in a SYTOX nuclear stain dye exclusion assay. Cellular death is illustrated as mean cell viability (N > 100 cells) with error bars corresponding to ± 1 SD. Student's t-test p-values: from $7.9x10^{-5}$ to 0.028 when compared to treatment with arsenite alone. Complete list of p-values is included in the Appendix, in Table A2.
Ars: arsenite.

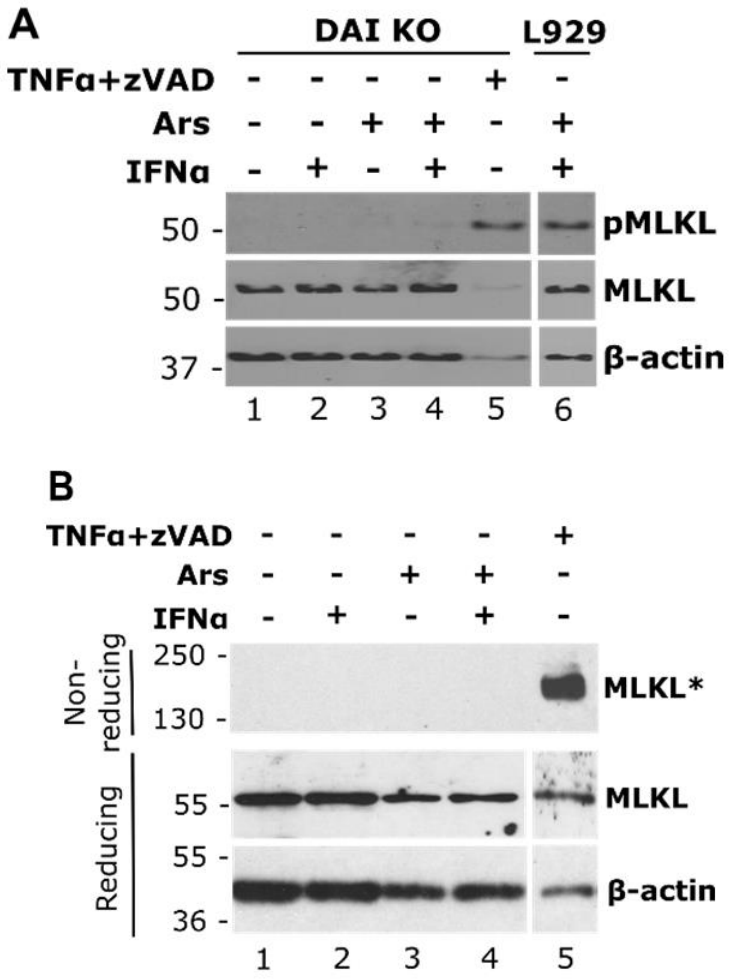

Figure 10. Lack of MLKL activation in DAI-deficient L929 cells. (A) Phosphorylation status of MLKL. DAI KO L929 cells were mock- or IFN-primed and subsequently treated with arsenite or TNFα and zVAD. 5 hours following the treatments, cells were lysed and subjected to immunoblotting in reduced conditions. (B) Trimerization status of MLKL. Performed as in B, except immunoblotting was conducted in both non-reduced and reduced conditions.
*Trimerized MLKL form is depicted.
Ars: arsenite.

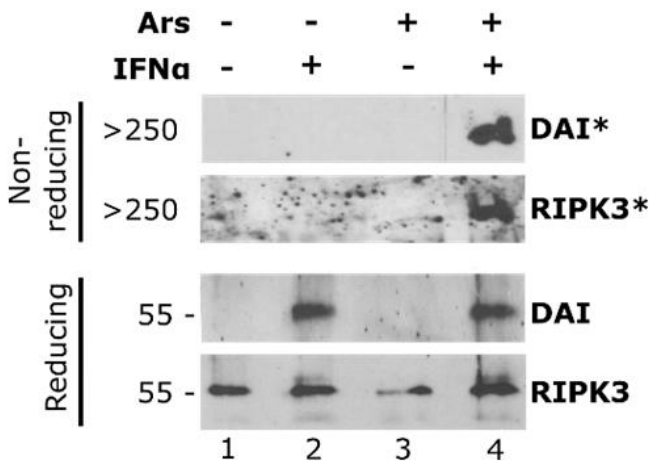

Figure 11. Necrosome formation in arsenite-treated L929 cells. DSP crosslinking. At 2 hours following the indicated treatments, DSP crosslinker was added to L929 cells. Following a 30-min. incubation, the cells were lysed and subjected to immunoblotting in non-reduced and reduced conditions.
*Aggregated DAI and RIPK3 forms are depicted.
Ars: arsenite.

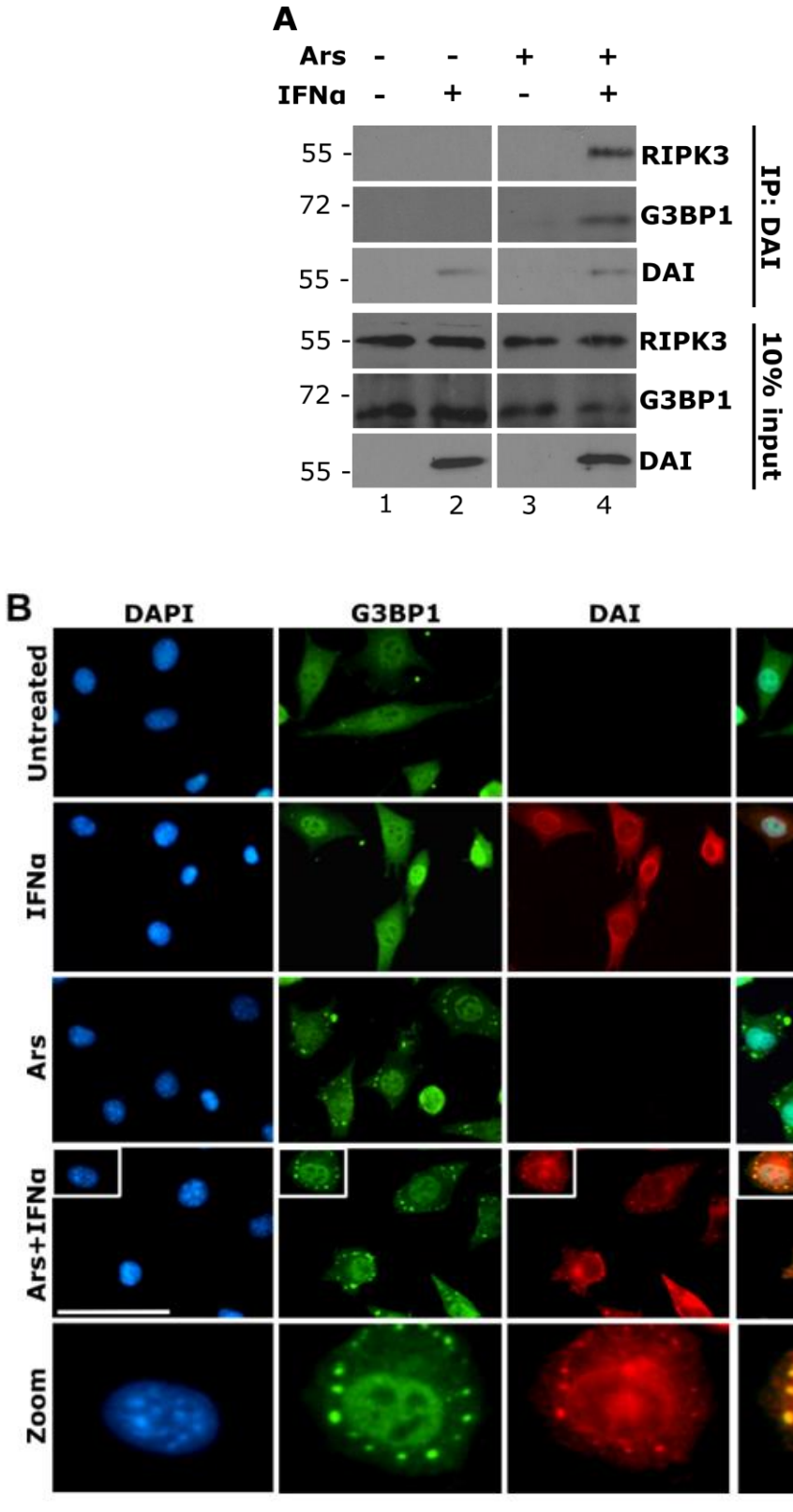
A
Ars - - + +
IFNα - + - +
55 -
72 -
55 -
RIPK3
G3BP1
DAI
IP: DAI
55 -
72 -
55 -
RIPK3
G3BP1
DAI
10% input
1 2 3 4
B
DAPI
G3BP1
DAI
Merge
Untreated
IFNα
Ars
Ars+IFNα
Zoom

Figure 12. DAI localizes to G3BP1-containing stress granules during arsenite-induced necroptosis. (A) Co-immunoprecipitation using DAI-specific antibody. Mock- or IFNα-primed L929 cells were mock or arsenite treated. At 2 hours post-treatment, cells were lysed and subjected to Co-IP using DAI-specific antibody. Immunoblotting followed using the indicated antibodies. (B) Immunofluorescence. Mock- or IFNα-primed L929 cells were mock or arsenite treated. At 1 hour post-treatment, cells were fixed and subjected to immunofluorescence using the indicated antibodies.
Size bar indicates 100 μm. Last row shows an enlargement of the marked cell in the Ars+IFNα row.
Ars: arsenite.

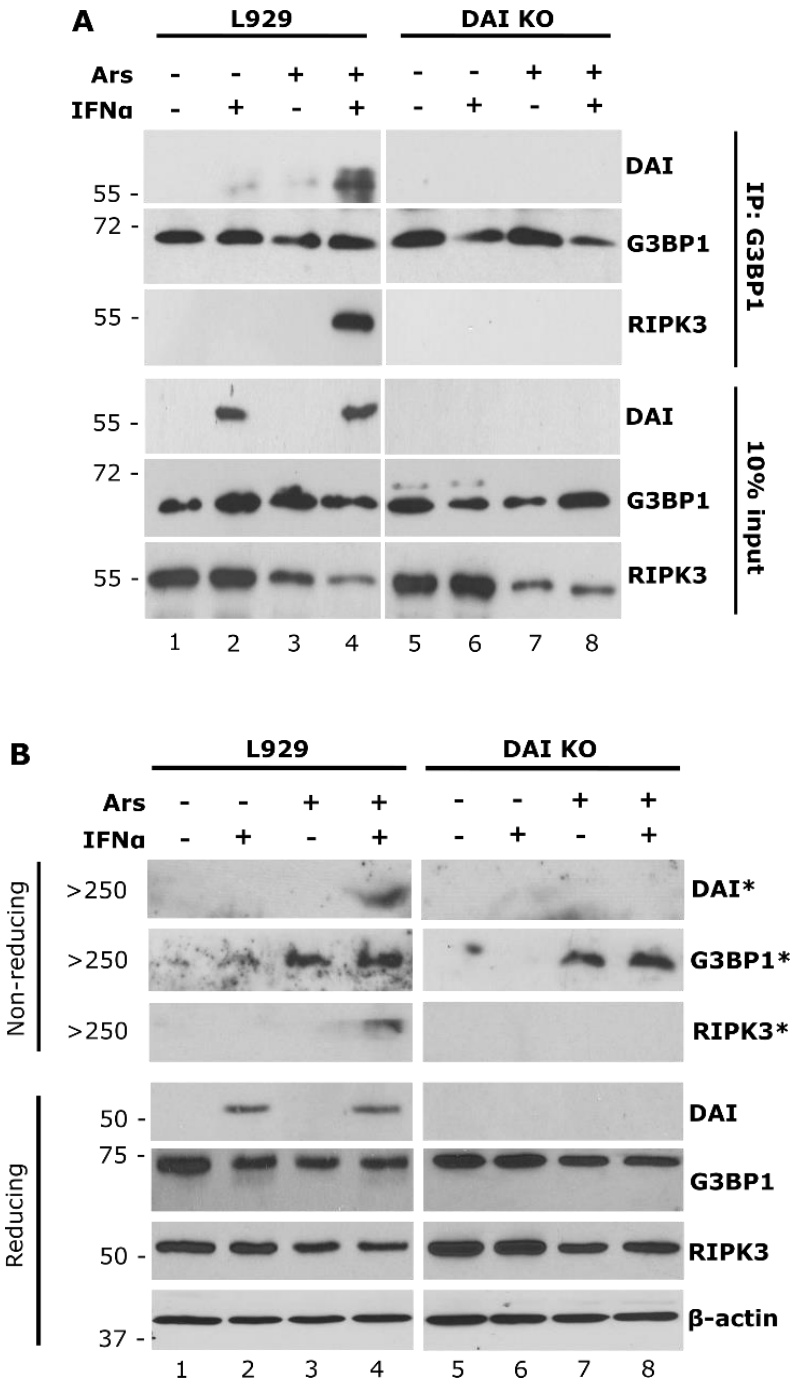
A
L929
DAI KO
Ars
IFNα
DAI
G3BP1
RIPK3
IP: G3BP1
10% input
55
72
1 2 3 4 5 6 7 8
B
Non-reducing
Reducing
>250
50
75
37
DAI*
G3BP1*
RIPK3*
β-actin

Figure. 13. DAI recruits RIPK3 to G3BP1-containing stress granules where they form DAI-RIPK3 necrosomes. (A) Co-immunoprecipitation using a G3BP1-specific antibody. Mock- or IFNα-primed L929 and DAI-deficient L929 cells were mock or arsenite treated. At 2 hours post-treatment, cells were lysed and subjected to Co-IP using a G3BP1-specific antibody. Immunoblotting followed using indicated antibodies. (B) DSP crosslinking. At 2 hours following the indicated treatments, DSP crosslinker was added to L929 and DAI-deficient L929 cells. Following a 30-min. incubation, the cells were lysed and subjected to immunoblotting in non-reduced and reduced conditions. *Aggregated DAI, G3BP1, and RIPK3 forms are depicted.
Ars: arsenite.

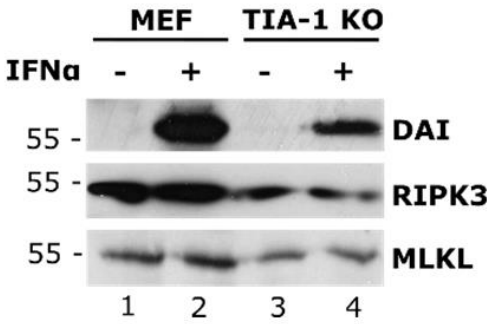

Figure 14. Levels of expression of necroptosis proteins in MEF cells. Mock- or IFNα-primed MEF and TIA-1-deficient MEF cells were lysed and subjected to Western immunoblotting using indicated antibodies. Similar levels of DAI were induced in MEF and TIA-1 KO MEF cells when normalized to RIPK3 and MLKL levels.

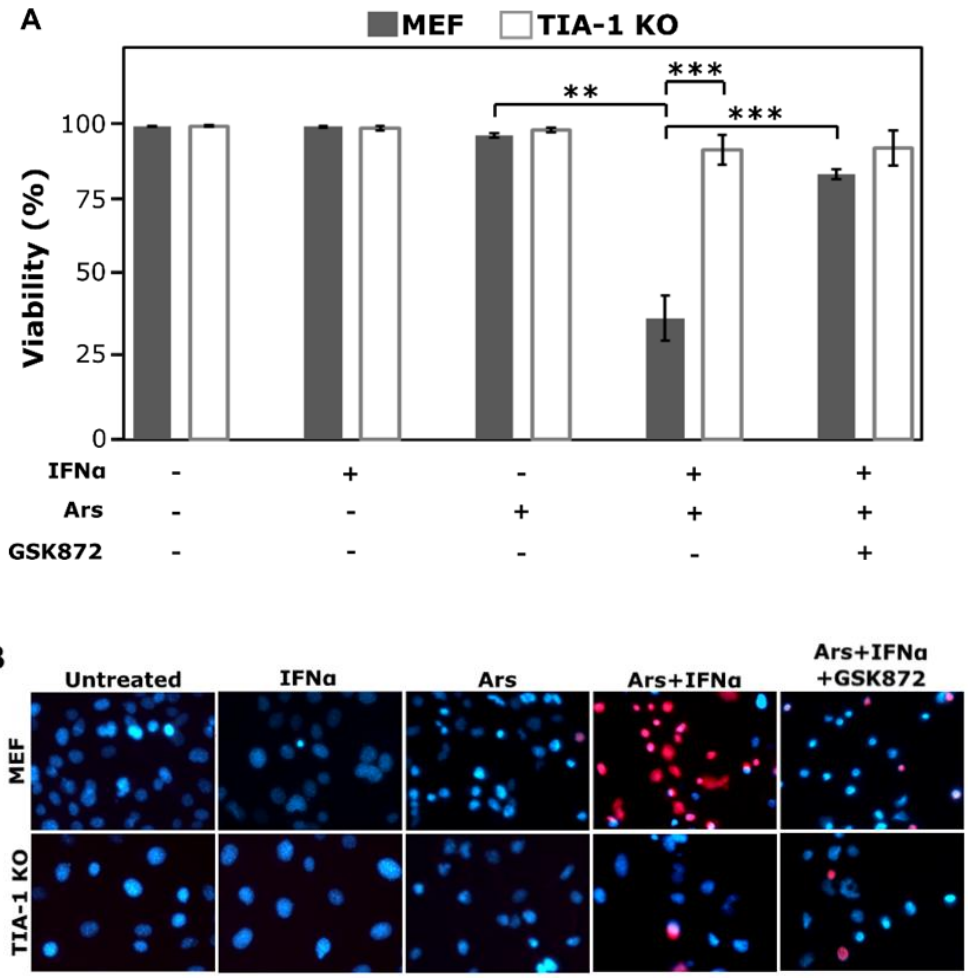

Figure 15. Arsenite-induced death is abolished in absence of granule formation. (A) Viability assay in MEF and TIA-1 KO MEF cells. Mock- or IFNα-primed MEF and TIA-1-deficient MEF underwent the indicated treatments. Cell viability was assessed in a propidium iodine nuclear stain dye exclusion assay 8 hours after the treatments. Cellular death is illustrated as mean cell viability (N > 500 cells) with error bars corresponding to ± 1 SD. Student's t-test p-values: Arsenite vs. Arsenite+IFNα (wild-type MEF), p= 0.0048, Arsenite+IFNα vs. Arsenite+IFNα+GSK'872 (wild-type MEF), p= 4.3×10^{-4}, Arsenite+IFNα in wild-type MEF vs. in TIA-1 KO MEF, p=4.2×10^{-4}. (B) Visualization of the viability assay from (A).

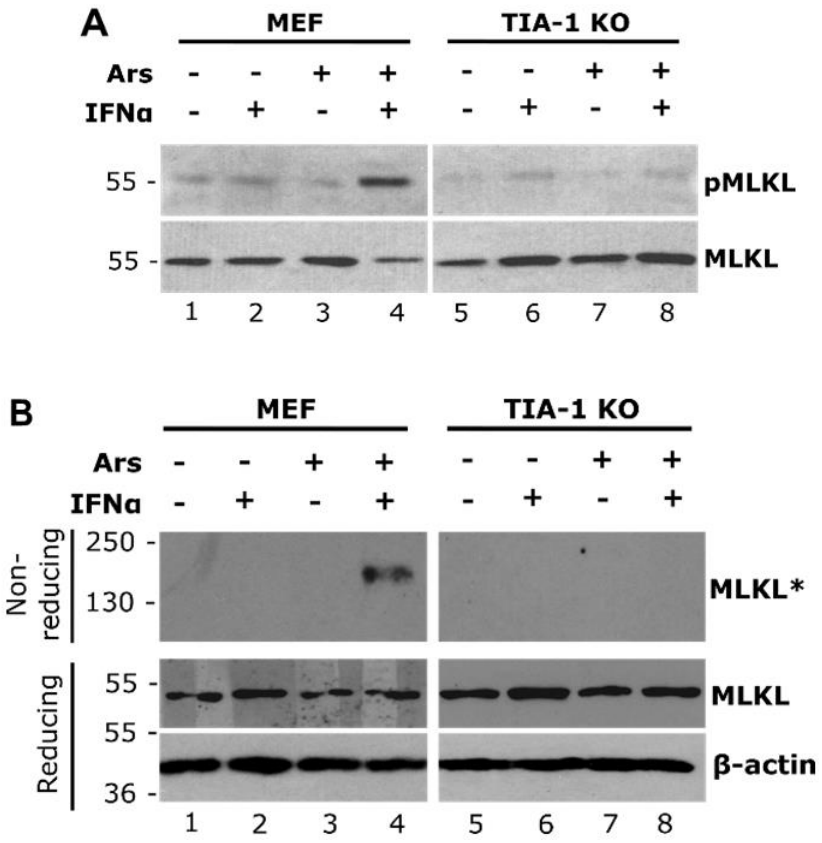

Figure 16. MLKL activation in MEF and TIA-1-deficient MEF cells. (A) Phosphorylation status of MLKL. Mock- or IFNα-primed MEF and TIA-1-deficient MEF cells were mock or arsenite treated. 5 hours following the treatments, cells were lysed and subjected to Western immunoblotting in reduced conditions. (B) Trimerization status of MLKL. Performed as in B, with the exception of immunoblotting being run in both non-reduced and reduced conditions. *Trimerized MLKL form is depicted.

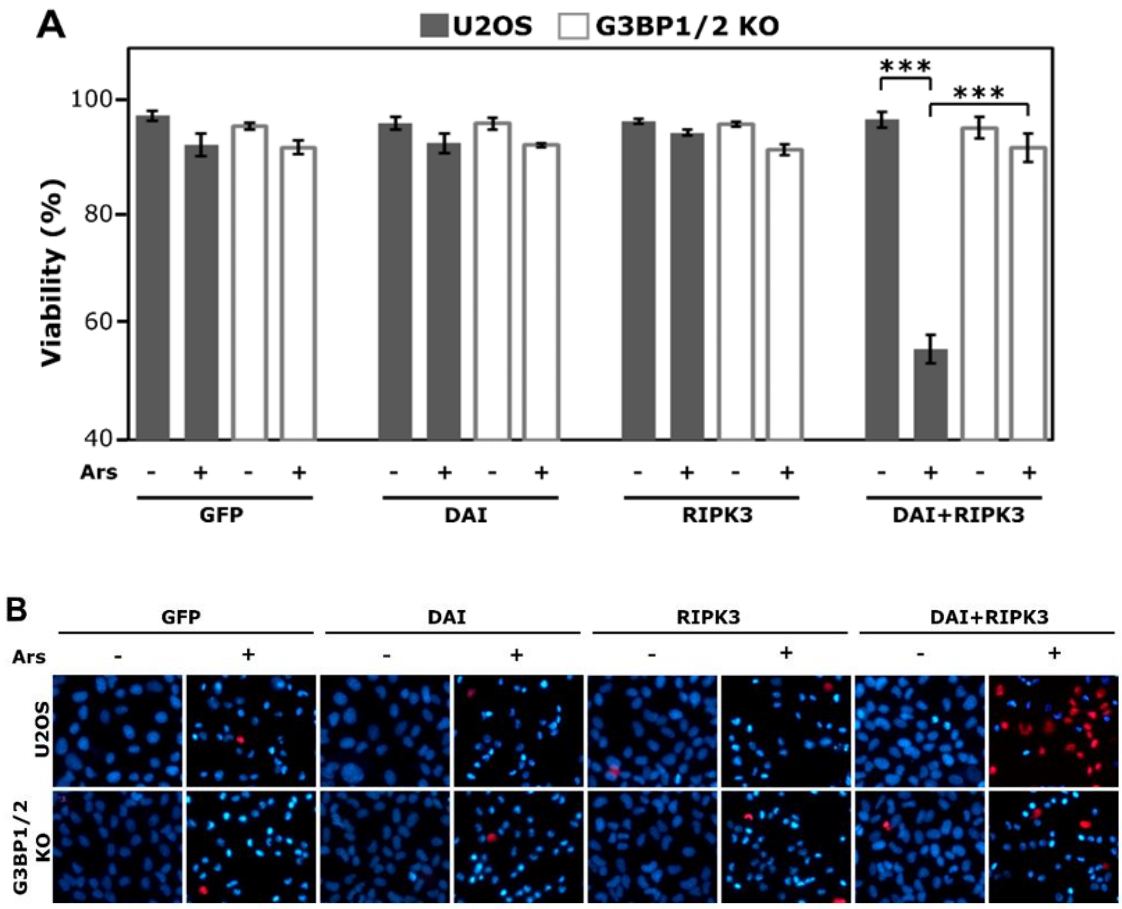

Figure 17. Arsenite-induced death in DAI- and RIPK3-transfected U2OS cells. (A) Viability assay in U2OS cells and G3BP1/2-deficient U2OS cells. The cells were transfected with the indicated plasmids and treated with arsenite 48 hours later. Cell viability was assessed as in A, 15 hours after the treatment. Cellular death is illustrated as mean cell viability (N > 3000 cells) with error bars corresponding to ± 1 SD. Student's t-test p-values (DAI+RIPK3 transfection): mock vs. arsenite, $p=1.2x10^{-4}$, U2OS vs. G3BP1/2 KO U2OS, $p=6.5x10^{-5}$. (B) Visualization of the viability assay from (A). *Ars: arsenite.*

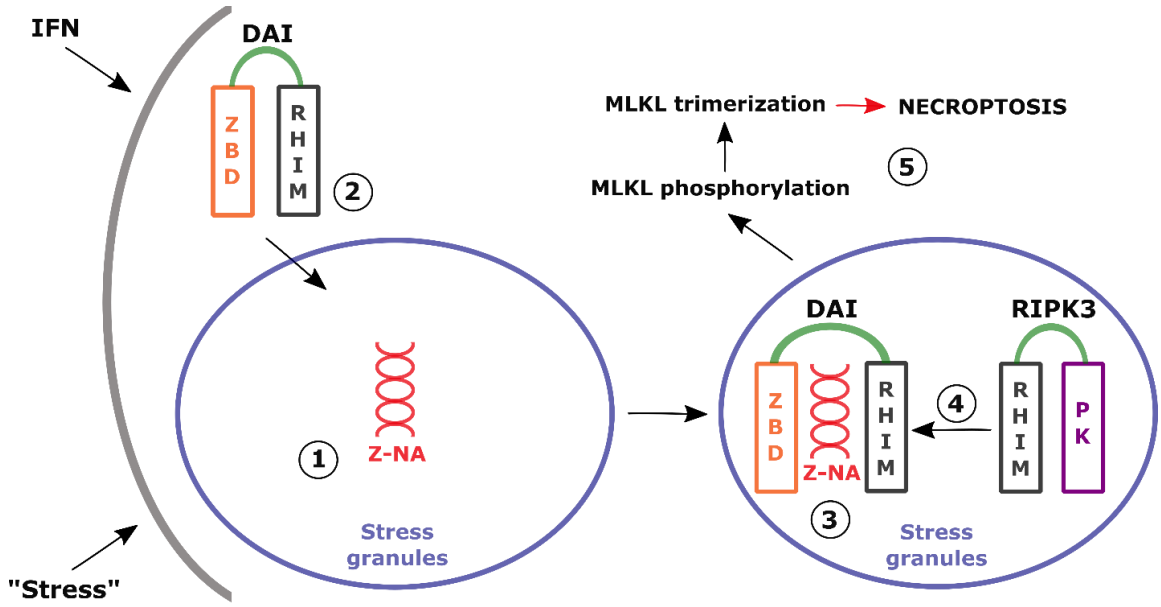

Figure 18. A model of stress-mediated necroptosis. Stress acting upon a cell leads to induction of a necroptosis-activating molecule, presumably a Z-form nucleic acid (Z-NA) (1). Z-NAs are believed to reside in stress granules as all known Z-DNA-binding proteins are known to localize to stress granules (118). When interferon induces DAI expression (2), DAI localizes to stress granules where it binds the Z-NAs. Binding of DAI to the necroptosis-activating Z-NAs leads to a conformational change in DAI, exposing its RHIM domain (3). DAI recruits RIPK3 to stress granules (4) where RHIM-mediated interaction between DAI and RIPK3 leads to formation of the necrosomes. Finally, necroptosis is executed via RIPK3-mediated phosphorylation of MLKL and MLKL trimerization (5).
Z-NA: Z-form nucleic acid; ZBD: Z-DNA-binding domain; PK: protein kinase.

Acknowledgments: We thank Dr. Nancy Kedersha for providing MEF, TIA-1 KO MEF, U2OS, and G3BP1/2 KO U2OS cells. We thank Dr. Karen Kibler for proofreading this manuscript. **Funding:** This work was supported by a grant from the National Institute of Allergy and Infectious Diseases (NIAID) at National Institutes of Health (NIH) (R01AI095394). **Author contributions:** M.S., B. Johnson, and B. Jacobs wrote the manuscript. B. Jacobs provided intellectual oversight and designed experiments. M.S., B. Johnson, M.M., J.W., and C.G. performed experiments and analyzed results. M.S. and B. Johnson performed the statistical analyses. **Competing interests:** Authors declare no competing interests. **Data and materials availability:** All data is available in the main text or the supplementary materials. Sharing of materials described in this analysis will be subject to standard material transfer agreements.

CHAPTER 3

STRESS GRANULES ARE REQUIRED FOR DAI-MEDIATED NECROPTOSIS INHIBITED BY VACCINIA VIRUS IMMUNE EVASION PROTEIN, E3

ABSTRACT

Necroptosis has previously been implicated as the innate immunity pathway activated during MCMV, HSV-1, and IAV infection. In our previous studies, we demonstrated that vaccinia virus (VACV) E3 protein mutant lacking the N-terminal Z-DNA-binding domain (VACV-E3LΔ83N) induced necroptosis independent of death receptors. Currently, we have investigated in detail the mechanism of necroptosis induced during VACV-E3LΔ83N infection. We show that VACV-E3LΔ83N-induced necroptosis is dependent on the cellular Z-DNA-binding protein, DAI. During VACV-E3LΔ83N infection of L929 cells, DAI forms a macromolecular complex (the necrosome) with RIPK3. Necrosome formation takes place only in presence of cytoplasmic stress granules, to which DAI is shown to localize. Formation of stress granules is required for activation of necroptosis in MEF cells infected with VACV-E3LΔ83N. Altogether, our data demonstrates that VACV-E3LΔ83N induces necroptosis in the known DAI-mediated pathway. Furthermore, we present a novel mechanism of stress granule-mediated necroptosis, offering insights into viral infectious cycles and host immunity.

INTRODUCTION

Eukaryotic cells can die as result of mechanical damage (unregulated necrosis) or via a highly controlled signaling pathway of programmed cell death (PCD) (53). Most commonly, PCD (especially apoptosis) occurs to delete unwanted, superfluous or potentially harmful cells, such as those undergoing transformation, and is normal part of eukaryotic development and physiology (40). Apoptosis is also known to clear infected cells, and thereby abrogate virus replication. In evolutionary response, many viruses evolved inhibitors of apoptosis, particularly inhibitors of caspases. In this evolutionary 'arms race' with pathogens, necroptosis may have evolved as an alternative, caspase-independent PCD pathway, and is part of innate immunity against viruses encoding apoptosis inhibitors (149).

The canonical necroptosis pathway is activated via stimulation of a death receptor: tumor necrosis factor (TNF) receptor (TNFR) or Fas/CD95, by their ligands: TNF or FasL, respectively (48, 56). This stimulation leads to recruitment of cIAP1/2, TRADD, TRAF, and receptor-interacting protein kinase 1 (RIPK1) to a membrane-bound protein complex. When RIPK1 is deubiquitinated by CYLD, RIPK1 can interact via RIP homotypic interaction motif (RHIM) with another protein kinase, RIPK3 (55, 57, 58). This interaction, in the presence of a caspase-8 inhibitor, causes activation of RIPK3, leading to its autophosphorylation and oligomerization (59, 60). Subsequently, RIPK3 phosphorylates mixed lineage kinase domain-like, MLKL (61, 62). Aside from RIPK3-mediated phosphorylation at serine 358 (S345 in mice), MLKL is phosphorylated at tyrosine 357 by TAM kinases. This second stage of MLKL phosphorylation results in

MLKL trimerization in the plasma membrane, leading to formation of pores (63-67). Water and sodium can enter the pores, resulting in cell swelling and eventual rupture.

Activation of RIPK3 and thereby necroptosis can also be brought about by RIPK3 interaction with DNA-dependent activator of IFN-regulatory factors, or DAI (also known as ZBP-1 or DLM-1). DAI has been shown to be the sensor of viral infection in cells infected with DNA viruses, like MCMV, and RNA viruses, like IAV. In these cells, DAI recognizes viral RNA and becomes activated, leading to its interaction via RHIM with RIPK3 and execution of necroptosis (74, 76-79).

DAI contains two Z-DNA-binding domains (ZBDs), named Zα and Zβ, and three RHIM-like domains (83). All cellular proteins containing ZBDs have been shown to localize to stress granules – cytoplasmic microdomains of stalled translational complexes and RNA-binding proteins: TIAR, TIA-1, or G3BP1/2 (23, 24, 82). Stress granules form in the cytoplasm in response to cellular stresses, like oxidative stress or viral infection. Since DAI localizes into stress granules and DAI is involved in necroptosis, we asked whether there is a correlation between stress granule formation and activation of necroptosis.

Another protein containing a ZBD is vaccinia virus (VACV) innate immune evasion protein, E3. In our previous studies, we demonstrated that VACV E3 protein mutant lacking the first 83 amino acids (VACV-E3L83N), hence the entire ZBD, induced necroptosis, otherwise inhibited by the wild-type virus (wtVACV) (75). This necroptosis was dependent on DAI as demonstrated in 293T cells, in which ectopic expression of RIPK3 and DAI was required for VACV-E3L83N-induced necroptosis. Furthermore, even though pathogenicity of VACV-E3L83N is attenuated in vivo, it was restored in

DAI-deficient mice (75). The mechanism of DAI-mediated necroptosis induction by VACV-E3L83N has remained enigmatic.

Currently, we show that VACV-E3L83N-induced death present in wild-type L929 cells is inhibited in DAI-deficient L929 cells. VACV-E3L83N infection does not lead to phosphorylation and trimerization of MLKL in DAI knock-out L929 cells. We show interaction of DAI with RIPK3 in cells infected with the mutant virus but not wild-type virus. This interaction results in formation of a macromolecular complex presumed to be the necrosome. Stress granule protein G3BP1 is present in this macromolecular complex and is shown to interact with DAI, indicating DAI localization into stress granules. RIPK3 only forms the necrosome when DAI is present. Finally, VACV-E3LΔ83N-induced necroptosis is completely dependent on stress granule formation as demonstrated by inhibition of death, MLKL phosphorylation, and MLKL trimerization in TIA-1-deficient MEF cells. Necroptosis induction does not depend on PKR, implicating a different mechanism of stress granule formation during vaccinia virus infection.

MATERIALS AND METHODS

Viruses and viral infections. The Western-Reserve (WR) strain of Vaccinia virus (wtVACV) was used in these studies. Creation of the mutant virus lacking the N-terminal 83 amino acids of E3 was described previously (89). Viral infections were performed as described previously (89).

Cells. Murine fibroblast L929 cells were obtained from ATCC. DAI, PKR, and MLKL knock-out L929 cells were created as described below. All L929 cells were cultured in the Minimum Essential Media (MEM) (Corning) supplemented with 5% fetal bovine serum (FBS). Mouse embryonic fibroblasts (MEF) and TIA-1 KO MEF were a kind gift from Dr. Nancy Kedersha (Brigham and Women's Hospital, Inc., Boston) (100). These cells were cultured in Dulbecco's Modification of MEM media (DMEM) (Corning) supplemented with 10% FBS and 2 µM L-Glutamine. All cells were grown at 37^{o}C in atmosphere supplemented with 5% CO_2.

Cell treatments. To determine the requirement for activity of RIP proteins, cells were pretreated with N-(6-(isopropylsulfonyl)quinolin-4-yl)benzo[d]thiazol-5-amine (GSK'872, RIPK3 inhibitor; GlaxoSmithKline) at 3 µM and 2,2-dimethyl-1-(5(S)-phenyl-4,5-dihydro-pyrazol1-yl)-propan-1-one (GSK'963, RIPK1 inhibitor; GlaxoSmithKline) at 5 µM, one hour prior the virus infection, and continuously treated thereafter. For induction of the canonical necroptosis pathway, cells were pretreated with carbobenzoxy-valyl-alanyl-aspartyl-[O-methyl]-fluoromethylketone (Z-VAD-FMK, pan-caspase inhibitor, ApexBio) at 100 µM, one hour prior to treatment with 20 ng/mL mouse tumor necrosis factor alpha (TNF-α, Sigma), and continuously treated thereafter.

Cell viability assay. To assess viability of L929 and MEF cells, the cells were seeded in 12-well CytoOne tissue culture-treated plates (USA Scientific) and pre-treated with 100 U/mL (L929) or 1000 U/mL (MEF) of mouse IFNα (Calbiochem) for 18 h before they were infected with the wtVACV or VACV-E3L83N at MOI of 5. Hoechst 33342 (H3570, Thermo Fisher) and Propidium Iodide Nucleic Acid Stain (P1304MP, Thermo Fisher Scientific) were applied in the overlay media following virus infection. Imaging was performed using EVOS FL auto imaging system (Invitrogen).

MLKL phosphorylation assay. L929 or MEF cells were seeded in a 6-well tissue culture-treated dish (VWR) and pre-treated with 100 U/mL (L929) or 1000 U/mL (MEF) of mouse IFNα (Calbiochem) for 18 h before they were infected with the wtVACV or VACV-E3L83N at MOI of 5. Following 5 hours of infection, the cells were scraped, pelleted, and subsequently lysed in RIPA lysis buffer as described below. Next, lysates were centrifuged in QIAshredder columns (79654, Qiagen) to aid MLKL extraction from the membrane-bound trimer. Western immunoblot analysis (described below) followed using primary antibodies specific for phosphorylated MLKL (mAb, S345, ab196436, abcam) and total MLKL (mAb, D6W1K, Cell Signaling Technology).

MLKL trimerization assay. L929 or MEF cells were seeded, treated, and lysed in RIPA lysis buffer like described for MLKL phosphorylation assay. Western immunoblot analysis was performed like described below with the following exceptions: SDS-PAGE was run in non-reducing conditions and proteins were transferred overnight onto a nitrocellulose membrane at low voltage (30 V). To detect MLKL trimers, primary antibodies specific for total MLKL (mAb, D6W1K, Cell Signaling Technology) were used.

Protein extraction and Western immunoblot analysis. For analysis of protein levels, cells were routinely scraped, pelleted, and lysed in RIPA lysis buffer (150 mM NaCl, 1% Nonidet P-40, 0.5% sodium deoxycholate, 0.1% SDS, 25 mM Tris pH 7.4) by 10-min. incubation on ice. Standard protocol for SDS-PAGE was followed. Proteins were transferred on a nitrocellulose membrane in 10 mM 3-(cyclohexylamino)-1-propane sulfonic acid (CAPS), 20% v/v methanol, pH 11. Antibodies used for immunoblotting were specific for ZBP1/DAI (mAb, Zippy-1, AG-20B-0010-C100, Adipogen), RIP3 (D4G2A, mAb, #95702, Cell Signaling Technology), G3BP1 (pAb, 13057-2-AP, Proteintech). Secondary antibodies used were goat anti-rabbit IgG or goat anti-mouse IgG, both HRP-linked (Cell Signaling Technology). Antibodies specific for β-actin were HRP-linked (sc-47778, Santa Cruz Biotechnology). Immunoreactive bands were visualized by chemiluminescence with SuperSignal West Pico PLUS or Dura Extended Duration substrate (ThermoFisher).

DSP crosslinking. L929 cells were seeded in a 6-well tissue culture-treated dish (VWR) and pre-treated with 100 U/mL of mouse IFNα (Calbiochem) for 18 h before they were infected with the wtVACV or VACV-E3L83N at MOI of 5. Following 2 hours of infection, the cells were scraped, pelleted, and resuspended in phosphate-buffered saline (PBS). To crosslink proteins, , dithiobis(succinimidyl propionate) (Lomant's Reagent, DSP) (22586, ThermoFisher Scientific) was added at 2 mM and the cell suspension was incubated at 25^{o}C for 30 min. Cells were pelleted, resuspended in RIPA lysis buffer (see above) and lysed for 10 min. on ice. Crosslinked protein complexes were subjected to a non-reducing SDS-PAGE, followed by an overnight (16-20 hour) transfer at 30V to a nitrocellulose membrane. Immunoblot protocol followed (described above).

Co-immunoprecipitation. L929 cells were seeded in a 6-well tissue culture-treated dish (VWR) and pre-treated with 100 U/mL of mouse IFNα (Calbiochem) for 18 h before they were infected with the wtVACV or VACV-E3L83N at MOI of 5. Following 2 hours of infection, the cells were scraped, pelleted, resuspended in non-denaturing lysis buffer [10 mM Tris-HCl, pH 7.5, 1 mM DTT, 2 mM MgCl2, 50 mM KCl, 1% Triton X-100, 1X HALT Protease/ Phosphatase Inhibitor Cocktail (78446, ThermoFisher)] and lysed by incubation for 10 min. on ice. Equal volume of Buffer I (20 mM Tris-HCl, pH 7.5, 0.4 mM NaCl, 1 mM DTT, 1 mM EDTA, 1% Triton X-100, 20% glycerol, 2 mM Na3VO4) was added. Lysates were precleared by incubation with Protein A/G PLUS-Agarose (Santa Cruz, sc-2003) for 30 min. at 4ºC with rotation. To capture protein complexes, the lysates were incubated with antibodies specific for ZBP1/DAI (mAb, Zippy-1, AG-20B-0010-C100, Adipogen) or G3BP1 (mAb, 66486-1-Ig, Proteintech) overnight at 4ºC with rotation. Protein complexes were isolated by addition of Protein A/G PLUS-Agarose (Santa Cruz, sc-2003) and incubation for 90 min. at 4ºC with rotation, followed by three 5-min. washes in Buffer I, and pelleting the beads with bound antibodies and protein complexes. Protein complexes were released by addition of 4x Laemmli (250 mM Tris, pH 6.8, 8% SDS, 50% glycerol, 0.04% bromophenol blue) with 50 mM DTT and boiling for 15 min. at 95ºC. Western immunoblot analysis followed like described above with the following exception: to detect DAI, antibody specific for ZBP1/DLM-1/DAI (NBP1- 76854, Novus Biologicals) was used.

Creation of DAI KO, PKR KO, and MLKL KO L929 cells. L929 cells at 50% confluency were infected with Edit-R Lentiviral particles containing Cas9 sgRNA (#VCAS10133, Dharmacon) at MOI 0.3 and incubated at 37°C for 4 hours, after which

L929 growth medium was added. Following 24-hour incubation, the medium was replaced with L929 growth medium containing 8 µg/mL blasticidin. Following selection, expression of Cas9 in cells was confirmed via Western immunoblot (#NBP2-36440L, Novus Biologicals). In order to knock out the DAI gene, Cas9-expressing L929 cells at 50% confluency were infected with a mixture of three Edit-R Lentiviral DAI-specific sgRNAs (sgRNA1: VSGM10144-246664134, sgRNA2: -246664138, sgRNA3: -246664139, Dharmacon) at an MOI of 0.3 and incubated at 37°C for 4 hours, after which L929 growth medium was added. After 24 hours, the medium was replaced with L929 growth medium containing 10 µg/mL puromycin. Following selection, surviving cells were seeded into a 96-well dish with one cell per well and were clonally expanded. The successful knock-out of the DAI gene was confirmed via Western immunoblot analysis (mAb, Zippy-1, AG-20B-0010-C100, Adipogen).

To create PKR KO L929 cells, the same protocol was followed, except a mixture of three Edit-R Lentiviral PKR-specific sgRNAs were used (GSGM11839-246831064 NM_011163-Exon5, GSGM11839-246831065 NM_011163-Exon7, GSGM11839-246831067 NM_011163-Exon4, Dharmacon). The successful knock-out of the PKR gene was confirmed via Western immunoblot analysis (mAb, D6W1K, Cell Signaling Technology).

To create MLKL KO L929 cells, the same protocol was followed, except a single Edit-R Lentiviral MLKL-specific sgRNA was used (VSGM10144-246701514, Dharmacon). The successful knock-out of the MLKL gene was confirmed via Western immunoblot analysis (mAb, D6W1K, Cell Signaling Technology).

Statistical analysis. All data is a representation of at least three independently conducted experiments. Normal-based 95% confidence interval (CI): mean ± 2 SD was used as the basis for statistical analysis. Fisher-Snedecor distribution (F test) with the significance level (α) of 0.05 was used to compare variances between groups. Two-sided Student's t-test (α of 0.05) was performed to assess statistical significance of the observed differences between samples. The t-distribution for equal or unequal variances was used based on the results of the F test.

RESULTS

VACV-E3LΔ83N infection does not induce death in MLKL-deficient L929 cells. Necroptosis is a RIPK3-dependent pathway (56, 73, 77). Activation of RIPK3 leads to its autophosphorylation and phosphorylation of mixed-lineage kinase-like (MLKL) protein (61, 62). As phosphorylation of MLKL has not been associated with any other cellular pathway, presence of the phosphorylated form of MLKL (pMLKL) is indicative of necroptosis. Previously, we showed that infection of IFN-primed L929 cells with VACV-E3LΔ83N led to RIPK3-dependent death as cell viability was rescued in presence of the RIPK3 inhibitor, GSK'872 (75). Furthermore, VACV-E3LΔ83N infection resulted in phosphorylation and trimerization of MLKL, indicative of execution of necroptosis (75). To confirm MLKL-dependence of the death pathway induced by the mutant virus, in this manuscript we knocked out the MLKL gene from L929 cells using CRISPR-Cas9 technology. Consistent with what was seen before, infection of IFN-primed L929 cells with VACV-E3LΔ83N leads to significant amount of death as opposed to infection with wtVACV (Fig. 19). Nonetheless, the death observed in VACV-E3LΔ83N-infected IFN-primed L929 cells was abolished in cells deficient in MLKL (Fig. 20), confirming that VACV-E3LΔ83N-induced death is dependent on MLKL, and therefore can be identified as necroptosis.

VACV-E3LΔ83N infection does not induce death in DAI-deficient L929 cells. We demonstrated before that VACV-E3LΔ83N virus is sensitive to IFN in wild-type L929 cells as opposed to wtVACV, which is fully IFN resistant (75). Furthermore, the VACV-E3LΔ83N induces necroptosis only in IFN-primed L929 cells. To decipher why

death was induced only in cells pretreated with IFN, we looked at protein levels of cell death proteins and discovered that expression of DAI, both at mRNA and protein level, was highly dependent on IFN treatment (75). Furthermore, we demonstrated that in 293T cells, which do not express DAI and RIPK3, VACV-E3LΔ83N induced rapid death only when the cells were transfected with plasmids expressing both DAI and RIPK3, and not RIPK3 alone (75). This data suggested that VACV-E3LΔ83N-induced death might be DAI-dependent.

To investigate dependence on DAI further, in this manuscript we created DAI-deficient L929 cells and performed a viability assay. Infection of DAI KO cells with wtVACV did not lead to death, regardless of IFN pre-treatment status (Fig. 21). Interestingly, infection with VACV-E3LΔ83N did not result in cell death of DAI KO L929 cells either, even in cells that were IFN-primed (Fig. 21). These results are different from what is observed in wild-type L929 cells (Fig. 19). Lack of VACV-E3L83N-induced death in DAI KO L929 cells indicates that cell death induced by the mutant virus is dependent on DAI in wild-type L929 cells.

Treatment of cells with tumor necrosis factor α (TNF-α) in presence of the pan-caspase inhibitor zVAD induces the canonical, death receptor-mediated form of necroptosis, dependent on RIPK1 (56, 57). Treatment of wild-type L929 cells led to rapid cell death (Fig. 19). Similarly, TNF-α and zVAD treatment of L929 cells deficient in DAI resulted in death (Fig. 21), which is consistent with the fact that death receptor-induced necroptosis is dependent on RIPK1, and not DAI.

MLKL is not phosphorylated in DAI-deficient L929 cells following VACV-E3LΔ83N infection. To confirm DAI-dependence of VACV-E3L83N-induced

necroptosis, we investigated the status of MLKL phosphorylation in DAI-deficient cells infected with our viruses. We did not observe MLKL phosphorylation following infection with wtVACV (Fig. 22, right panel). Furthermore, infection with VACV-E3L83N did not result in presence of pMLKL either, even in IFN-primed DAI KO L929 cells. In agreement with our previously published work, infection of wild-type cells with wtVACV did not lead to phosphorylation of MLKL (Fig. 22, left panel). We observed presence of MLKL phosphorylation in IFN-primed wild-type L929 cells following VACV-E3LΔ83N infection. This data indicated that VACV-E3LΔ83N-induced phosphorylation of MLKL is DAI-dependent in L929 cells.

VACV-E3LΔ83N-induced trimerization of MLKL is lost in DAI KO L929 cells. Phosphorylated MLKL is considered the executioner of necroptotic death. In conditions of necroptosis, the phosphorylated form of MLKL localizes into plasma membrane where it trimerizes, leading to formation of pores (68-70). Such puncturing of the plasma membrane leads to ionic imbalance and influx of water into the cells, which results in cellular swelling and eventual rupture (71). There are a few mechanisms of inhibition of trimerization of phosphorylated MLKL (65-67). Therefore, it is not sufficient to demonstrate presence of pMLKL to report on necroptosis induction.

Consistently with our previous studies, infection of IFN-primed L929 cells with VACV-E3LΔ83N results in MLKL phosphorylation and subsequent trimerization (Fig. 22, left panel). wtVACV does not induce trimerization of MLKL, which aligns with the fact that wtVACV did not induce death or phosphorylation of MLKL in these cells. Trimerization of MLKL was also abolished in IFN-primed DAI-deficient L929 cells (Fig. 22, right panel) following infection with the mutant virus, which remains consistent with

lack of death and phosphorylation of MLKL in these cells following infection with VACV-E3LΔ83N virus.

Altogether, this data demonstrated that DAI is required for necroptosis induced by VACV-E3LΔ83N infection of L929 cells.

VACV-E3LΔ83N induces macromolecular complex formation by DAI and RIPK3. We have established that infection of cells with VACV-E3LΔ83N leads to necroptosis dependent on DAI. During DAI-mediated necroptosis, DAI is known to interact with RIPK3, forming a complex referred to as the necrosome (77). In order to investigate if infection of cells with the mutant vaccinia virus results in necrosome formation, we performed DSP crosslinking. When cells were infected with the wild-type virus, no high-molecular-weight complex formation was observed, even though cells were primed with IFN (Fig. 23A). Following VACV-E3LΔ83N infection of L929 cells, formation of a large macromolecular complex was observed. This complex contained both DAI and RIPK3, indicating that infection with VACV-E3LΔ83N leads to formation of a DAI-RIPK3 necrosome.

DAI interacts with RIPK3 in IFN-primed L929 cells infected with VACV-E3LΔ83N but not wtVACV. Presence of a macromolecular complex containing DAI and RIPK3 does not necessarily indicate direct interaction between the two proteins. In order to confirm that DAI directly associates with RIPK3 to form the necrosome, we performed a co-immunoprecipitation assay. Infection of L929 cells with wtVACV did not lead to interaction between DAI and RIPK3, which is consistent with the lack of cell death during wtVACV infection (Fig. 23B). In contrast, DAI interacted with RIPK3 in IFN-primed L929 cells infected with VACV-E3LΔ83N. Altogether, co-

immunoprecipitation and crosslinking data demonstrated DAI-RIPK3 necrosome complex formation in conditions of necroptosis induced by VACV-E3LΔ83N.

DAI localizes to stress granules following infection of IFN-primed L929 cells with VACV-E3LΔ83N. This manuscript demonstrates that necroptosis induced during infection of L929 cells with VACV-E3LΔ83N is dependent on the cellular protein DAI. As a Z-DNA-binding protein, DAI is known to localize to stress granules (82, 118). We asked whether DAI localizes to stress granules in conditions of VACV-E3LΔ83N-induced necroptosis by looking at its interaction with one of the stress granule proteins, G3BP1. We performed a co-immunoprecipitation experiment utilizing a DAI-specific antibody. We observed association of DAI with G3BP1 in IFN-primed L929 cells infected with VACV-E3LΔ83N, which might indicate DAI's localization into stress granules in cells infected with the mutant virus (Fig. 24A). In contrast, DAI did not interact with G3BP1 in cells infected with wtVACV. Furthermore, RIPK3 also co-precipitated with DAI (Fig. 23B). Altogether, this data suggests that in IFN-primed L929 cells infected with VACV-E3LΔ83N, DAI localizes to stress granules where it forms the necrosome with RIPK3 and this leads to activation of necroptosis. Furthermore, these results suggest that localization of these necrosome components to stress granules is a required step of necroptosis induction as infection of cells with wtVACV does not result in DAI-G3BP1 interaction and necroptosis. We investigated this requirement in detail below.

DAI recruits RIPK3 to stress granules during VACV-E3LΔ83N-induced necroptosis. Having demonstrated that DAI and RIPK3 localize to stress granules in conditions of necroptosis induced by VACV-E3LΔ83N, we wanted to investigate

whether DAI is required for localization of RIPK3 into granules. We demonstrated earlier that DAI and RIPK3 form a macromolecular complex in IFN-primed L929 cells infected with the mutant virus (Fig. 23A). When the same assay was performed in DAI-deficient L929 cells, RIPK3 did not form the macromolecular complex seen in wild-type L929 cells (Fig. 24B, right panel). Consistent with our immunoprecipitation data showing DAI localization to stress granules, G3BP1 was part of a macromolecular complex detectable in cells infected with the mutant virus, further confirming that necrosome is assembled in stress granules. Interestingly, in DAI-deficient L929 cells, VACV-E3LΔ83N infection leads to formation of a macromolecular complex containing G3BP1, but not RIPK3, indicative of stress granule formation and requirement of DAI to recruit RIPK3 to the granules to induce necroptosis (Fig. 24B, right panel). Intriguingly, infection of cells with wtVACV does not lead to formation of a macromolecular complex containing G3BP1. This might suggest that wtVACV inhibits granule formation and therefore inhibits necroptosis.

VACV-E3LΔ83N does not induce necroptosis in TIA-1-deficient MEF cells. We have shown so far that following infection of IFN-primed L929 cells with VACV-E3LΔ83N, DAI localizes into stress granules where it recruits RIPK3 to form the necrosome and execute necroptosis. We wanted to ask whether activation of VACV-E3LΔ83N-induced necroptosis is actually dependent on formation of stress granules. We utilized MEF cells deficient in TIA-1 that display a limited ability to form stress granules (23). Similarly to L929 cells, infection of wild-type MEF cells with VACV-E3LΔ83N leads to rapid death when the cells are primed with IFN (Figs. 26A and 26C). This death is dependent on RIPK3 as it is inhibited by RIPK3 inhibitor, GSK'872. wtVACV

infection did not have an effect on MEF cell viability. The VACV-E3LΔ83N-induced death was abolished in TIA-1-deficient MEF cells, indicating that stress granules are required for VACV-E3LΔ83N-mediated induction of RIPK3-dependend death (Figs. 26B and 26C).

To confirm the identity of VACV-E3LΔ83N-induced death in MEF cells, we looked at levels of the phosphorylated form of MLKL. Following VACV-E3LΔ83N infection, MLKL was phosphorylated in IFN-primed wild-type MEF cells, but not in TIA-1 KO cells (Fig. 27). Infection with wtVACV did not lead to phosphorylation of MLKL. Similarly, infection of MEF cells with the mutant virus resulted in trimerization of MLKL (Fig. 27), which was lost when cells were deficient in TIA-1, ultimately demonstrating that VACV-E3LΔ83N-induced necroptosis is dependent on formation of stress granules. wtVACV infection did not result in trimerization of MLKL in TIA-1 KO, consistent with the ability of the virus to inhibit necroptosis.

We have shown that necroptosis is dependent on formation of stress granules, which does not occur during wtVACV infection. Therefore, inhibition of stress granule formation by wtVACV might be the mechanism underlying wtVACV-mediated inhibition of necroptosis.

VACV-E3LΔ83N-induced necroptosis is independent of PKR. Activation of protein kinase dependent on RNA (PKR) is a major mechanism leading to stress granule formation following viral infection (6, 7). We asked whether induction of granule formation during VACV-E3LΔ83N infection results from activation of PKR. To this purpose, we created PKR-deficient L929 cells. Infection of IFN-primed PKR KO L929 cells with VACV-E3LΔ83N resulted in rapid death comparable to death seen in wild-

type L929 cells (Fig. 28). wtVACV infection did not have an effect on the viability of PKR KO cells, just like in wild-type cells. Furthermore, VACV-E3LΔ83N infection led to phosphorylation of MLKL and trimerization of MLKL (Fig. 29), demonstrating that VACV-E3LΔ83N induces necroptosis in absence of PKR. These data indicate that PKR activation is not responsible for granule formation during VACV-E3LΔ83N infection. Furthermore, these results suggest that inhibition of stress granule formation by wtVACV occurs via a mechanism other than inhibition of PKR. The exact mechanism is currently under investigation.

DISCUSSION

In our previous studies, we demonstrated that vaccinia virus is able to inhibit necroptosis (75). Infection with vaccinia virus mutant lacking 83 amino acids at the N terminus of the virus immune evasion protein, E3, led to induction of necroptosis. The pathway was dependent on DAI that had to be transfected into DAI-deficient 293T cells in order for necroptosis to occur following VACV-E3LΔ83N infection. Furthermore, siRNA-mediated knock-down of DAI from L929 cells inhibited the VACV-E3LΔ83N-induced necroptosis (75). In this manuscript, we look closer at the mechanism of DAI-mediated necroptosis induced by the mutant virus and discover dependence of this innate immunity pathway on formation of cellular stress granules.

We confirmed the identity of VACV-E3LΔ83N-induced death as necroptosis as infection with the mutant virus did not lead to death in absence of MLKL (Fig. 20). To confirm DAI-dependence of VACV-E3LΔ83N-induced necroptosis, we created DAI-deficient L929 cells and demonstrated that VACV-E3LΔ83N-induced necroptosis is abolished in this cell line. Infection of these cells with VACV-E3LΔ83N did not lead to death (Fig. 21) or phosphorylation and trimerization of MLKL (Fig. 22). The canonical pathway of necroptosis induced via stimulation of the TNF death receptor and inactivation of caspases with zVAD inhibitor still occurred in these cells as the death receptor-induced necroptosis is independent of DAI (56, 57).

Activation of DAI-dependent necroptosis by viruses has been observed before: infection with influenza A virus (IAV) (an RNA virus) and murine cytomegalovirus (MCMV) (a DNA virus) lead to DAI-mediated necroptosis, during which DAI is known

to interact with RIPK3 following DAI-mediated recognition of virus infection (76-79, 85). We investigated whether infection of cells with VACV-E3LΔ83N would result in DAI-RIPK3 interaction and necrosome formation. Our co-immunoprecipitation data (Fig. 23B) shows that RIPK3 was pulled down with DAI-specific antibody in conditions of necroptosis induced by the mutant virus. No interaction of DAI with RIPK3 was observed in cells infected with wtVACV, indicating that the wild-type virus is able to inhibit formation of the necrosome and therefore we do not observe death in cells infected with wtVACV.

During death receptor-induced necroptosis, the necrosome is comprised of multiple copies of RIPK1 and RIPK3, therefore forming a macromolecular complex (60, 140). It has been unknown whether similar macromolecular complex is formed during DAI-mediated necroptosis. Our data show that DAI and RIPK3 both form a macromolecular complex in IFN-primed L929 cells infected with the mutant virus (Fig. 23A). Consistently with all other observations, no necrosome was formed in cells infected with the wild-type virus.

We showed that G3BP1, a stress granule protein, interacted with DAI, indicating localization of DAI into cellular stress granules in cells infected with VACV-E3LΔ83N, but not wtVACV (Fig. 24A). Furthermore, G3BP1 formed a macromolecular complex similar to the one formed by DAI and RIPK3 during VACV-E3LΔ83N-induced necroptosis (Fig. 24B). Interestingly, the G3BP1 macromolecular complex did not form in cells infected with the wtVACV, implicating lack of stress granule formation in cells infected with the wild-type virus. In fact, wtVACV has been shown to inhibit stress granule formation in infected cells in other studies (150). Because inhibition of SG

formation correlated with lack of necroptosis induction, we next investigated if SGs are required for necroptosis.

We demonstrate that in absence of stress granule formation, VACV-E3LΔ83N was unable to induce necroptosis: infection of TIA-1 KO MEF cells with VACV-E3LΔ83N did not result in death, or phosphorylation and trimerization of MLKL (Figs. 26 and 27). Necroptosis was induced successfully in wild-type MEF cells infected with the mutant virus. This data demonstrated significance of stress granule formation for necroptosis induced by the mutant virus. We began to confirm the significance of stress granule formation for necroptosis using a different cell line. Transfection of human U2OS cells with DAI and RIPK3 resulted in cell death following VACV-E3LΔ83N infection. In contrast, death was inhibited in DAI+RIPK3 transfected G3BP1/2 KO U2OS cells, which are also unable to form granules (data not shown).

Altogether, our data showed that formation of stress granules is required for activation of VACV-E3LΔ83N-induced necroptosis dependent on DAI. DAI contains two Z-NA-binding domains and thereby has been shown to localize to stress granules before (82, 118). The ZBDs of DAI are homologous to the ZBD of vaccinia virus E3. In fact, swapping the Zα domain of E3 with the Zα domain of DAI maintains virus pathogenicity, which is otherwise lost when the domain is missing or mutated (84). This indicates that E3 and DAI may compete for biding to a Z-NA during infection, rendering it possible for wtVACV to inhibit necroptosis induction.

The importance of DAI ZBDs has been demonstrated in other studies. Maelfait et al. (85) showed that mutations of these domains prevented necroptosis induced by MCMV-M45mutRHIM virus, which otherwise occurs with DAI with functional ZBDs.

Moreover, knock-in mice expressing DAI with mutations in its ZBDs (Zbp1Za1a2 / Za1a2) failed to efficiently clear MCMV-M45mutRHIM infection, unlike wild-type mice. In another study, DAI was shown to recognize viral Z-RNA during IAV infection, which was required for induction of necroptosis (78, 79). The mechanism of DAI-mediated recognition of vaccinia virus infection is currently under investigation, including deciphering which of the two ZBDs of DAI (Zα or Zβ) plays a role in VACV-E3LΔ83N-induced necroptosis.

Our results suggest that the ability of wtVACV to inhibit stress granule formation may be the underlying mechanism of necroptosis inhibition by the wild-type virus. Vaccinia virus produces double-stranded RNA (dsRNA) during its replication cycle as result of overlapping bidirectional transcription from both strands of the double-stranded genomic DNA (87). dsRNA is typically recognized by the cellular RNA-dependent protein kinase, PKR, which inhibits cellular translation by phosphorylating eIF2α, resulting in stress granule formation (3, 6, 7). The C terminus of vaccinia virus E3 protein contains a dsRNA-binding domain, which masks the presence of viral dsRNA and inhibits activation of PKR. Nonetheless, although VACV-E3LΔ83N contains an intact dsRBD (Fig. 5), it has been shown to induce PKR and eIF2α phosphorylation in HeLa cells (151). To test if the stress granule formation during VACV-E3LΔ83N infection results from the inability of this ZBD mutant to inhibit PKR, we performed necroptosis assays in PKR KO L929 cells. Surprisingly, infection of these cells with the mutant virus led to loss of cell viability and phosphorylation and trimerization of MLKL, characteristic of necroptosis (Figs. 28 and 29). This data showed that VACV-E3LΔ83N-induced

necroptosis is independent of PKR and that wtVACV blocks the stress granule formation in a mechanism different from inhibition of PKR.

Poxvirus infection results in induction of oxidative stress (152). Oxidative stress leads to formation of Z-NAs (145, 146), which may accumulate in cells infected with vaccinia virus. wtVACV E3 contains the intact ZBD that can bind to Z-NAs (Fig. 5), which might inhibit SG formation (84). In contrast, the truncated E3 protein of VACV-E3LΔ83N, lacking the entire ZBD, is unable to bind to Z-NA and therefore to block SG assembly. Once SGs are formed, DAI can be recruited by the residing Z-NA. DAI will then recruit RIPK3 to SGs, where the two proteins will form the necrosome, which will then execute necroptosis. Significance of oxidative stress for VACV-E3LΔ83N-induced necroptosis is currently under investigation.

Our studies shed a light on how viruses counteract necroptosis and help us better understand the viral mechanisms of inhibition of host innate immunity responses. We believe that this knowledge will contribute to more effective drug development and vaccine design. These VACV studies also complement the oxidative stress data (Chapter 2), further strengthening the notion of necroptosis dependence on stress granules under various scenarios of cellular stress.

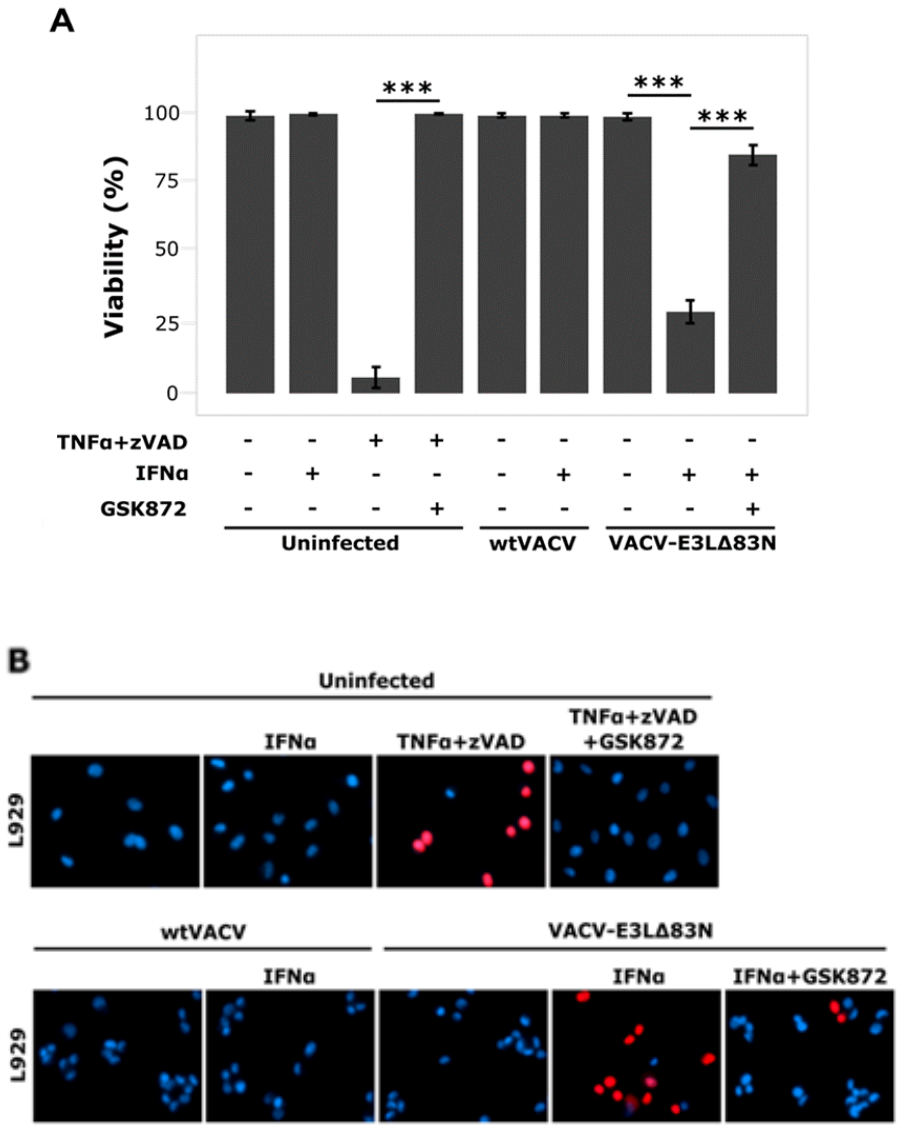

Figure 19. VACV-E3LΔ83N induces RIPK3-dependent death in IFN-primed L929 cells. (A) Viability assay in L929 cells. Mock- or IFNα-primed cells were treated as indicated or infected with wtVACV or VACV-E3LΔ83N. Viability was measured in propidium iodide nuclear stain dye exclusion assay 6 hours later. Cellular death is illustrated as mean cell viability (N > 500 cells) ±1 SD. Student's t-test p-values: TNFα+zVAD vs. TNFα+zVAD+GSK'872: $p=5.1x10^{-4}$, VACV-E3LΔ83N vs. VACV-E3LΔ83N +IFN: $p=9.4x10^{-6}$, VACV-E3LΔ83N +IFN vs. VACV-E3LΔ83N +IFN+GSK'872: $p= 5.9x10^{-5}$. (B) Microscopy images of the viability assay in (A).

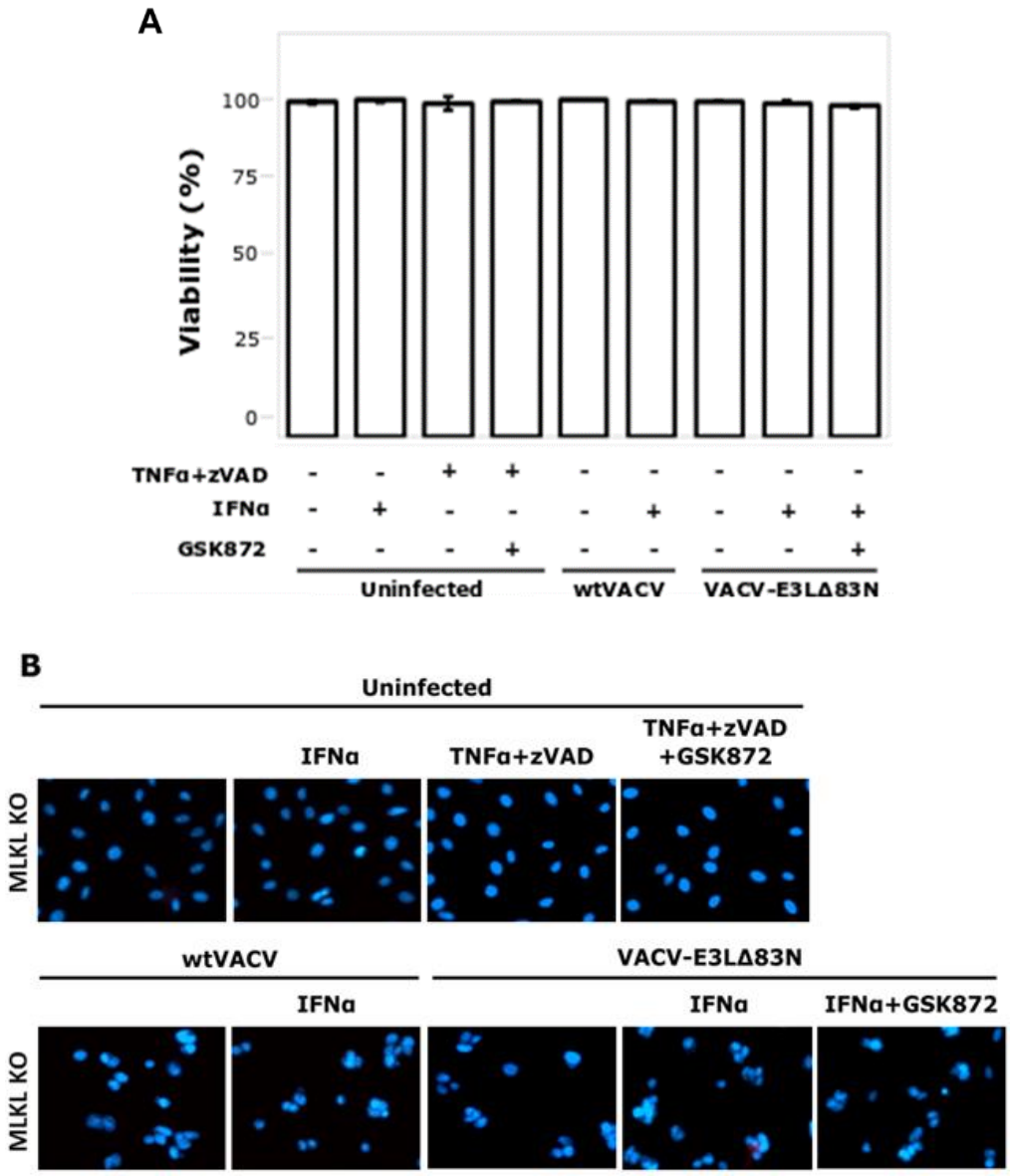

Figure 20. Lack of VACV-E3LΔ83N-induced death in MLKL-deficient L929 cells. (A) Viability assay in MLKL-deficient L929 cells. Mock- or IFNα-primed cells were treated as indicated or infected with wtVACV or VACV-E3LΔ83N. Viability was measured in propidium iodide nuclear stain dye exclusion assay 6 hours later. Cellular death is illustrated as mean cell viability (N > 500 cells) ±1 SD. (B) Microscopy images of the viability assay in (A).

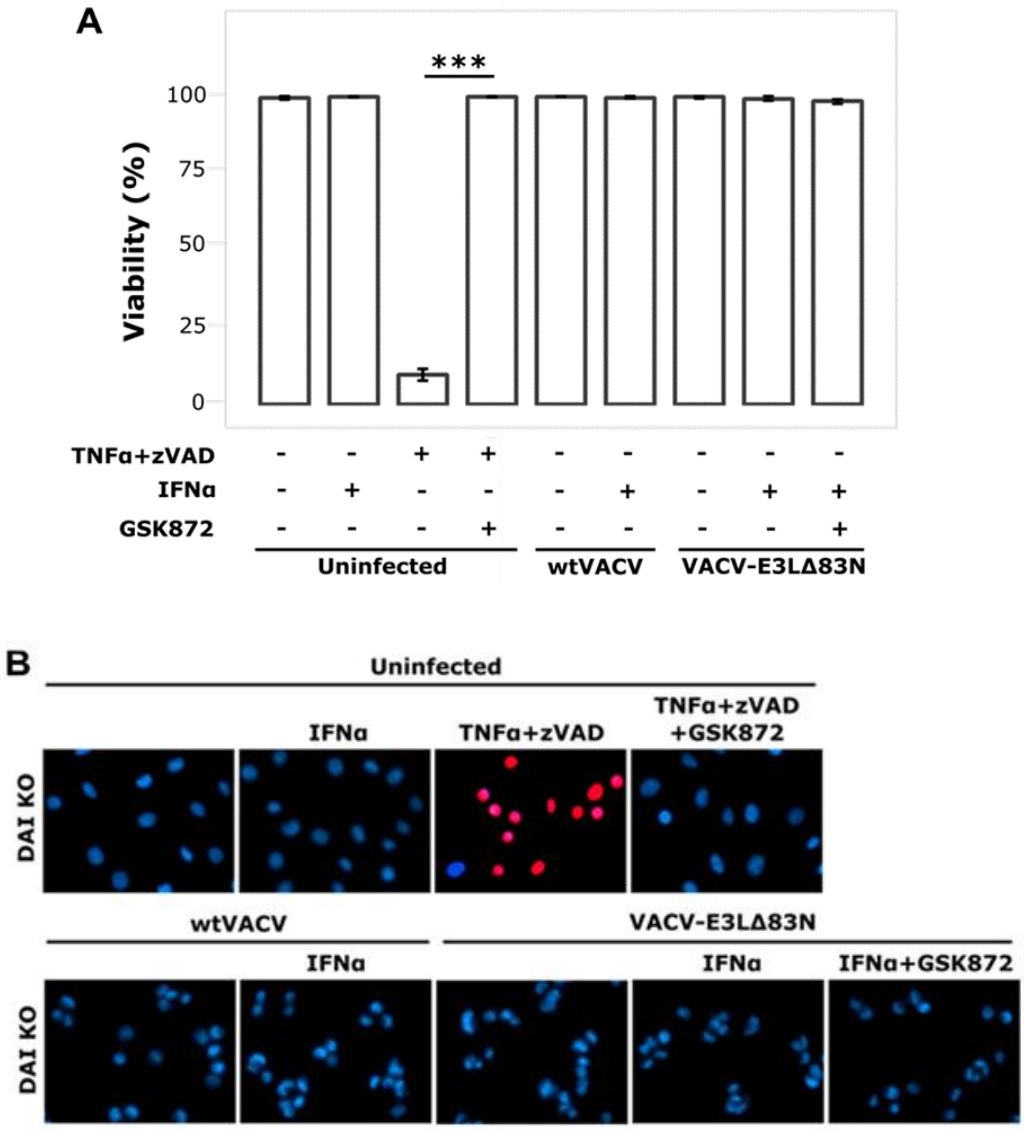

Figure 21. VACV-E3LΔ83N-induced death is dependent on DAI. (A) Viability assay in DAI-deficient L929 cells. Mock- or IFNα-primed cells were treated as indicated or infected with wtVACV or VACV-E3LΔ83N. Viability was measured in propidium iodide nuclear stain dye exclusion assay 6 hours later. Cellular death is illustrated as mean cell viability (N > 500 cells) ±1 SD. Student's t-test p-value: TNFα+zVAD vs. TNFα+zVAD+GSK'872: $p=9.5x10^{-5}$. (B) Microscopy images of the viability assay in (A).

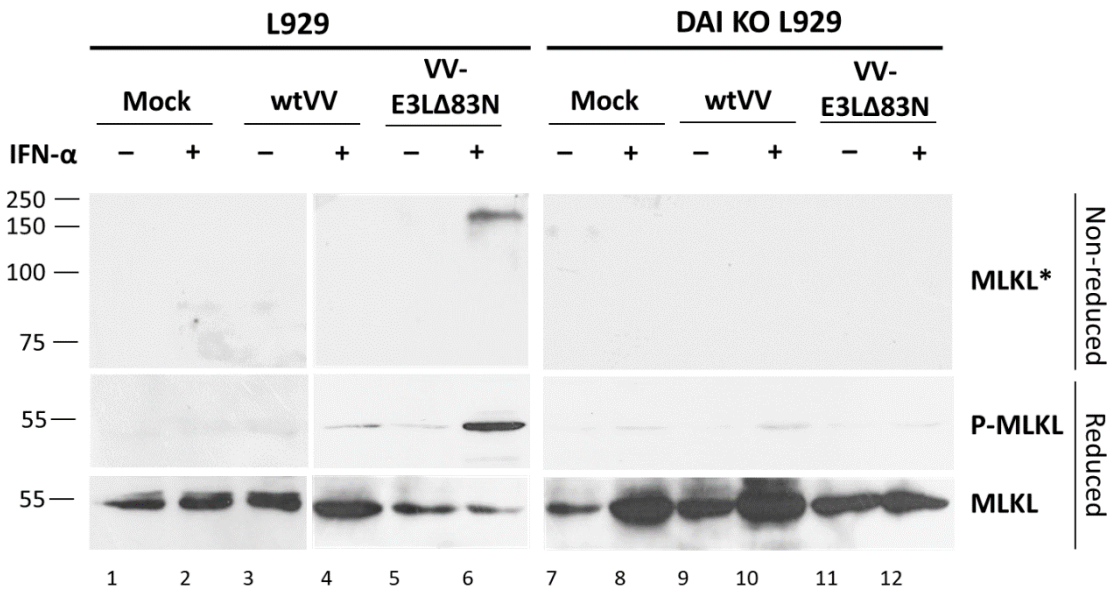

Figure 22. Lack of MLKL activation in DAI-deficient L929 cells infected with VACV-E3LΔ83N. Phosphorylation and trimerization status of MLKL. DAI KO L929 cells were mock- or IFNα-primed and subsequently infected with wtVACV or VACV-E3LΔ83N or left uninfected. After 5 hours, cells were lysed and subjected to immunoblotting in non-reduced and reduced conditions.
*Trimerized MLKL form is depicted

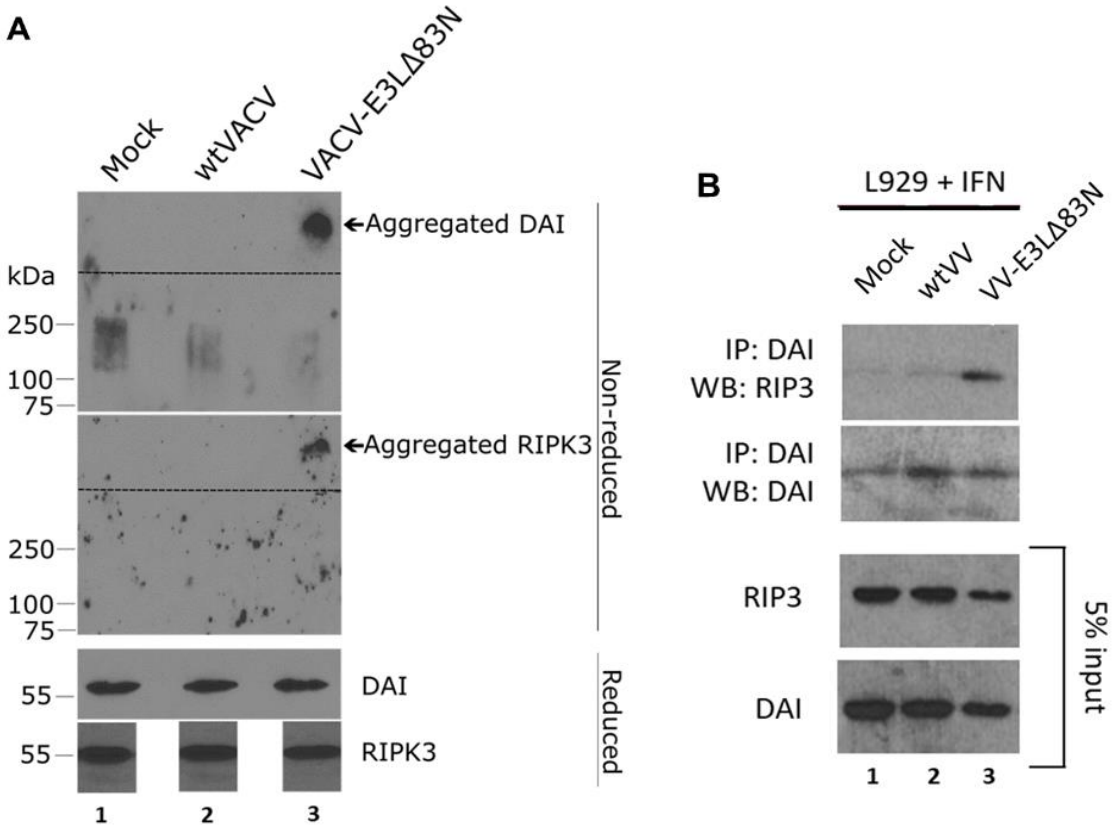

Figure 23. Necrosome formation in L929 cells infected with VACV-E3LΔ83N. (A) DSP crosslinking. At 2 hours following infection with the indicated viruses, DSP crosslinker was added to L929 cells. Following a 30-min. incubation, the cells were lysed and subjected to immunoblotting in non-reduced and reduced conditions. Macromolecular complex with DAI and RIPK3 formed in cells infected with mutant virus only. (B) Co-immunoprecipitation using DAI-specific antibody. Mock- or IFNα-primed L929 cells were infected with wtVACV or VACV-E3LΔ83N or left uninfected. At 2 hours post-treatment, cells were lysed and subjected to Co-IP using DAI-specific antibody. Immunoblotting followed using the indicated antibodies. RIPK3 co-precipitated with DAI only in cells infected with the mutant virus.
Figure 23A is also presented as Figure 32. Figure 23B is also presented as Figure 33.

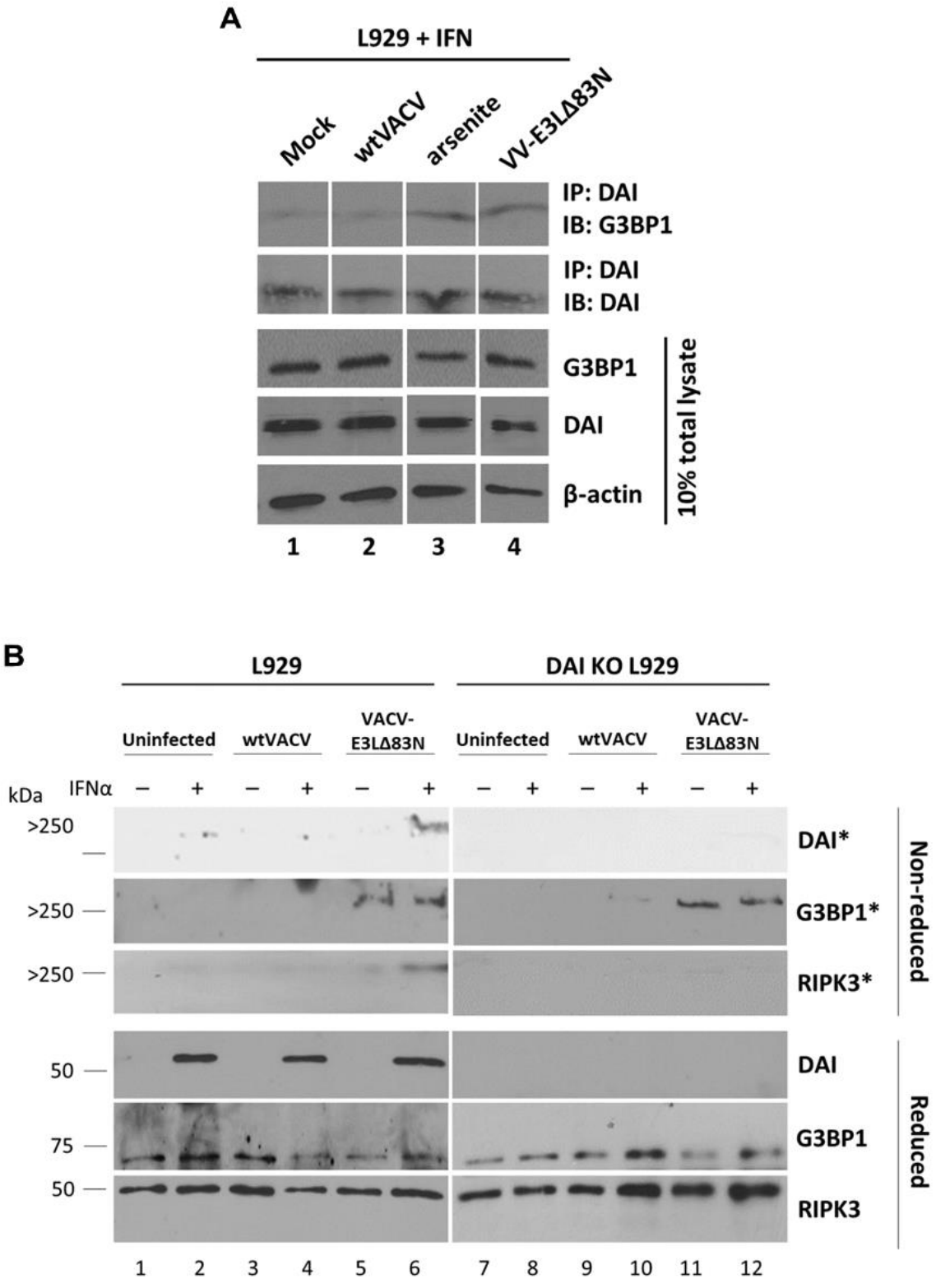
A
L929 + IFN
Mock
wtVACV
arsenite
VV-E3LΔ83N
IP: DAI
IB: G3BP1
IP: DAI
IB: DAI
G3BP1
DAI
β-actin
10% total lysate
1
2
3
4
B
L929
DAI KO L929
Uninfected
wtVACV
VACV-E3LΔ83N
Uninfected
wtVACV
VACV-E3LΔ83N
kDa
IFNα
– + – + – + – + – + – +
>250
>250
>250
50
75
50
DAI*
G3BP1*
RIPK3*
DAI
G3BP1
RIPK3
Non-reduced
Reduced
1 2 3 4 5 6 7 8 9 10 11 12

Figure 24. DAI-mediated necrosome formation in VACV-E3LΔ83N-induced stress granules. (A) Co-immunoprecipitation using G3BP1-specific antibody. Mock- or IFNα-primed L929 cells were infected with wtVACV or VACV-E3LΔ83N, left uninfected, or treated with arsenite. After 2 hours, cells were lysed and subjected to Co-IP using G3BP1-specific antibody. Immunoblotting followed using the indicated antibodies. DAI co-precipitated with G3BP1 only in conditions of necroptosis (cells infected with the mutant virus or treated with arsenite). (B) DSP crosslinking. At 2 hours following infection with the indicated viruses, DSP crosslinker was added to L929 and DAI KO L929 cells. Following a 30-min. incubation, the cells were lysed and subjected to immunoblotting in non-reduced and reduced conditions. Macromolecular complex with DAI and RIPK3 formed only in L929 cells infected with the mutant virus. Macromolecular complex with G3BP1 formed in cells infected with the mutant virus only.

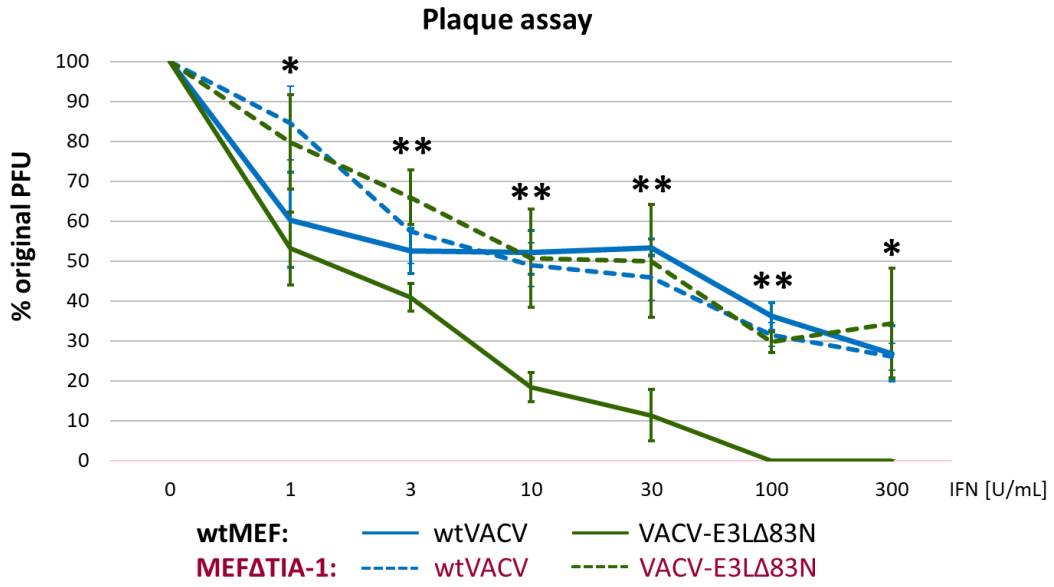

Figure 25. IFN sensitivity assay in MEF and MEF deficient in TIA-1. Mock- or IFNα-primed cell monolayers were infected with wtVACV or VACV-E3LΔ83N. After 48 hours, cell monolayers were stained and plaques were counted. Percentage of original plaque-forming units (PFUs) is plotted against the dosage of IFNα used. Lack of TIA-1, and therefore ability to form stress granules, increased IFN resistance of the mutant virus to the levels seen for the wt virus.

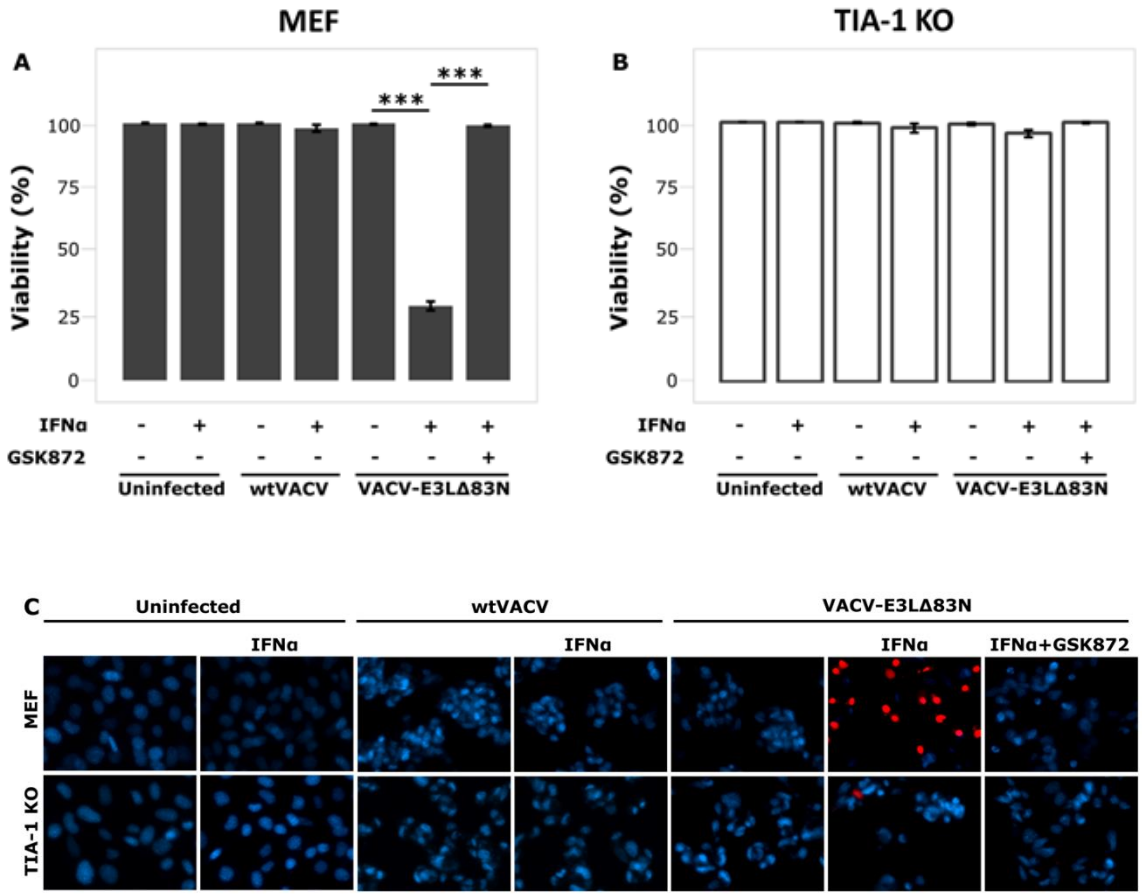

Figure 26. VACV-E3LΔ83N induces RIPK3-mediated death dependent on formation of stress granules in MEF cells. (A) Viability assay in MEF cells. Mock- or IFNα-primed cells were infected with wtVACV or VACV-E3LΔ83N or left uninfected. Viability was measured in propidium iodide nuclear stain dye exclusion assay 8 hours later. Cellular death is illustrated as mean cell viability (N > 500 cells) ±1 SD. Student's t-test p-values: VACV-E3LΔ83N vs. VACV-E3LΔ83N +IFN: $p=2.1x10^{-4}$, VACV-E3LΔ83N +IFN vs. VACV-E3LΔ83N +IFN+GSK'872: $p= 3.2x10^{-7}$. (B) Viability assay in TIA-1-deficient MEF cells performed in the same manner as in (A). Student's t-test p-value: VACV-E3LΔ83N+IFN (TIA-1 KO MEF) vs. wtVACV: $8.6x10^{-7}$. (C) Microscopy images of the viability assays in (A) and (B).

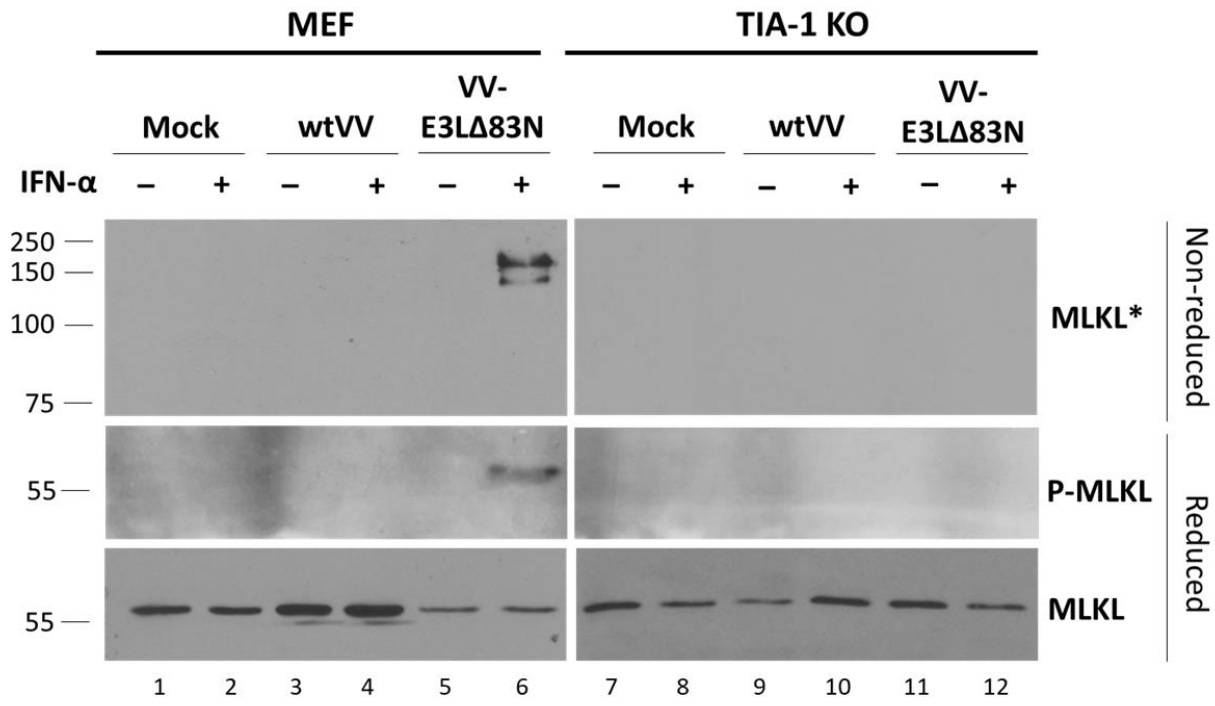

Figure 27. VACV-E3LΔ83N infection leads to MLKL activation in MEF cells but not in TIA-1-deficient MEF cells. Phosphorylation and trimerization status of MLKL. MEF and TIA-1 KO MEF cells were mock- or IFNα-primed and subsequently infected with wtVACV or VACV-E3LΔ83N or left uninfected. After 5 hours, cells were lysed and subjected to immunoblotting in non-reduced and reduced conditions.
*Trimerized MLKL form is depicted

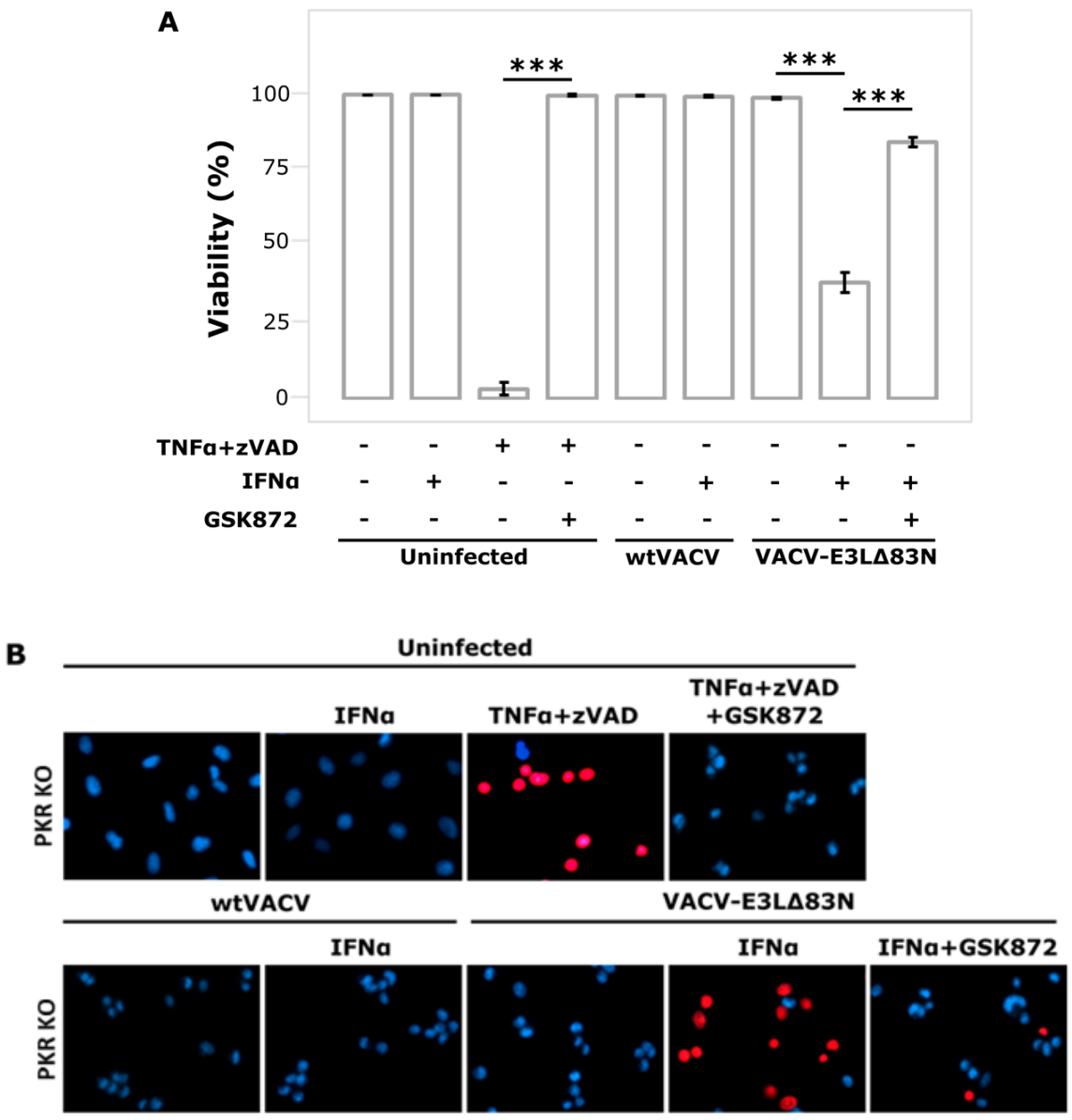

Figure 28. VACV-E3LΔ83N-induced death is independent of PKR in L929 cells. (A) Viability assay in PKR-deficient L929 cells. Mock- or IFNα-primed cells were infected with wtVACV or VACV-E3LΔ83N or left uninfected. Viability was measured in propidium iodide nuclear stain dye exclusion assay 6 hours later. Cellular death is illustrated as mean cell viability (N > 500 cells) ±1 SD. Student's t-test p-values: TNFα+zVAD vs. TNFα+zVAD+GSK'872: $p=1.3x10^{-4}$, VACV-E3LΔ83N vs. VACV-E3LΔ83N +IFN: $p=8.6x10^{-4}$, VACV-E3LΔ83N +IFN vs. VACV-E3LΔ83N +IFN+GSK'872: $p= 2.5x10^{-5}$. (B) Microscopy images of the viability assay in (A).

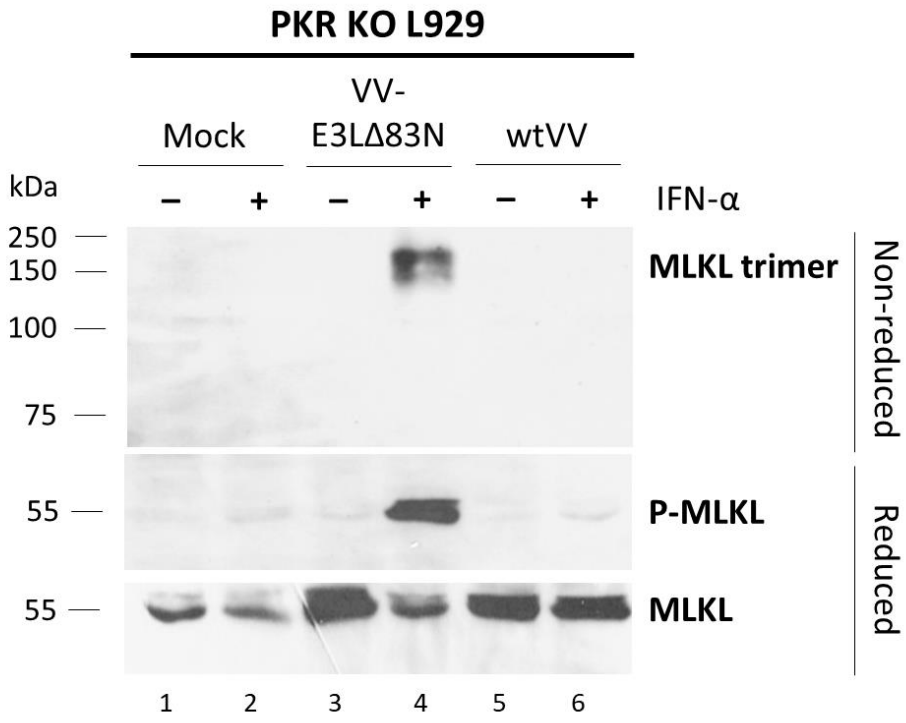

Figure 29. MLKL activation following VACV-E3LΔ83N infection in PKR-deficient L929 cells. Phosphorylation and trimerization status of MLKL. PKR KO L929 cells were mock- or IFNα-primed and subsequently infected with wtVACV or VACV-E3LΔ83N or left uninfected. After 5 hours, cells were lysed and subjected to immunoblotting in non-reduced and reduced conditions.

CHAPTER 4

DETECTING NECROPTOSIS IN VIRUS-INFECTED CELLS

ABSTRACT

Necroptosis has been implicated as a critical cell death pathway in cancers, Alzheimer's and other neurodegenerative diseases, and virus-infected cells. Necroptosis occurs when mixed-lineage kinase domain-like protein (MLKL) punctures the cytoplasmic membrane allowing a rapid influx of water leading to a loss of cellular integrity. As its role in human disease becomes apparent, methods identifying necroptosis will need to be further developed and optimized. Here, we describe identification of necroptosis through quantifying cell death with pathway inhibitors and using Western blots to identify end points of MLKL activation and protein-protein interactions leading to it.

INTRODUCTION

Necroptosis is a relatively newly identified form of programmed cell death, that unlike apoptosis and pyroptosis, is independent of caspases (111, 112). Necroptotic cell death has been implicated in the response to infection, death receptor activation, and activation of TLR 3 and TLR 4. Necroptosis has been detected in brains of patients with Alzheimer's disease and Parkinson's disease and has been implicated in age-related macular degeneration and in skin inflammation (153-155).

While independent of caspase activation, necroptosis is dependent on the serine/threonine protein kinase, RIPK3. In fact, active caspase 8, one key initiator caspase for apoptosis, can inhibit necroptosis by cleaving RIPK3 (156). Once activated, RIPK3 can phosphorylate MLKL, the executioner of necroptosis (61, 62, 125). Phosphorylation of MLKL on serine 358 in humans and serine 345 in mice is necessary but not sufficient to induce necroptotic cell death (66, 67). A second step, trimerization, is dependent on highly phosphorylated inositol phosphates and on tyrosine phosphorylation (T357) of MLKL by the TAM kinases (63-65).

There are three sensors, RIPK1, DAI and TRIF, that act upstream of RIPK3 that can lead to RIPK3 activation. RIPK1 senses activation of death receptors (157). DAI senses Z-form nucleic acid, associated with viral infection, while TRIF senses signaling by TRL3 and TLR4 (73, 77). RIPK1, DAI, and TRIF can bind to RIPK3 through interaction of mutual RIP homotypic interaction motifs, RHIMs, leading to RIPK3 phosphorylation and activation (158). Once activated, RIPK3 can phosphorylate MLKL, initiating the pathway leading to necroptotic cell death.

In this manuscript we will describe methods to detect cell death and determine if the cell death is RIPK3-kinase-dependent and associated with MLKL-serine and tyrosine phosphorylation and MLKL trimerization. While the requirement for RIPK1 kinase activity can be evaluated using RIPK1 specific kinase inhibitors and RIPK1 phospho-specific antiserum, no similar reagents are available to evaluate activation of DAI or TRIF. However, co-immune precipitation can be used to ask if DAI and TRIF are bound to RIPK3, which is presumed to be necessary for DAI and TRIF-dependent activation of RIPK3. We have also recently shown that DAI-dependent necroptosis is associated with formation of large cross-linkable complexes, that contain DAI and RIPK3 (159). Cross-linking can be done in living cells and in tissue from experimental animals and necropsy tissue from humans. Thus, cross-linking can be used to determine if DAI activation is associated with disease.

2 Materials

2.1 Cell viability by dye exclusion with inhibitors

Prepare all inhibitor stocks in sterile DMSO or water, as indicated. Dilute into the working concentration in warm medium. There are many alternative live/dead nucleic acid stains, but these are our preference due to cost and availability.

a) Hoescht: Allows for nuclear staining in blue fluorescent channels. Prepare stock solution at 1 mM DMSO, storing at -20C until use at 1µM.
b) Propidium Iodide (PI): Stains nucleic acids, but is excluded from living cells. Detectable in the red channel. Prepare stock at 1 mg/mL in water and use at 1 µg/ml.
c) Fluorescent microscope or cell counter with RFP and DAPI channels.
d) RIPK3: While lack of RIP3 involvement can rule out necroptosis, it has been shown to be involved in other death pathways and cannot be used to conclusively confirm it.
    a. GSK 872: Prepare stock at 10 mM in DMSO (store at -80C) and use at working concentration depends on cell line but generally between 1 uM-10 µM. Inhibits RIPK3 kinase activity in both human and mouse cells.
e) RIPK1: Much like RIPK3, RIPK1 is involved in other cell death pathways and cannot solely be used to determine if necroptosis is occurring. Unlike RIPK3, RIPK1-independent necroptosis can still occur.

a. GSK 963: Prepare stock 10 mM in DMSO, aliquot and store at -80C. Thaw and dilute to working concentration at 1 uM-10 uM in cell media. Inhibits kinase activity of both human and mouse RIPK1.

b. Nec-1s: Prepare 10 mM solution in DMSO and store at -20C for up to 1 month. Fully bring to room temperature before using at a concentration of 100 µM. Validated in human cells, mouse cells, and murine models.

f) MLKL: At the cell membrane MLKL executes necroptosis by forming pores allowing for unregulated ion transfer. It requires serine phosphorylation, homologous trimerization, cell membrane relocation, and a tyrosine phosphorylation before executing necroptosis. Inhibition of MLKL can be used to positively determine necroptosis occurred.

a. Necrosulfonamide (NSA) inhibits only human MLKL after serine phosphorylation but before pore formation. Prepare a stock solution of 10 mM in DMSO and store at -20C. Thaw and use at 1-10 µM.

2.2 MLKL serine phosphorylation

1. Approximately $1x10^6$ cells per sample to be tested.
2. Halt™ Protease and Phosphatase Inhibitor Cocktail (100X) (78446, ThermoFisher) or equivalent
3. DTT prepared at 500 mM in DMSO and stored at -20C.

4. Triton-X lysis buffer: Prepare a Triton-X lysis buffer to the following final concentrations in sterile water: 5 mM EDTA, 10 mM Tris-Cl pH 8.0, 50 mM NaCl, 1% (v/v) Triton-X 100. **see Note 1**
5. 4X SDS-PAGE loading buffer: Prepare the loading buffer to the following concentrations: 0.24% SDS, 0.2% bromophenol blue, 20% glycerol in sterile water. **see Note 2**
6. 10% polyacrylamide gels can be purchased or prepared.
7. Nitrocellulose membranes
8. CAPS transfer buffer: Resuspend 10 mM CAPS (3-(cyclohexylamino)-1-propane sulfonic acid) in sterile water and adjust pH to 11. Just before use add 20% v/v methanol.
9. Tris buffered saline with tween (TBST): Dissolve NaCl (137 mM), KCl (2.7 mM), and Tris base (19 mM) in sterile water. Titrate pH to 7.4 and add Tween-20 to 0.05% (v/v).
10. Membrane Blocking Buffer (MBB): Non-fat milk (NFM) diluted to 5% (w/v) in TBST
11. BSA dilution buffer (BDB): 3% (v/v) bovine serum albumin (BSA) in TBST
12. Antibody dilution buffer (ADB): Non-fat milk (NFM) diluted to 3% (w/v) in TBST
13. Reagents for detecting secondary antibodies.
14. Stripping buffer: 7.25 mM TrisCl, 0.1% Sodium Dodecyl Sulfate, with 0.1% (v/v) β-Mercaptoethanol added just before use
15. Primary and secondary antibodies s**ee Note 3**

2.3 MLKL trimerization

1. Approximately $1x10^6$ cells per sample to be tested.
2. Halt™ Protease and Phosphatase Inhibitor Cocktail (100X) (78446, ThermoFisher) or equivalent
3. DTT prepared at 500 mM in DMSO and stored at -20C.
4. 4X SDS-PAGE loading buffer. **see Note 2**
5. 7.5% polyacrylamide gels can be purchased or prepared.
6. Nitrocellulose membranes
7. CAPS transfer buffer
8. TBST
9. Primary and secondary antibodies and appropriate buffers **see Note 3**
10. Reagents for detecting secondary antibodies.
11. Stripping buffer

2.4 Co-Immunoprecipitation

1. Approximately $1x10^6$ cells per sample to be tested.
2. Halt™ Protease and Phosphatase Inhibitor Cocktail (100X) (78446, ThermoFisher) or equivalent
3. DTT prepared at 500 mM in DMSO and stored at -20C.
4. Non-denaturing lysis buffer (NDB): Dilute Tris-HCl, pH=7.5 to 10 mM, $MgCl_2$ to 2 mM, KCl to 50 mM, and Triton X-100 to 1% (v/v) in sterile water. **see Note 1**

5. Buffer I: Prepare Tris-HCl, pH=7.5 at 20 mM, NaCl at 0.4 mM, EDTA at 1 mM Triton X-100 at 1% (v/v), glycerol at 20%(v/v), and Na_3VO_4 at2 mM in sterile water.
6. Protein A/G PLUS-Agarose (Santa Cruz, sc-2003), 40 µL of 50% slurry/sample (20 µl for lysate pre-clearing and 20 µl for immunoprecipitation)
7. Primary antibody to pull down protein complexes **see Note 3**
8. 10% polyacrylamide gels can be purchased or prepared.
9. Nitrocellulose membranes
10. CAPS transfer buffer
11. TBST
12. Primary and secondary antibodies and appropriate buffers **see Note 3**
13. Reagents for detecting secondary antibodies.
14. Stripping buffer

2.5 Necrosome crosslinking

1. Approximately $1x10^6$ cells or 5-25mg of animal tissue per sample to be tested.
2. dithiobis[succinimidylpropionate] (DSP) crosslinker, 22585, ThermoScientific: Prepare 100 µL of 25 mM DSP, by resuspending 1 mg of DSP in 100 µL DMSO. **see Note 4**
3. Halt™ Protease and Phosphatase Inhibitor Cocktail (100X) (78446, ThermoFisher) or equivalent.

4. RIPA lysis buffer: 1% NP40, 0.1% SDS, 0.5% Sodium deoxycholate, DTT prepared at 500mM in DMSO and stored at -20C.
5. 4X SDS-PAGE loading buffer. DO NOT ADD DTT.
6. 10% polyacrylamide gels can be purchased or prepared.
7. Nitrocellulose membranes
8. CAPS transfer buffer
9. TBST
10. Primary and secondary antibodies and appropriate buffers **see Note 3**
11. Reagents for detecting secondary antibodies.
12. Stripping buffer

3 Methods

3.1 Cell viability by dye exclusion

Cell viability and dye exclusion can only be used to identify necroptosis in conjunction with necroptosis inhibitors. It is critical to set up inhibitors for this experiment according to their use as described in the Materials section 2.1 and demonstrated in **Figure 2**. Furthermore, establishing the time of membrane disruption as indicated by dye exclusion makes determining the timelines for Methods 3.2, 3.3, 3.4, and 3.5 much simpler. **See Note 5** for more information.

1. One day prior to testing, plate cells in a tissue culture dish suitable for fluorescent imaging.
2. Prepare working concentrations of Hoescht dye and inhibitors of the necroptosis pathway by diluting into cell growth media. Pre-treat cells by aspirating media and replacing with dye and inhibitors and incubating for 1hr under normal cell growth conditions (i.e. 37°C, 5% CO_2). All samples should have Hoescht dye; inhibitors should be used as appropriate.
3. Begin the experiment by aspirating dye media and adding a chemical death inducer or infecting with virus. If using inhibitors, include them in death inducer and viral preparations **see Note 6.**

4. Prepare 10X PI in cell growth media and add to cells (1/10 v/v) at least 15min before first timepoint. Gently swirl cells to allow dispersion of dye. PI can be left on cells for the course of the experiment.
5. Image cells using DAPI channel (Hoescht) and RFP channel (PI). Phase contrast can also be used for qualitative analysis of cell morphology.
6. Count all cells (blue) and dead cells (red).

3.2 MLKL serine phosphorylation

MLKL serine phosphorylation is the first step of MLKL activation by RIPK3. MLKL is also phosphorylated on a tyrosine residue, but at the time of this writing there are no commercially available antibodies specific to this phosphorylation site. To look at subsequent activation, Method 3.1 Cell death by dye exclusion, Method 3.3 MLKL Trimerization, and Method 3.4 Co-immunoprecipitation (with anti-Tyrosine Phospho antibody) can be used, for timepoints, **see Note 5.**

1. Prepare $1x10^6$ cells by infecting or treating with chemical reagents suspected of inducing necroptosis **see Note 6.**
2. At various time-points scrape cells into media using the blunt end of a P1000 pipette tip.
3. Centrifuge @ 1000 xg for 10’ and gently remove media from pellet **see Note 7.**
4. Resuspend pellet thoroughly in 60 µL of Triton-X lysis buffer with protease and phosphatase inhibitors.

5. Incubate cells on ice for 5’.
6. Centrifuge cells for 15’ at max speed at 4°C.
7. Keep the supernatant and add to 4X MLKL loading buffer + DTT s**ee Note 8.**
8. Heat all samples for at least 10’ at 95°C.
9. Load onto a 10% polyacrylamide gel **see Note 9.**
10. Run slowly (70V) until the ladder is in the separating gel. After this, the speed can be increased to 100V until the 50 kDa marker is 2/3 of the way down the gel.
11. Transfer to nitrocellulose membrane in 1X CAPS transfer buffer with added methanol for 1 hr at 100V.
12. Block for 1 hr with MBB. Rinse with TBST until no longer cloudy.
13. Add primary antibody (serine phospho-MLKL) overnight at 4°C, rinse 1x with TBST **see Note 3.**
14. Wash with TBST 3x at RT for 5 min.
15. Add secondary antibody and incubate 2 hr at RT in ADB.
16. Wash with TBST 3x at RT for 15 min.
17. Expose and image blot.
18. Strip the blot by incubating in Stripping Buffer (**see Note 10**) for 15 minutes at 56°C.
19. Block with MBB for 1hr at RT. Rinse with TBST until no longer cloudy.
20. Add primary MLKL antibody overnight at 4°C. s**ee Note 3.**
21. Rinse 3x with TBST at RT for 5 min.
22. Add secondary antibody. Incubate 2 hr at RT in ADB.

23. Wash with TBST 3x at RT for 5 min.

24. Expose and image blot.

3.3 MLKL trimerization

MLKL trimerization is a straightforward way to measure one of the final steps of MLKL activation before execution of cell death. After MLKL is trimerized, it moves to the cell surface creating pores which facilitate rapid cell death. This method takes advantage of MLKL trimers being resistant to denaturization by SDS and boiling while fully denaturing with DTT. For timepoints, **see Note 5.**

1. Prepare $1x10^6$ cells by infecting or treating with chemical reagents suspected of inducing necroptosis **see Note 6.**
2. At various time points scrape cells into media using the blunt end of a p1000 pipette tip.
3. Centrifuge @ 1000 x g for 10’ and gently remove media from pellet **see Note 6.**
4. Resuspend pellet thoroughly in 100 µL of 1X MLKL loading buffer <u>without DTT</u>. Separate half of sample and add DTT **see Note 11.**
5. Add all of sample to the Qiashredder and spin at maximum speed for 3’.
6. Heat all samples for at least 10’ at 95°C.
7. Load onto a 7.5% polyacrylamide gel **see Note 9.**
8. Run slowly (70V) until the 50 kDa marker is 2/3 of the way down the gel.

9. Transfer to nitrocellulose membrane 18 hrs at 15V in 4°C in CAPS transfer buffer with magnetic spinner turned to slow.
10. Block for 1 hr with MBB.
11. Add primary antibody (MLKL **see Note 3)** overnight at 4°C (rinse with TBST).
12. Wash with TBST 3x at RT for 5 min.
13. Add secondary antibody and incubate 2 hr at RT in ADB.
14. Wash with TBST 3x at RT for 15 min.
15. Expose and develop blot

3.4 Co-Immunoprecipitation

We have validated this co-immunoprecipitation protocol to identify interactions between DAI and RIPK3 and to detect MLKL Tyrosine phosphorylation **see Figure 3**. We can also find interactions between RIP3 and DAI by Co-IP **see Figure 4.** Each of these pull-downs will require a different timeline **see Note 5.**

1. Prepare $2x10^6$ cells by infecting or treating with chemical reagents suspected of inducing necroptosis **see Note 6.**
2. At 2 hours post-treatment or post-infection, aspirate the media and wash cells with 1 mL cold PBS.
3. Scrape cells into cold PBS using the blunt end of a p1000 and transfer the suspension to a microcentrifuge tube.
4. Centrifuge at 1000 x g for 10 min. at 4°C.

5. Remove PBS (supernatant) carefully, not disturbing the pellet **see Note 6.**
6. Lyse cells by resuspending the pellet in 100 µL ice-cold NDB and incubating on ice for 5 min.
7. Add 120 µL ice-cold Buffer I **see Note 12.**
8. Measure 80 µL of 25% (v/v) raw bead slurry per sample (Protein A/G agarose) and spin the slurry at 500 x g for 5 min **see Note 13.**
9. Wash the pellet of beads with 1 mL Buffer I and spin again.
10. Perform a total of 3 washes **see Note 12**.
11. Pre-clear samples, by adding 20 µl of washed 50% Protein A/G PLUS-Agarose slurry to the collected cell lysates.
12. Incubate with rotation at 4°C for 30-60 min.
13. Pellet beads (500 x g for 5 min) **see Note 14.**
14. Transfer 200 µL of the supernatant into a fresh tube for immunoprecipitation (discard beads used for pre-clearing. The other 40 µL of the lysate will be the Total Lysate Control **see Note 14.**
15. Add the bait antibody (**see Note 3)** to the 200 µL of cell lysate.
16. Incubate with rotation overnight at 4°C.
17. Add 20 µL of the previously prepared 50% Protein A/G PLUS-Agarose slurry to each sample.
18. Incubate with rotation for 60-90 min. at 4°C.
19. Pellet the bead-antibody-protein complexes by centrifugation at 500 x g for 5 min and set aside the supernatant to be kept as a control **see Note 14**.

20. Wash the beads to remove proteins with non-specific binding by adding 1 mL of Buffer I.
21. Centrifuge at 500 x g for 5 min. Preserve a fraction of the supernatant as a control s**ee Note 14**.
22. Repeat the wash for a total of 3 times.
23. When removing supernatant after last wash, leave about 15 µl of Buffer I on top of the bead slurry in the tube. Add at least 15 µL of 2X Denaturing loading buffer containing 20-50 µM DTT.
24. To release the antibody-protein complexes from the beads, heat the samples at 95°C for 10-15 min.
25. Pellet the beads by centrifugation at 500 x g for 10 min. Transfer the supernatant to fresh tube. The pellet can be kept as a control for successful release of antibody-protein complexes **see Note 14.**
26. Run two 10% PAGE-SDS gels at 100V. One gel should be run for the immunoprecipitated fraction, and another one for the Total Lysate Control from step 14.
27. Transfer to nitrocellulose membrane in 1X CAPS transfer buffer with added methanol for 1 hr at 100V.
28. Block for 1 hr with MBB. Rinse with TBST until no longer cloudy.
29. Add primary antibody overnight at 4°C in ADB **see Note 3** and **Note 15** (rinse with TBST).
30. Rinse 3x with TBST at RT for 5 min.
31. Add secondary antibody. Incubate 2 hr at RT in ADB.

32. Wash with TBST 3x at RT for 5 min.
33. Expose and image blot.
34. Strip the blot by incubating in Stripping Buffer (**see Note 9**) for 15 minutes at 56°C.
35. Block 1hr at RT. Rinse with TBST until no longer cloudy.
36. Add primary antibody overnight at 4°C (rinse with TBST) **see Note 3** and **Note 15.**
37. Rinse 3x with TBST at RT for 5 min.
38. Add secondary antibody. Incubate 2 hr at RT in ADB.
39. Wash with TBST 3x at RT for 5 min.
40. Expose and image blot.

3.5 Necrosome crosslinking

Necrosome crosslinking uses an amine-reactive crosslinker, DSP, to covalently cross link all proteins in the necrosome shifting their weight on a PAGE gel to >250kDa (**Figure 5)**. It is helpful for looking at interactions between proteins that cannot easily be detected by Co-IP (method 3.4) and can readily be used to analyze animal and human tissue samples frozen in liquid nitrogen. It is not as specific as Co-IP but can be used with other methods to demonstrate protein inclusion in the necrosome. For timelines, **see Note 5.**

1. For tissue culture experiments prepare $2x10^6$ cells by infecting or treating with chemical reagents suspected of inducing necroptosis **see Note 6.**

2. At 2 hours post-treatment or post-infection, aspirate the media and wash cells with 1 mL room-temperature reaction buffer (1x PBS) **see Note 16.**
3. Scrape cells into the PBS using the blunt end of a p1000 and transfer the suspension to a microcentrifuge tube.
4. Centrifuge at 1000 x g for 10 min.
5. Remove PBS (supernatant) carefully, not disturbing the pellet, **see Note 7.**
6. For treatments done in vivo (mice) or tissues collected from a diseased individual (human), homogenize about 5 mg tissue per sample by grinding in liquid nitrogen. The protocol can be scaled up for 25 mg **see Note 17.**
7. Resuspend cells or ground tissue in PBS at a concentration of 5 mg/100 µl.
8. Add 1 µL Halt™ Protease and Phosphatase Inhibitor Cocktail (in case some cells disrupt).
9. Add 8 µL of freshly prepared (**see Note 4)** 25 mM DSP crosslinker for a final concentration of 2 mM **see Note 18**.
10. Incubate at room temperature for 30 min or on ice for 2 hr with rotation **see Note 17.**
11. Add 2 µL of stop solution: 1M Tris pH 7.5 (for a final concentration of 20 mM)
12. Incubate for 15 min at room temperature with rotation **see Note 17.**
13. Centrifuge at 1000 x g for 10 min. at 4°C.
14. Remove the supernatant carefully, **see Note 7.**
15. Add 120 µL of ice-cold RIPA lysis buffer **see Note 1** and incubate on ice for 10 min **see Note 17.**

16. Add 60 µL of 4x SDS sample buffer without DTT **see Note 14.**
17. Load onto a 10% polyacrylamide gel **see Note 9.**
18. Run at 80 V until the sample is past the stacking gel then at 130 V through the separating gel.
19. Transfer to nitrocellulose membrane 18hrs at 20V in 4°C in CAPS transfer buffer with a low speed magnetic stirrer **see Note 19.**
20. Block for 1 hr at RT.
21. Add primary antibody overnight at 4°C (rinse with TBST) **see Note 3**.
22. Rinse 3x with TBST at RT for 5 min.
23. Add secondary antibody. Incubate 2 hr at RT in ADB.
24. Wash with TBST 3x at RT for 5 min.
25. Expose and develop blot **see Note 20.**
26. For total lysate controls, reduce 50 µL of the crosslinked samples by adding DTT to a final concentration of 50 µM (5.5 µL for 50 µL samples) and incubating the sample first at 37°C for 1 hr then at 95°C for 5-10 min.
27. Load on a 10% polyacrylamide gel.
28. Run at 80 V until the sample is past the stacking gel then at 130 V through the separating gel.
29. Transfer to nitrocellulose membrane in 1X CAPS transfer buffer with added methanol for 1 hr at 100V.
30. Block for 1 hr with MBB. Rinse with TBST until no longer cloudy.
31. Add primary antibody overnight at 4°C (rinse with TBST) **see Note 3**.
32. Rinse 3x with TBST at RT for 5 min.

33. Add secondary antibody. Incubate 2 hr at RT in ADB.

34. Wash with TBST 3x at RT for 5 min.

35. Expose and image blot **see Note 20.**

4 Notes

Note 1: Just before lysing cells add protease and phosphatase inhibitors.

Note 2: Just before denaturing protein, add DTT to 4x loading buffer to a final concentration of 4mM.

Note 3: Table 1 contains information on the antibodies we used for these protocols.

Note 4: DSP is very moisture sensitive and must be stored desiccated at 4C and be equilibrated to room temperature before opening. Because the NHS-ester moiety readily hydrolyzes and becomes non-reactive, prepare each use fresh and discarding any unused solution.

Note 5: Once necroptosis is initiated, cells die very quickly. As such the timepoints used to harvest protein to study these phenomena are critical. Each time a new cell line or treatment will be studied, the first step is to establish a timeline. The fastest way to do this is to use Method 3.1 dye exclusion to take images of the cells at 30 min intervals to determine the time of membrane rupture. Table 2 contains data from our observations on the best times to perform these assays in L929 cells.

Note 6: If infecting cells with virus, follow virus-specific infection protocols to infect >99% of cells and grow under standard culture conditions until desired timepoint.

Note 7: Dead volumes of 10-50µL should be left on pellets to avoid disturbing fragile cells.

Note 8: The samples for this experiment do not freeze well. Upon thawing pMLKL will barely be distinguishable between positive and negative control. Have the gel ready to run the same day as the experiment is conducted.

Note 9: If you are pouring the gel, the interface between the stacking and separating gels must be perfect. Isopropanol can be substituted for saturated isobutanol for a cleaner transition.

Note 10: Add 0.1% β-mercaptoethanol to stripping buffer immediately before use.

Note 11: Very fresh β-mercaptoethanol can be used in place of DTT. However, we have seen that this application is highly sensitive to oxidation and recommend using DTT for more consistent results.

Note 12: If necessary, lysates can be stored at -80°C until a more suitable time for processing.

Note 13: The commercial beads we use come as 25% (v/v) slurry. They need to be resuspended to a 50% (v/v) final concentration of beads. For this experiment, each sample requires 20 µL of the 50% slurry for both preclearing and the immunoprecipitation. For 10 samples, that will be 20 µL x 2 x 10 = 400 µL of 50% final slurry concentration. Therefore, you will need 400 µL x 2 = 800 µL of the 25% slurry. After washing the 800 µL of 25% slurry, you have roughly 200 µL of solid beads and add 200 µL buffer I to dilute to the final concentration of 400 µL 50% slurry.

Note 14: These can be kept at -80°C as a control.

Note 15: When probing the co-immunoprecipitation blots, you will look for both the protein targeted by the bait antibody in the IP and associated proteins. The first primary antibody probe should be against associated proteins. Stripping and re-probing for other

associated proteins can be done up to two more times. The final probe should be against the protein pulled down during the IP.

Note 16: Alternatively, 10-25 mM HEPES, bicarbonate/carbonate, borate buffers pH 7-9 can be used as the reaction buffer.

Note 17: For 25 mg of tissue several of the times need to be extended. Step 10, crosslink by rotating for 1 hour at RT or 4 hr at 4°C. Step 12, incubate with the stop solution for 30 min at RT with rotation. Step 15, lyse with RIPA for 30 mins at 4°C (with rotation).

Note 18: A final concentration of 1-2 µM is recommended. 2 µM works for L929 cells and brain tissue samples, but the concentration may need adjusting for other tissues and cell types.

Note 19: Do not discard the stacking gel; many macromolecular complexes will be present in this part of gel. The entire gel (stacking + separating) should be transferred.

Note 20: Blots can be stripped and probed up to 3 times. The cross-linked and total lysate control blots should be probed with the same antibodies.

Table 1: Antibodies used in these protocols.

Protein	Antibody clone	Species detected	Assays	Blocking buffer	Concentration	Dilution buffer
DAI	Zippy-1 AG-20B-0010-C100	Mouse, Human	WB	MBB	500 ng/mL (1:2000)	ADB
			Co-IP		5 ng/µL	Buffer I
RIPK3	CST D4G2A	Mouse	WB	MBB	85 ng/mL (1:2000)	ADB
Phospho-Tyrosine	Sigma 05-321X	Any	Co-IP		2.5 ng/µL	Buffer I
MLKL (Serine phospho)	CST D6E3G	Mouse	WB	MBB	28 ng/mL (1:1000)	BDB
MLKL (total)	CST D6W1K	Mouse	WB	BDB	313 ng/mL (1:1000)	BDB

Table 2: Optimal timepoints (in hours post-treatment) for these assays in L929 cells.

Method	**Assay**	**TNF +ZVD**	**VACV E3Δ83N**
3.1	Dye exclusion	4-6	6-8
3.2	MLKL serine phosphorylation	2-4	4-5
3.3	MLKL trimerization	4	5-6
3.4	Tyrosine phospho-MLKL co-IP	4	4-5
3.4	DAI-RIP3 co-IP	N/A	1-3
3.5	Necrosome aggregation		1-3

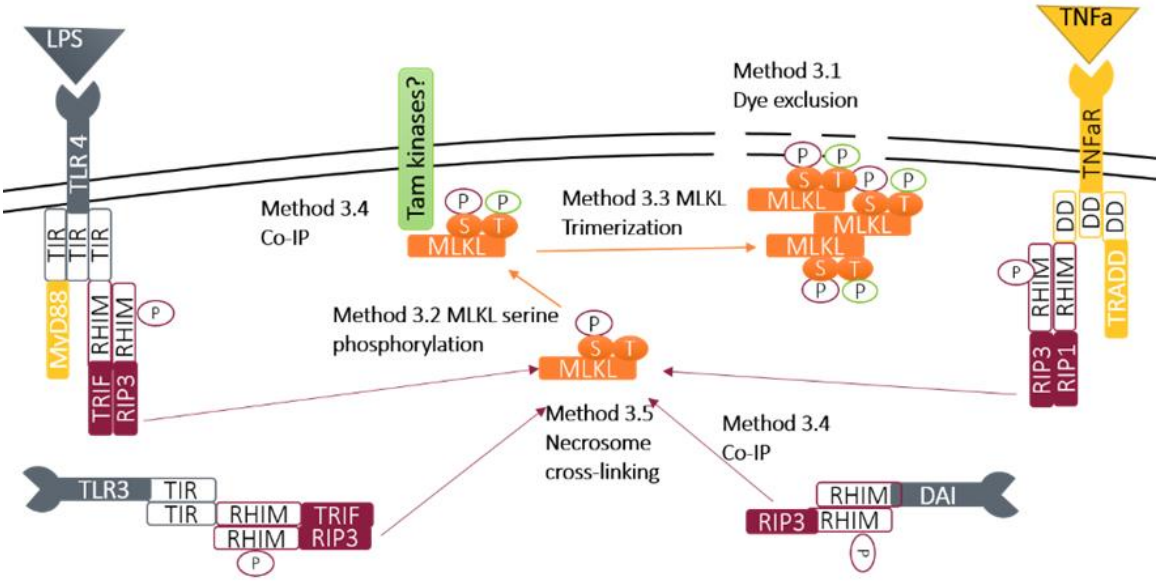

Figure 30. Overview showing how necroptosis can be induced and detected. This chapter describes how to detect the different stages of necroptotic death. We can detect initiation of RIPK3 activation with CoIP (Method 3.4). Then we can detect RIPK3 induction of the necrosome with crosslinking (Method 3.5). Next, we can detect MLKL serine phosphorylation (Method 3.2) and tyrosine phosphorylation (Method 3.5). We also describe detection of MLKL trimerization (Method 3.2) and cell death (Method 3.1). The inhibitors we have described in Method 3.1 are critical for determining how the cells are dying.

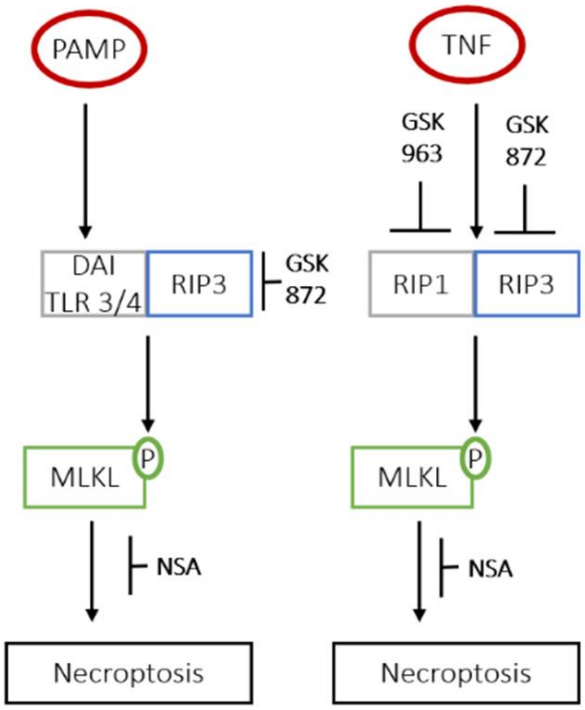

Figure 31. Inhibitors used to determine mechanism of cell death. Membrane permeablization is the final step before cell death. Detecting membrane permeablization in the presence of kinase inhibitors of different proteins involved in necroptotic death is a critical first step for determining whether or not necroptosis might be involved and how long it takes for cells to die. Nec-1s and GSK 963 both inhibit RIPK1 kinase activity. GSK 872 inhibits RIPK3 kinase activity. Necrosulfonamide (NSA) inhibits MLKL post serine phosphorylation, and ZVAD inhibits pan-caspase activity.

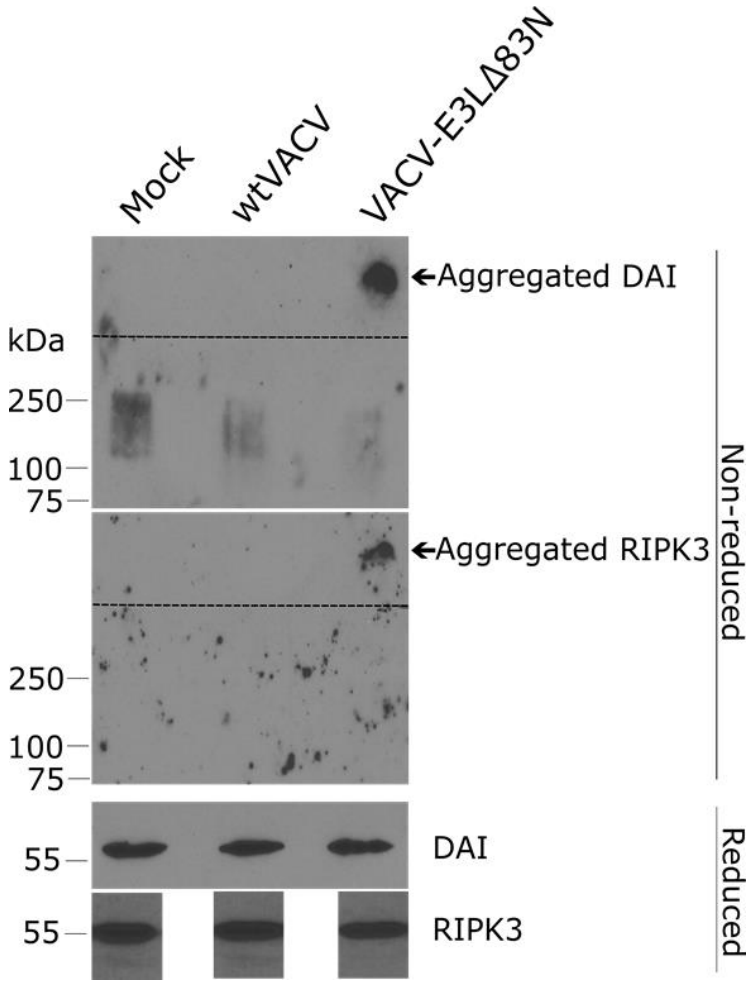

Figure 32. Cross-linking to determine mediator of necroptosis. L929 cells pre-treated with type 1 IFN were infected with VACV-E3LΔ83N. At 2 hours post infection, cells were harvested and cross-linked according to the protocol described in Method 3.4. Lysates were then run on Western blots and probed with antibodies against DAI and RIPK3.
This figure is also presented as Figure 23A.

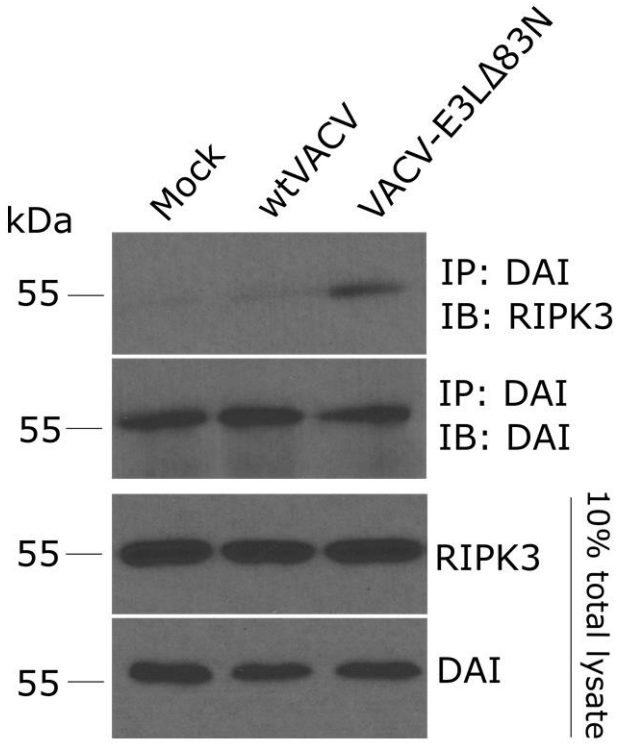

Figure 33. Co-IP to determine mediator of necroptosis. L929 cells pre-treated with type 1 IFN were infected with VACV-E3LΔ83N. At 2 hours post infection, lysates were harvested and subjected to immunoprecipitation by antibodies specific for DAI as described in Method 3.3. Immunoprecipitated protein and input lysate were run on Western blots and probed with antibody for RIPK3.
This figure is also presented as Figure 23B.

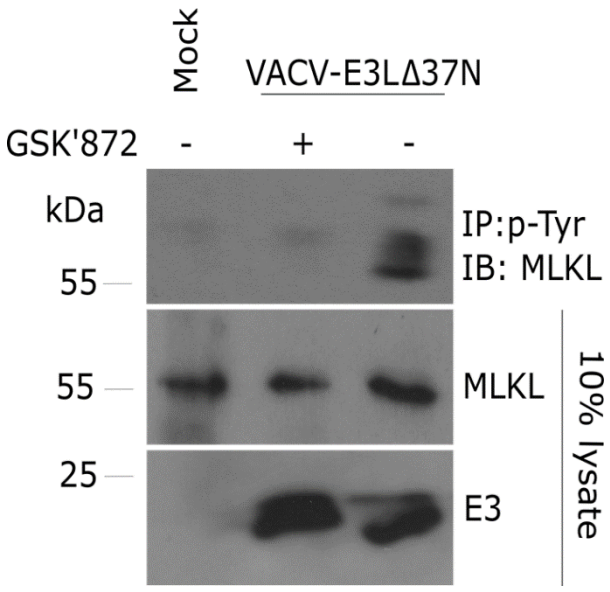

Figure 34: Co-IP to measure MLKL tyrosine phosphorylation. L929 cells pre-treated with type 1 interferon (IFN) were infected with VACV-E3LΔ37N and harvested at 4 hours post infection. Lysates then were immunoprecipitated as described in Method 3.3 using phosphotyrosine specific antibody. Immunoprecipitated proteins and input lysate were run on a Western blot and probed for MLKL.

Acknowledgments: This article (Chapter 4 of this dissertation) will be published in *Methods in Molecular Biology (Clifton, N.J.)* in 2021. Authors: Samantha Cotsmire, Mateusz Szczerba, Bertram Jacobs. See reference (160).

We would like to thank Nobuko Fukushima and James Bonner for technical assistance and Dr. Heather Koehler and Dr. Edward Mocarski for sharing expertise in necroptosis through consultation and protocol optimization. **Funding:** This work was supported by a grant from the National Institute of Allergy and Infectious Diseases (NIAID) at National Institutes of Health (NIH) (R01AI095394). **Author contributions:** Samantha Cotsmire, Mateusz Szczerba, and Bert Jacobs wrote the manuscript. B. J. provided intellectual oversight and designed experiments. S.C. and M.S. performed experiments and analyzed results. **Competing interests:** Authors declare no competing interests. **Data and materials availability:** All data is available in the main text or the supplementary materials. Sharing of materials described in this analysis will be subject to standard material transfer agreements.

CHAPTER 5

SUMMARY AND OUTLOOK

These studies have investigated the importance of stress granules in the necroptosis pathway induced following oxidative stress and viral infection. Necroptosis is a programmed cell death (PCD) pathway dependent on the serine/threonine protein kinase, RIPK3. Necroptosis has been implicated in a variety of human diseases, including neurodegenerative diseases (e.g., multiple sclerosis) (119), cancer (133), cardiovascular diseases (134, 135), ethanol-induced liver damage (136), inflammaging (137), skin inflammation (161) as well as viral and bacterial infections [reviewed in (138)]. Stress granules (SGs) are induced during cellular stress and their function have long been thought of as pro-survival (1-3). Here, we show that stress granules are required for necroptosis activation both following oxidative stress induced by arsenite (Chapter 2) as well as during poxviral infection (Chapter 3). Our studies give new insights into stress granule functions as well as mechanisms of necroptosis induction, contributing to better understanding of innate immunity and etiology of human diseases.

We began our studies with investigation of the function of the N terminal domain of vaccinia virus (VACV) E3 protein. wtVACV E3 protein is comprised of two domains conserved within the *Poxviridae* family (Fig. 5):

a) the C-terminal domain is a double-stranded RNA (dsRNA)-binding domain (dsRBD) that functions to mask presence of dsRNA produced during VACV replication, and thereby inhibits activation of the cellular enzymes PKR and 2’5’ OAS (90-92)

b) the N-terminal domain is a Z-DNA-binding domain (ZBD) whose function was initially only observable in animal models. It was shown that the N terminus of E3 binds to Z-form DNA and that this ability corresponded to viral pathogenicity in mice (84).

For a long time, mutations in the E3 ZBD, and even deletion of the entire ZBD (VACV-E3LΔ83N mutant, Fig. 5), did not have a significant effect on the virus replication or phenotype in cell culture. Nonetheless, the E3 protein N terminus was necessary for viral pathogenesis in mice (84). VACV-E3LΔ83N pathogenicity in mice was rescued by deletion of the type I IFN receptor (IFNα/βR$^{-/-}$), indicating a role of the E3 ZBD for IFN resistance (95). This prompted our studies of IFN resistance of VACV-E3LΔ83N virus in mouse cell lines. It was observed that VACV-E3LΔ83N is sensitive to IFN during infection of L929 cells (75). Furthermore, infection with the virus resulted in a rapid cell death, manifested by cellular rupture of L929 cells infected with VACV-E3LΔ83N. This death was demonstrated to be dependent on RIPK3 and independent of caspases. Furthermore, VACV-E3LΔ83N led to phosphorylation and trimerization of MLKL, and therefore this death pathway was identified as necroptosis (75). These results were confirmed in current studies, showing that death induced by VACV-E3LΔ83N was completely abolished in MLKL KO L929 cells (Fig. 20).

Activation of RIPK3 takes place following its interaction with one of the other RHIM domain-harboring proteins: RIPK1, TRIF, or DAI (59, 73, 77). VACV-E3LΔ83N-induced necroptosis was not affected by inhibition of RIPK1 activity with GSK'963 (75), and therefore was independent of RIPK1. Viral infections have been shown before to activate DAI: MCMV and HSV-1 (DNA viruses) and IAV (RNA virus) all induced

necroptosis that was dependent on DAI (76-79, 85, 162). DAI was a good candidate to be the activator of VACV-E3LΔ83N-induced necroptosis, as DAI expression is dependent on IFN and VACV-E3LΔ83N-induced necroptosis was observed only in IFN-primed L929 cells (75). In fact, we show that VACV-E3LΔ83N-induced necroptosis was abolished in DAI KO L929 cells: infection with VACV-E3LΔ83N did not result in death (Fig. 21) or activation (phosphorylation and trimerization) of MLKL (Fig. 22). Therefore, we demonstrated that VACV-E3LΔ83N-induced necroptosis was dependent on DAI.

DAI is a Z-DNA-binding protein and all proteins containing ZBDs have been shown to localize to stress granules (82, 118). Stress granules form in the cytoplasm during cellular stress (see Overall Introduction and Figs. 1 and 2) and are generally considered to be pro-survival: they store the non-translating mRNAs of house-keeping genes, letting the cell direct its resources to expression of stress-induced genes, moderating the effects of the ongoing stress (33, 100). Although stress granules were not shown to be directly involved in cellular death, we asked if they could play a role in necroptosis due to the fact of DAI dependence of some necroptosis pathways and typical DAI localization in the cell.

We began investigating involvement of stress granules in necroptosis by using arsenite. Arsenite is the most canonical inducer of stress granules in cells (97). Arsenite causes oxidative stress, leading to activation of HRI kinase, which phosphorylates eIF2α, thereby leading to formation of stress granules. We were able to observe death in IFN-primed L929 cells following arsenite treatment (Fig. 6). This death was dependent on RIPK3. We also showed that arsenite treatment led to phosphorylation and trimerization of MLKL (Fig. 7), and therefore identified this arsenite-induced death as necroptosis.

Similar to VACV-E3LΔ83N infection, arsenite-induced necroptosis was dependent on DAI, as arsenite treatment did not lead to death (Fig. 9) or activation of MLKL (Fig. 10) in DAI KO L929 cells. Induction of DAI-mediated necroptosis by a stress-granule inducer implicated potential role of stress granules for necroptosis.

Deciphering the molecular mechanism of necroptosis in more detail, we were able to detect formation of the DAI-RIPK3 necrosomes both in cells subjected to oxidative stress (Figs. 11) as well as cells infected with vaccinia virus (Figs. 23). Both DAI and RIPK3 formed macromolecular complexes in conditions of necroptosis, consistent with RIPK1-RIPK3 macromolecular complex formation known from previous studies, required for the canonical death receptor-induced necroptosis (60, 140). This implicates a potential significance of DAI-mediated necroptosis in neurodegenerative diseases (see below). Furthermore, we showed localization of DAI into stress granules in cells subjected to oxidative stress (Fig. 12) and infected with VACV-E3LΔ83N (Fig. 24) and demonstrated that necrosome formation takes place in SGs. To finally ask if SGs are required for necroptosis, we looked at necroptosis induction in cell lines that do not form granules: TIA-1 KO MEF cells and G3BP1/2 KO U2OS cells. Our data showed that neither arsenite (Figs. 15 and 17) nor VACV (Fig. 26) induced death in cells unable to form granules. Furthermore, MLKL activation was abolished in those cells, both during oxidative stress (Fig. 16) and VACV infection (Fig. 27). Altogether, our data demonstrated that DAI-mediated necroptosis is dependent on formation of stress granules, identifying a new function for these RNP cytoplasmic foci as well as discovering a new step in activating necroptosis.

Prolonged oxidative stress leads to damage of macromolecules (proteins, lipids, and nucleic acids), resulting in tissue damage, release of DAMPs, and inflammation, which can underlie a variety of diseases: Alzheimer's disease, Parkinson's disease, diabetes, cancer, cardiovascular diseases, stroke, septic shock, rheumatoid arthritis, and atherosclerosis [reviewed in (132)]. As necroptosis has been implicated in many of these diseases as well (see above), it is interesting to ask whether oxidative stress-induced necroptosis is the underlying mechanism of some of these human diseases.

Alzheimer's disease is characterized by formation of fibrillar peptides, assembling into β-amyloid structures (141, 142). Furthermore, IFN-mediated inflammation as well as accumulation of stress granules have been reported in brains of Alzheimer's patients (120, 121, 139). Finally, increased oxidation and thereby elevated levels of Z-form nucleic acids (Z-NAs) (see Chapter 2 Discussion) are other hallmarks of Alzheimer's disease and related neurodegenerative disorders (148). We show that DAI, a protein harboring ZBDs, mediates necroptosis induced by oxidative stress. DAI expression is dependent on IFN, and the protein localizes to stress granules formed during oxidative stress. Furthermore, we show that DAI and RIPK3 form macromolecular complexes, believed to be the necrosomes, just like the RIPK1-RIPK3 necrosomes formed during the canonical death receptor-induced necroptosis (60). RIPK1 and RIPK3 have been shown to assemble into filamentous structures exhibiting the characteristics of typical β-amyloids, similar to protein fibrils formed in Alzheimer's patients (140). It would be interesting to investigate if DAI and RIPK3 can form fibrils similar to those formed by RIPK1 and RIPK3.

To begin to investigate if DAI is involved in neurodegeneration, we obtained brain tissue from Alzheimer's patients and performed DSP crosslinking to test for presence of the same macromolecular complexes as seen in tissue culture. We were able to detect DAI-containing complexes in Alzheimer's patients at much higher levels compared to the healthy brains (Fig. 35). Furthermore, similar complexes were formed containing the stress granule protein TIA-1 only in Alzheimer's brains, implicating presence of stress granules. Finally, Tau aggregates were present only in the diseased brains. Furthermore, we have recently shown that expression of pathogenic Tau leads to RIPK3-dependent MLKL phosphorylation and neuronal death in mice (manuscript in preparation). More studies are currently being performed to demonstrate activation and execution of DAI-mediated necroptosis in Alzheimer's disease.

As described before, oxidative stress, like any other of the cellular stresses, can have detrimental effects on the cellular macromolecules: proteins, lipids, and nucleic acids (128, 130, 131). Oxidation of RNA increases its propensity to flip into the Z configuration (see Chapter 2 Discussion) (145). Referred to as damaged RNA, Z-form RNA has been detected in cells treated with arsenite before (146). Although referred to as Z-DNA-binding domains, ZBDs of DAI can bind both Z-DNA (and in a lesser degree B-DNA) and Z-RNA. The underlying cause for this phenomenon is the fact that Z-DNA and Z-RNA both exist in left-handed form and display similar structural features, unlike the right-handed DNA and RNA (79, 163, 164). In fact, DAI has been shown before to bind to RNA (and activate necroptosis), believed to be Z-RNA, produced during IAV and MCMV infections (78, 79, 85). Our hypothesis is that arsenite treatment induces Z-RNA formation that localizes to stress granules where it is bound by the DAI Zα domain,

leading to activation of RIPK3, phosphorylation of MLKL and necroptotic cell death. This hypothesis is currently under investigation using antibodies specific for 8-oxoguanine (present in damaged/oxidized RNA) (145): using co-immunoprecipitation and immunofluorescence, we are testing to see if DAI is associated with 8-oxoguanine-containing nucleic acid (Z-RNA) in cells treated with arsenite.

Existence of a Z-form RNA is now relatively well-established through structural studies (163), yet knowledge about the biological function of this type of molecule is primitive. Only a speculative function in necroptosis has been ascribed to Z-form nucleic acids based on the mutational data on DAI (76, 85). Current necroptosis studies with antibodies specific for Z-RNA would demonstrate the very first biological function of this molecule.

Necroptosis induced by VACV-E3LΔ83N, just like the arsenite-induced necroptosis, is dependent on DAI and stress granules. This might be an implication of VACV-E3LΔ83N-induced necroptosis being activated by Z-RNA as well. In fact, we were able to detect Z-NA in cells infected with VACV, but not in uninfected cells (Koehler, Cotsmire, Langland, and Jacobs, manuscript submitted). Wild-type vaccinia virus was able to inhibit necroptosis induction as no death (Fig. 19), phosphorylation of MLKL, or trimerization of MLKL (Fig. 22) was observed in cells infected with the wild-type virus. Furthermore, there was no necrosome formation in cells infected with wtVACV (Fig. 23). Wild-type VACV expresses full-length E3 protein that contains a ZBD similar to the one in DAI. It has been shown before that ZBDs of both proteins are functionally interchangeable as substituting the E3 ZBD for the one of DAI preserves the virus pathogenicity, which otherwise is absent when the ZBD is mutated or missing (84).

This indicates that during infection, E3 and DAI may compete for biding to a Z-RNA, rendering it possible for wtVACV to inhibit necroptosis induction.

Interestingly, no macromolecular complex containing G3BP1 was detected in cells infected with wtVACV (Fig. 24), indicating that wtVACV is able to inhibit formation of stress granules. This data remains consistent with previous reports of wtVACV blocking formation of granules while granules were observed in cells infected with VACV mutant lacking the E3L gene (VACV-ΔE3L) (150). This data indicates that E3 protein is involved in inhibition of SG assembly. As described before, E3 protein harbors a dsRNA-binding domain at its C terminus, and therefore can inhibit activation of PKR – one of the eIF2α kinases, activation of which leads to stress granule formation (90-92). As wtVACV can block PKR activation, it would suggest that the virus can block stress granule formation. Our current studies show that infection with VACV-E3LΔ83N leads to stress granule-dependent necroptosis. This mutant virus harbors an E3 protein with intact dsRBD and missing the entire ZBD (Fig. 5). The intact dsRBD should allow for inhibition of PKR by the mutant virus. In fact, at early times post-infection, both wtVACV and VACV-E3LΔ83N successfully block PKR activation and eIF2α phosphorylation (151). Nonetheless, at late times post-infection, VACV-E3LΔ83N fails to inhibit PKR in HeLa cells. dsRNA begins to accumulate at later times post-infection with the mutant virus (Cotsmire and Jacobs, manuscript in preparation). The mechanism behind this phenomenon is not fully understood. Therefore, VACV-E3LΔ83N might be able to inhibit PKR initially, but not at later times post-infection. We wanted to ask if inhibition of PKR is the underlying mechanism behind wtVACV-mediated inhibition of SG formation. We tested if PKR-mediated phosphorylation of eIF2α is required for

VACV-E3LΔ83N-induced necroptosis. Infection of the PKR-deficient L929 cells still led to rapid RIPK3-dependent death (Fig. 28) as well as activation of MLKL (Fig. 29), indicating that necroptosis is not dependent on PKR. It will be crucial to investigate if eIF2α phosphorylation and formation of SGs take place in PKR KO L929 cells infected with the mutant virus, which would show that VACV-E3LΔ83N-induced SG assembly is PKR-independent.

It was demonstrated before that siRNA-mediated inhibition of PKR rescued IFN resistance of VACV-E3LΔ83N in immortalized 129 MEF cells. The IFN sensitivity of the virus was also reversed in PKR-deficient 129 MEF cells. However, the virus pathogenicity was not rescued in PKR KO mice, indicating that a PKR-independent mechanism limits the mutant virus pathogenicity (95). Similarly, the VACV-E3LΔ83N replication in cells was not affected by PKR-mediated phosphorylation of eIF2α as the virus replicated in HeLa cells (151). We started asking whether necroptosis induced by VACV-E3LΔ83N (shown here to be independent of PKR) could be responsible for decreased mutant virus pathogenicity. We show that in cell culture with L929 cells, viral replication is limited in conditions of necroptosis (Fig. 36) and replication can be rescued, at least to a certain degree, by the RIPK3 inhibitor, GSK'872. Furthermore, we demonstrate activation of necroptosis in C57BL/6 mice infected intranasally with VACV-E3LΔ83N, but not in mice infected with wtVACV (Fig. 37). This data begins to explain why VACV-E3LΔ83N is not pathogenic in mice. In fact, knock-out of necroptosis proteins DAI, RIPK3, and MLKL rescued VACV-E3LΔ83N pathogenicity and IFN resistance in mice (Subramanian, Szczerba, Kibler, and Jacobs, manuscript in preparation).

It still is not fully understood why wtVACV inhibits SG formation, and therefore necroptosis, whereas VACV-E3LΔ83N does not. The only difference between these two viruses is presence or absence of the ZBD at the E3 protein N terminus (Fig. 5). In fact, the mechanism of necroptosis induction by the mutant VACV might resemble the one induced by arsenite. Poxvirus infection is known to induce oxidative stress (152). As described before, oxidative stress leads to formation of Z-form nucleic acids (145, 146). These Z-NAs can be bound by the ZBD of wtVACV E3 protein, which may inhibit formation of stress granules. The E3 protein of VACV-E3LΔ83N lacks the ZBD. Therefore, Z-NAs can be recruited to stress granules, which will recruit DAI and activate the necroptosis pathway. It is unknown if DAI itself might be required for SG assembly. Although proteins with ZBDs are known to localize to SGs, the requirement of Z-NA binding by these proteins to form granules is unknown. Nonetheless, intrinsically disordered regions (IDRs) play important roles in SG formation (19-21). The RHIM domains of RIPK1 and RIPK3 are embedded in these proteins' IDRs (140, 165, 166). Like RIPK1 and RIPK3, the RHIM domains of DAI are predicted to be embedded in an IDR region (data not shown), which might present importance of DAI in the SG assembly process. It will be interesting to see if, during wtVACV infection, wt E3 binds to a Z-NA as tested via a co-immunoprecipitation assay or immunofluorescence experiment with Z-NA-specific antibodies (145, 146). On the other hand, DAI would be expected to associate with the same nucleic acid in cells infected with the mutant virus. Furthermore, it would be crucial to test if VACV-E3LΔ83N still is able to induce necroptosis when HRI kinase is knocked out or knocked down in order to ask if induction of oxidative stress is indeed responsible for the observed cell death. Finally, if negative,

the mechanism of SG formation in cells infected with VACV-E3LΔ83N should be investigated. Phosphorylation of eIF2α is only one of three manners in which induction of formation of SGs takes place. Other pathways include:

a) inhibition of eIF4F complex assembly, including disruption of eIF4E interaction with eIF4G (sodium selenite, H_2O_2, tRNA-derived stress-induced RNAs or tiRNAs) and inhibition of the RNA helicase eIF4A function (pateamine A, hippuristanol, silvestrol, 15-deoxy-Δ(12,14)-prostaglandin J2) (27)
b) inhibition of the ubiquitin-dependent proteasome system (UPS) (Z-Leu-Leu-Leu-al or MG132, lactacystin, N-acetyl-Leu-Leu-norleucinal or MG101) (29, 30)

Looking at VACV-E3LΔ83N-mediated stress granule formation in PKR KO cells, and subsequently HRI KO cells, will be crucial. We expect for SGs to form in PKR KO, and not in HRI KO cells. If SGs form in HRI KO cells infected with the mutant virus, we will investigate the other two pathways leading to SG formation.

In the future, it would be interesting to investigate the process of SG formation, both in arsenite-treated cells and cells infected with VACV. IDRs of RBPs TIA-1/-R and G3BP1/2 participate in the process of concentrating the RNP complexes of mRNA and bound proteins (including RBPs) into stress granules (19-21, 167). Phosphorylation of serine 149 within G3BP1 IDR is responsible for regulation of G3BP1-driven SG assembly (24, 27, 99). It would be interesting to see how posttranslational modifications of IDRs of involved proteins play a role in SG formation during arsenite treatment and viral infection of cells.

The subsets of mRNAs targeted into stress granules in conditions of different cellular stresses tend to overlap, yet only to a certain degree (168). It would be interesting to perform a mass spectrometry and high-throughput sequencing analysis of granules isolated from the arsenite- and VACV-stressed cells to identify transcripts as well as proteins specifically targeted during each of the stresses into SGs (169).

Stress granules formed during infection of cells with VACV-ΔE3L have been shown to differ from canonical stress granules formed during arsenite treatment. The virally induced granules, referred to as antiviral granules (AVGs) by the authors of the study (150), did not disassemble upon treatment of cells with cycloheximide, whereas arsenite-induced stress granules did. Cycloheximide inhibits tRNA-mRNA translocation during protein synthesis, and thereby blocks the elongation step of translation. We might expect that granules formed during VACV-E3LΔ83N infection will be similar to those induced by VACV-ΔE3L, and different from arsenite-induced granules. Once again, deciphering the components of both kinds of granules might shed a light into the observed difference in behavior between SGs and AVGs.

The presented work deciphers a novel, stress granule-mediated mechanism of cell death induction. Stress granules can be the non-membraneous organelle with underappreciated role in antiviral innate immunity and human diseases. Stress granules have been shown to display an antiviral function before by sequestering viral mRNAs and proteins needed for successful infectious cycle (150). In fact, some viruses are known to block SG formation, like IAV, which is also known to induce necroptosis (170). Moreover, oxidation-driven necroptosis induction may underlie a variety of human diseases (see above). Our work offers a novel insight into host responses to poxviral

infection, demonstrates a novel mechanism of necroptosis induction and a new outcome of cellular stress. Furthermore, potential novel function for Z-form nucleic acids is suggested. Finally, our studies bring up the question about viral involvement in the onset of Alzheimer's disease as oxidation, one of the hallmarks of AD, might be caused by viral infection (171-173).

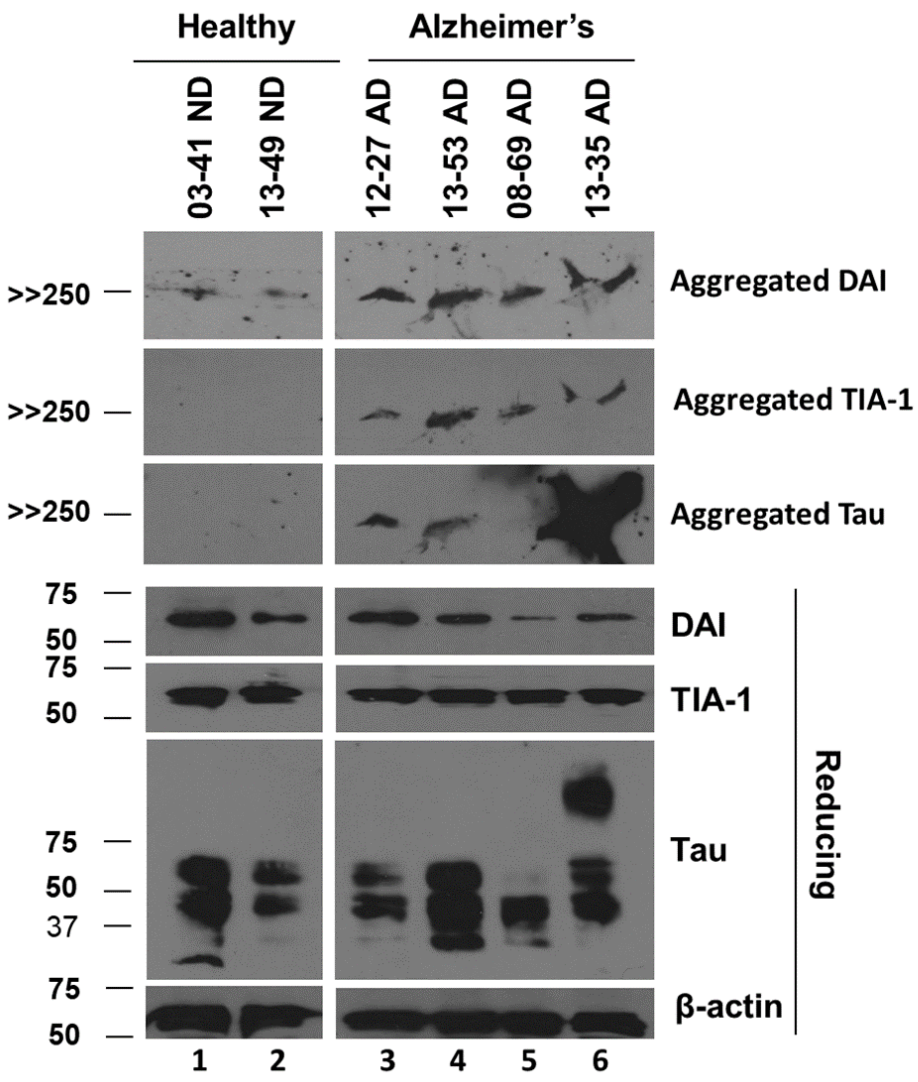

Figure 35: Activation of DAI, TIA-1 and Tau in Alzheimer's brains via DSP crosslinking. Healthy and Alzheimer's brains were homogenized in liquid nitrogen. DSP crosslinking was performed as described in Chapter 4. Formation of a high-molecular-weight complex with DAI and TIA-1, indicative of induction of necroptosis and presence of stress granules, respectively, was observed in all Alzheimer's brains and no healthy brains. Aggregation of Tau (hallmark of AD) was observed in 3 out of 4 Alzheimer's brains (lack of Tau aggregation was seen in a patient with no active Tau formation based on the reduced gel, lane 5).

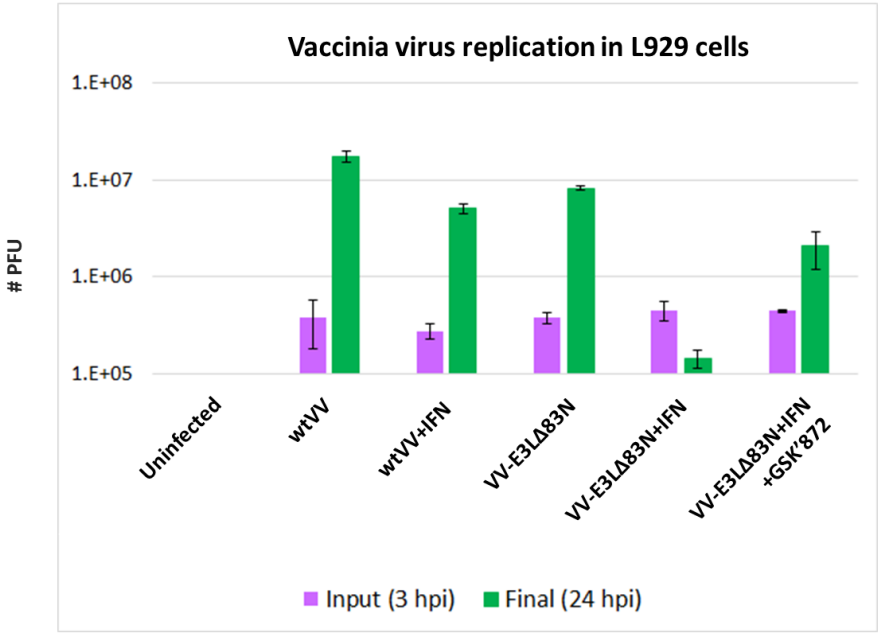

Figure 36: Programmed necrosis limits viral replication in cell culture. Confluent monolayers of mock- or IFN-primed (18 hours) L929 cells were pre-treated (1 hour) with GSK'872 or left untreated. Subsequently, the cells were infected with wtVACV, VACV-E3LΔ83N, or left uninfected. Cells were lysed at 3 and 24 hpi, and the released virus was titered in BSC40 cells. wtVACV replicated successfully regardless of the IFN treatment status. VACV-E3LΔ83N replicated in cells untreated with IFN. In conditions of necroptosis (VACV-E3LΔ83N infection of IFN-primed cells), viral replication was inhibited. Viral replication was rescued by inhibition of necroptosis by the RIPK3 inhibitor, GSK'872.

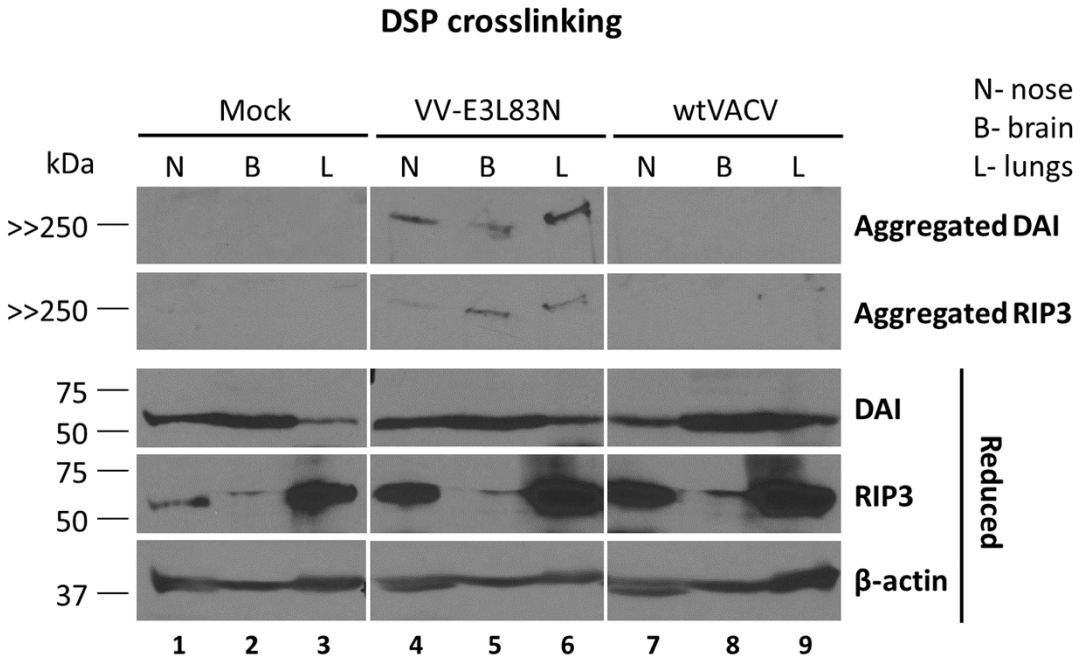

Figure 37: VACV-E3LΔ83N intranasal infection of C57BL/6 mice leads to induction of necroptosis in nose, brain, and lungs. C57BL/6 mice were infected intranasally with wtVACV, VACV-E3LΔ83N, or left uninfected. After 4 days, nose, brain, and lung tissues were collected and homogenized in liquid nitrogen. DSP crosslinking was performed as described in Chapter 4. Formation of a high-molecular-weight complex with DAI and RIPK3, indicative of necroptosis induction, was observed in all the tissues only in mice infected with the mutant virus.

REFERENCES

1. **Harding HP, Novoa I, Zhang Y, Zeng H, Wek R, Schapira M, Ron D.** 2000. Regulated translation initiation controls stress-induced gene expression in mammalian cells. Mol Cell 6:1099-108.

2. **Wek RC, Jiang HY, Anthony TG.** 2006. Coping with stress: eIF2 kinases and translational control. Biochem Soc Trans 34:7-11.

3. **Donnelly N, Gorman AM, Gupta S, Samali A.** 2013. The eIF2α kinases: their structures and functions. Cell Mol Life Sci 70:3493-511.

4. **Chen JJ.** 2007. Regulation of protein synthesis by the heme-regulated eIF2alpha kinase: relevance to anemias. Blood 109:2693-9.

5. **Lu L, Han AP, Chen JJ.** 2001. Translation initiation control by heme-regulated eukaryotic initiation factor 2alpha kinase in erythroid cells under cytoplasmic stresses. Mol Cell Biol 21:7971-80.

6. **Meurs E, Chong K, Galabru J, Thomas NS, Kerr IM, Williams BR, Hovanessian AG.** 1990. Molecular cloning and characterization of the human double-stranded RNA-activated protein kinase induced by interferon. Cell 62:379-90.

7. **Williams BR.** 1999. PKR; a sentinel kinase for cellular stress. Oncogene 18:6112-20.

8. **Harding HP, Zhang Y, Bertolotti A, Zeng H, Ron D.** 2000. Perk is essential for translational regulation and cell survival during the unfolded protein response. Mol Cell 5:897-904.

9. **Harding HP, Zhang Y, Ron D.** 1999. Protein translation and folding are coupled by an endoplasmic-reticulum-resident kinase. Nature 397:271-274.

10. **Deval C, Chaveroux C, Maurin AC, Cherasse Y, Parry L, Carraro V, Milenkovic D, Ferrara M, Bruhat A, Jousse C, Fafournoux P.** 2009. Amino acid limitation regulates the expression of genes involved in several specific biological processes through GCN2-dependent and GCN2-independent pathways. Febs j 276:707-18.

11. **Grallert B, Boye E.** 2007. The Gcn2 kinase as a cell cycle regulator. Cell Cycle 6:2768-72.

12. **Asano K, Clayton J, Shalev A, Hinnebusch AG.** 2000. A multifactor complex of eukaryotic initiation factors, eIF1, eIF2, eIF3, eIF5, and initiator tRNA(Met) is an important translation initiation intermediate in vivo. Genes Dev 14:2534-46.

13. **Dever TE.** 2002. Gene-specific regulation by general translation factors. Cell 108:545-56.

14. **Sudhakar A, Ramachandran A, Ghosh S, Hasnain SE, Kaufman RJ, Ramaiah KV.** 2000. Phosphorylation of serine 51 in initiation factor 2 alpha (eIF2 alpha) promotes complex formation between eIF2 alpha(P) and eIF2B and causes inhibition in the guanine nucleotide exchange activity of eIF2B. Biochemistry 39:12929-38.

15. **Kedersha N, Chen S, Gilks N, Li W, Miller IJ, Stahl J, Anderson P.** 2002. Evidence that ternary complex (eIF2-GTP-tRNA(i)(Met))-deficient preinitiation complexes are core constituents of mammalian stress granules. Mol Biol Cell 13:195-210.

16. **Sanders DW, Kedersha N, Lee DSW, Strom AR, Drake V, Riback JA, Bracha D, Eeftens JM, Iwanicki A, Wang A, Wei MT, Whitney G, Lyons SM, Anderson P, Jacobs WM, Ivanov P, Brangwynne CP.** 2020. Competing Protein-RNA Interaction Networks Control Multiphase Intracellular Organization. Cell 181:306-324.e28.

17. **Van Treeck B, Protter DSW, Matheny T, Khong A, Link CD, Parker R.** 2018. RNA self-assembly contributes to stress granule formation and defining the stress granule transcriptome. Proc Natl Acad Sci U S A 115:2734-2739.

18. **Youn JY, Dunham WH, Hong SJ, Knight JDR, Bashkurov M, Chen GI, Bagci H, Rathod B, MacLeod G, Eng SWM, Angers S, Morris Q, Fabian M, Côté JF, Gingras AC.** 2018. High-Density Proximity Mapping Reveals the Subcellular Organization of mRNA-Associated Granules and Bodies. Mol Cell 69:517-532.e11.

19. **Brangwynne CP.** 2013. Phase transitions and size scaling of membrane-less organelles. J Cell Biol 203:875-81.

20. **Keating CD.** 2012. Aqueous phase separation as a possible route to compartmentalization of biological molecules. Acc Chem Res 45:2114-24.

21. **Nott TJ, Petsalaki E, Farber P, Jervis D, Fussner E, Plochowietz A, Craggs TD, Bazett-Jones DP, Pawson T, Forman-Kay JD, Baldwin AJ.** 2015. Phase transition of a disordered nuage protein generates environmentally responsive membraneless organelles. Mol Cell 57:936-947.

22. **Tompa P.** 2005. The interplay between structure and function in intrinsically unstructured proteins. FEBS Lett 579:3346-54.

23. **Gilks N, Kedersha N, Ayodele M, Shen L, Stoecklin G, Dember LM, Anderson P.** 2004. Stress granule assembly is mediated by prion-like aggregation of TIA-1. Mol Biol Cell 15:5383-98.

24. **Tourrière H, Chebli K, Zekri L, Courselaud B, Blanchard JM, Bertrand E, Tazi J.** 2003. The RasGAP-associated endoribonuclease G3BP assembles stress granules. J Cell Biol 160:823-31.

25. **Kahvejian A, Svitkin YV, Sukarieh R, M'Boutchou MN, Sonenberg N.** 2005. Mammalian poly(A)-binding protein is a eukaryotic translation initiation factor, which acts via multiple mechanisms. Genes Dev 19:104-13.

26. **Tarun SZ, Jr., Sachs AB.** 1995. A common function for mRNA 5' and 3' ends in translation initiation in yeast. Genes Dev 9:2997-3007.

27. **Panas MD, Ivanov P, Anderson P.** 2016. Mechanistic insights into mammalian stress granule dynamics. J Cell Biol 215:313-323.

28. **Sonenberg N, Hinnebusch AG.** 2009. Regulation of translation initiation in eukaryotes: mechanisms and biological targets. Cell 136:731-45.

29. **Jiang HY, Wek RC.** 2005. Phosphorylation of the alpha-subunit of the eukaryotic initiation factor-2 (eIF2alpha) reduces protein synthesis and enhances apoptosis in response to proteasome inhibition. J Biol Chem 280:14189-202.

30. **Mazroui R, Di Marco S, Kaufman RJ, Gallouzi IE.** 2007. Inhibition of the ubiquitin-proteasome system induces stress granule formation. Mol Biol Cell 18:2603-18.

31. **Banani SF, Lee HO, Hyman AA, Rosen MK.** 2017. Biomolecular condensates: organizers of cellular biochemistry. Nat Rev Mol Cell Biol 18:285-298.

32. **Jain S, Wheeler JR, Walters RW, Agrawal A, Barsic A, Parker R.** 2016. ATPase-Modulated Stress Granules Contain a Diverse Proteome and Substructure. Cell 164:487-98.

33. **Cougot N, Babajko S, Séraphin B.** 2004. Cytoplasmic foci are sites of mRNA decay in human cells. J Cell Biol 165:31-40.

34. **Kedersha N, Cho MR, Li W, Yacono PW, Chen S, Gilks N, Golan DE, Anderson P.** 2000. Dynamic shuttling of TIA-1 accompanies the recruitment of mRNA to mammalian stress granules. J Cell Biol 151:1257-68.

35. **Jiang HY, Wek SA, McGrath BC, Lu D, Hai T, Harding HP, Wang X, Ron D, Cavener DR, Wek RC.** 2004. Activating transcription factor 3 is integral to the eukaryotic initiation factor 2 kinase stress response. Mol Cell Biol 24:1365-77.

36. **Marciniak SJ, Yun CY, Oyadomari S, Novoa I, Zhang Y, Jungreis R, Nagata K, Harding HP, Ron D.** 2004. CHOP induces death by promoting protein synthesis and oxidation in the stressed endoplasmic reticulum. Genes Dev 18:3066-77.

37. **Jiang HY, Wek SA, McGrath BC, Scheuner D, Kaufman RJ, Cavener DR, Wek RC.** 2003. Phosphorylation of the alpha subunit of eukaryotic initiation factor 2 is required for activation of NF-kappaB in response to diverse cellular stresses. Mol Cell Biol 23:5651-63.

38. **Brush MH, Weiser DC, Shenolikar S.** 2003. Growth Arrest and DNA Damage-Inducible Protein GADD34 Targets Protein Phosphatase 1α to the Endoplasmic Reticulum and Promotes Dephosphorylation of the α Subunit of Eukaryotic Translation Initiation Factor 2. Molecular and Cellular Biology 23:1292-1303.

39. **Lockshin RA, Williams CM.** 1964. Programmed cell death—II. Endocrine potentiation of the breakdown of the intersegmental muscles of silkmoths. Journal of Insect Physiology 10:643-649.

40. **Fuchs Y, Steller H.** 2011. Programmed cell death in animal development and disease. Cell 147:742-58.

41. **Yuan J, Kroemer G.** 2010. Alternative cell death mechanisms in development and beyond. Genes Dev 24:2592-602.

42. **Duprez L, Wirawan E, Vanden Berghe T, Vandenabeele P.** 2009. Major cell death pathways at a glance. Microbes Infect 11:1050-62.

43. **Kerr JF, Wyllie AH, Currie AR.** 1972. Apoptosis: a basic biological phenomenon with wide-ranging implications in tissue kinetics. Br J Cancer 26:239-57.

44. **Fuentes-Prior P, Salvesen GS.** 2004. The protein structures that shape caspase activity, specificity, activation and inhibition. Biochem J 384:201-32.

45. **Thornberry NA, Lazebnik Y.** 1998. Caspases: enemies within. Science 281:1312-6.

46. **Youle RJ, Strasser A.** 2008. The BCL-2 protein family: opposing activities that mediate cell death. Nat Rev Mol Cell Biol 9:47-59.

47. **Riedl SJ, Salvesen GS.** 2007. The apoptosome: signalling platform of cell death. Nat Rev Mol Cell Biol 8:405-13.

48. **Peter ME, Krammer PH.** 2003. The CD95(APO-1/Fas) DISC and beyond. Cell Death Differ 10:26-35.

49. **Chipuk JE, Bouchier-Hayes L, Green DR.** 2006. Mitochondrial outer membrane permeabilization during apoptosis: the innocent bystander scenario. Cell Death Differ 13:1396-402.

50. **Boatright KM, Salvesen GS.** 2003. Mechanisms of caspase activation. Curr Opin Cell Biol 15:725-31.

51. **Bergsbaken T, Fink SL, Cookson BT.** 2009. Pyroptosis: host cell death and inflammation. Nat Rev Microbiol 7:99-109.

52. **Lamkanfi M, Dixit VM.** 2010. Manipulation of host cell death pathways during microbial infections. Cell Host Microbe 8:44-54.

53. **Galluzzi L, Vitale I, Aaronson SA, Abrams JM, Adam D, Agostinis P, Alnemri ES, Altucci L, Amelio I, Andrews DW, Annicchiarico-Petruzzelli M, Antonov AV, Arama E, Baehrecke EH, Barlev NA, Bazan NG, Bernassola F, Bertrand MJM, Bianchi K, Blagosklonny MV, Blomgren K, Borner C, Boya P, Brenner C, Campanella M, Candi E, Carmona-Gutierrez D, Cecconi F, Chan FK, Chandel NS, Cheng EH, Chipuk JE, Cidlowski JA, Ciechanover A, Cohen GM, Conrad M, Cubillos-Ruiz JR, Czabotar PE, D'Angiolella V, Dawson TM, Dawson VL, De Laurenzi V, De Maria R, Debatin KM, DeBerardinis RJ, Deshmukh M, Di Daniele N, Di Virgilio F, Dixit VM, Dixon SJ, et al.** 2018. Molecular mechanisms of cell death: recommendations of the Nomenclature Committee on Cell Death 2018. Cell Death Differ 25:486-541.

54. **Vanlangenakker N, Vanden Berghe T, Krysko DV, Festjens N, Vandenabeele P.** 2008. Molecular mechanisms and pathophysiology of necrotic cell death. Curr Mol Med 8:207-20.

55. **Moriwaki K, Chan FK.** 2013. RIP3: a molecular switch for necrosis and inflammation. Genes Dev 27:1640-9.

56. **Dondelinger Y, Aguileta MA, Goossens V, Dubuisson C, Grootjans S, Dejardin E, Vandenabeele P, Bertrand MJ.** 2013. RIPK3 contributes to TNFR1-mediated RIPK1 kinase-dependent apoptosis in conditions of cIAP1/2 depletion or TAK1 kinase inhibition. Cell Death Differ 20:1381-92.

57. **Micheau O, Tschopp J.** 2003. Induction of TNF receptor I-mediated apoptosis via two sequential signaling complexes. Cell 114:181-90.

58. **Mahoney DJ, Cheung HH, Mrad RL, Plenchette S, Simard C, Enwere E, Arora V, Mak TW, Lacasse EC, Waring J, Korneluk RG.** 2008. Both cIAP1 and cIAP2 regulate TNFalpha-mediated NF-kappaB activation. Proc Natl Acad Sci U S A 105:11778-83.

59. **Moquin D, Chan FK.** 2010. The molecular regulation of programmed necrotic cell injury. Trends Biochem Sci 35:434-41.

60. **Wu XN, Yang ZH, Wang XK, Zhang Y, Wan H, Song Y, Chen X, Shao J, Han J.** 2014. Distinct roles of RIP1-RIP3 hetero- and RIP3-RIP3 homo-interaction in mediating necroptosis. Cell Death Differ 21:1709-20.

61. **Sun L, Wang H, Wang Z, He S, Chen S, Liao D, Wang L, Yan J, Liu W, Lei X, Wang X.** 2012. Mixed lineage kinase domain-like protein mediates necrosis signaling downstream of RIP3 kinase. Cell 148:213-27.

62. **Wang H, Sun L, Su L, Rizo J, Liu L, Wang LF, Wang FS, Wang X.** 2014. Mixed lineage kinase domain-like protein MLKL causes necrotic membrane disruption upon phosphorylation by RIP3. Mol Cell 54:133-146.

63. **Dondelinger Y, Declercq W, Montessuit S, Roelandt R, Goncalves A, Bruggeman I, Hulpiau P, Weber K, Sehon CA, Marquis RW, Bertin J, Gough PJ, Savvides S, Martinou JC, Bertrand MJ, Vandenabeele P.** 2014. MLKL compromises plasma membrane integrity by binding to phosphatidylinositol phosphates. Cell Rep 7:971-81.

64. **Dovey CM, Diep J, Clarke BP, Hale AT, McNamara DE, Guo H, Brown NW, Jr., Cao JY, Grace CR, Gough PJ, Bertin J, Dixon SJ, Fiedler D, Mocarski ES, Kaiser WJ, Moldoveanu T, York JD, Carette JE.** 2018. MLKL Requires the Inositol Phosphate Code to Execute Necroptosis. Mol Cell 70:936-948.e7.

65. **Najafov A, Mookhtiar AK, Luu HS, Ordureau A, Pan H, Amin PP, Li Y, Lu Q, Yuan J.** 2019. TAM Kinases Promote Necroptosis by Regulating Oligomerization of MLKL. Mol Cell 75:457-468.e4.

66. **Rodriguez DA, Weinlich R, Brown S, Guy C, Fitzgerald P, Dillon CP, Oberst A, Quarato G, Low J, Cripps JG, Chen T, Green DR.** 2016. Characterization of RIPK3-mediated phosphorylation of the activation loop of MLKL during necroptosis. Cell Death Differ 23:76-88.

67. **Tanzer MC, Tripaydonis A, Webb AI, Young SN, Varghese LN, Hall C, Alexander WS, Hildebrand JM, Silke J, Murphy JM.** 2015. Necroptosis signalling is tuned by phosphorylation of MLKL residues outside the pseudokinase domain activation loop. Biochem J 471:255-65.

68. **Cai Z, Jitkaew S, Zhao J, Chiang HC, Choksi S, Liu J, Ward Y, Wu LG, Liu ZG.** 2014. Plasma membrane translocation of trimerized MLKL protein is required for TNF-induced necroptosis. Nat Cell Biol 16:55-65.

69. **Chen X, Li W, Ren J, Huang D, He WT, Song Y, Yang C, Li W, Zheng X, Chen P, Han J.** 2014. Translocation of mixed lineage kinase domain-like protein to plasma membrane leads to necrotic cell death. Cell Res 24:105-21.

70. **Hildebrand JM, Tanzer MC, Lucet IS, Young SN, Spall SK, Sharma P, Pierotti C, Garnier JM, Dobson RC, Webb AI, Tripaydonis A, Babon JJ, Mulcair MD, Scanlon MJ, Alexander WS, Wilks AF, Czabotar PE, Lessene G, Murphy JM, Silke J.** 2014. Activation of the pseudokinase MLKL unleashes the four-helix bundle domain to induce membrane localization and necroptotic cell death. Proc Natl Acad Sci U S A 111:15072-7.

71. **Su L, Quade B, Wang H, Sun L, Wang X, Rizo J.** 2014. A plug release mechanism for membrane permeation by MLKL. Structure 22:1489-500.

72. **He S, Liang Y, Shao F, Wang X.** 2011. Toll-like receptors activate programmed necrosis in macrophages through a receptor-interacting kinase-3-mediated pathway. Proc Natl Acad Sci U S A 108:20054-9.

73. **Kaiser WJ, Sridharan H, Huang C, Mandal P, Upton JW, Gough PJ, Sehon CA, Marquis RW, Bertin J, Mocarski ES.** 2013. Toll-like receptor 3-mediated necrosis via TRIF, RIP3, and MLKL. J Biol Chem 288:31268-79.

74. **Guo H, Omoto S, Harris PA, Finger JN, Bertin J, Gough PJ, Kaiser WJ, Mocarski ES.** 2015. Herpes simplex virus suppresses necroptosis in human cells. Cell Host Microbe 17:243-51.

75. **Koehler H, Cotsmire S, Langland J, Kibler KV, Kalman D, Upton JW, Mocarski ES, Jacobs BL.** 2017. Inhibition of DAI-dependent necroptosis by the Z-DNA binding domain of the vaccinia virus innate immune evasion protein, E3. Proc Natl Acad Sci U S A 114:11506-11511.

76. **Sridharan H, Ragan KB, Guo H, Gilley RP, Landsteiner VJ, Kaiser WJ, Upton JW.** 2017. Murine cytomegalovirus IE3-dependent transcription is required for DAI/ZBP1-mediated necroptosis. EMBO Rep 18:1429-1441.

77. **Upton JW, Kaiser WJ, Mocarski ES.** 2012. DAI/ZBP1/DLM-1 complexes with RIP3 to mediate virus-induced programmed necrosis that is targeted by murine cytomegalovirus vIRA. Cell Host Microbe 11:290-7.

78. **Kuriakose T, Man SM, Malireddi RK, Karki R, Kesavardhana S, Place DE, Neale G, Vogel P, Kanneganti TD.** 2016. ZBP1/DAI is an innate sensor of influenza virus triggering the NLRP3 inflammasome and programmed cell death pathways. Sci Immunol 1.

79. **Thapa RJ, Ingram JP, Ragan KB, Nogusa S, Boyd DF, Benitez AA, Sridharan H, Kosoff R, Shubina M, Landsteiner VJ, Andrake M, Vogel P, Sigal LJ, tenOever BR, Thomas PG, Upton JW, Balachandran S.** 2016. DAI Senses Influenza A Virus Genomic RNA and Activates RIPK3-Dependent Cell Death. Cell Host Microbe 20:674-681.

80. **Fu Y, Comella N, Tognazzi K, Brown LF, Dvorak HF, Kocher O.** 1999. Cloning of DLM-1, a novel gene that is up-regulated in activated macrophages, using RNA differential display. Gene 240:157-63.

81. **Takaoka A, Wang Z, Choi MK, Yanai H, Negishi H, Ban T, Lu Y, Miyagishi M, Kodama T, Honda K, Ohba Y, Taniguchi T.** 2007. DAI (DLM-1/ZBP1) is a cytosolic DNA sensor and an activator of innate immune response. Nature 448:501-5.

82. **Deigendesch N, Koch-Nolte F, Rothenburg S.** 2006. ZBP1 subcellular localization and association with stress granules is controlled by its Z-DNA binding domains. Nucleic Acids Res 34:5007-20.

83. **Kaiser WJ, Upton JW, Mocarski ES.** 2008. Receptor-interacting protein homotypic interaction motif-dependent control of NF-kappa B activation via the DNA-dependent activator of IFN regulatory factors. J Immunol 181:6427-34.

84. **Kim YG, Muralinath M, Brandt T, Pearcy M, Hauns K, Lowenhaupt K, Jacobs BL, Rich A.** 2003. A role for Z-DNA binding in vaccinia virus pathogenesis. Proc Natl Acad Sci U S A 100:6974-9.

85. **Maelfait J, Liverpool L, Bridgeman A, Ragan KB, Upton JW, Rehwinkel J.** 2017. Sensing of viral and endogenous RNA by ZBP1/DAI induces necroptosis. Embo j 36:2529-2543.

86. **McFadden G.** 2005. Poxvirus tropism. Nat Rev Microbiol 3:201-13.

87. **Moss B.** 2013. Poxvirus DNA replication. Cold Spring Harb Perspect Biol 5.

88. **Seet BT, Johnston JB, Brunetti CR, Barrett JW, Everett H, Cameron C, Sypula J, Nazarian SH, Lucas A, McFadden G.** 2003. Poxviruses and immune evasion. Annu Rev Immunol 21:377-423.

89. **Brandt TA, Jacobs BL.** 2001. Both carboxy- and amino-terminal domains of the vaccinia virus interferon resistance gene, E3L, are required for pathogenesis in a mouse model. J Virol 75:850-6.

90. **Chang HW, Jacobs BL.** 1993. Identification of a conserved motif that is necessary for binding of the vaccinia virus E3L gene products to double-stranded RNA. Virology 194:537-47.

91. **Chang HW, Watson JC, Jacobs BL.** 1992. The E3L gene of vaccinia virus encodes an inhibitor of the interferon-induced, double-stranded RNA-dependent protein kinase. Proc Natl Acad Sci U S A 89:4825-9.

92. **Rivas C, Gil J, Mělková Z, Esteban M, Díaz-Guerra M.** 1998. Vaccinia virus E3L protein is an inhibitor of the interferon (i.f.n.)-induced 2-5A synthetase enzyme. Virology 243:406-14.

93. **Iordanov MS, Paranjape JM, Zhou A, Wong J, Williams BR, Meurs EF, Silverman RH, Magun BE.** 2000. Activation of p38 mitogen-activated protein kinase and c-Jun NH(2)-terminal kinase by double-stranded RNA and encephalomyocarditis virus: involvement of RNase L, protein kinase R, and alternative pathways. Mol Cell Biol 20:617-27.

94. **Chang HW, Uribe LH, Jacobs BL.** 1995. Rescue of vaccinia virus lacking the E3L gene by mutants of E3L. J Virol 69:6605-8.

95. **White SD, Jacobs BL.** 2012. The amino terminus of the vaccinia virus E3 protein is necessary to inhibit the interferon response. J Virol 86:5895-904.

96. **Liu Z, Lv Y, Zhao N, Guan G, Wang J.** 2015. Protein kinase R-like ER kinase and its role in endoplasmic reticulum stress-decided cell fate. Cell Death Dis 6:e1822.

97. **McEwen E, Kedersha N, Song B, Scheuner D, Gilks N, Han A, Chen JJ, Anderson P, Kaufman RJ.** 2005. Heme-regulated inhibitor kinase-mediated phosphorylation of eukaryotic translation initiation factor 2 inhibits translation, induces stress granule formation, and mediates survival upon arsenite exposure. J Biol Chem 280:16925-33.

98. **Wek SA, Zhu S, Wek RC.** 1995. The histidyl-tRNA synthetase-related sequence in the eIF-2 alpha protein kinase GCN2 interacts with tRNA and is required for activation in response to starvation for different amino acids. Mol Cell Biol 15:4497-506.

99. **Kedersha N, Panas MD, Achorn CA, Lyons S, Tisdale S, Hickman T, Thomas M, Lieberman J, McInerney GM, Ivanov P, Anderson P.** 2016. G3BP-Caprin1-USP10 complexes mediate stress granule condensation and associate with 40S subunits. J Cell Biol 212:845-60.

100. **Kedersha NL, Gupta M, Li W, Miller I, Anderson P.** 1999. RNA-binding proteins TIA-1 and TIAR link the phosphorylation of eIF-2 alpha to the assembly of mammalian stress granules. J Cell Biol 147:1431-42.

101. **Solomon S, Xu Y, Wang B, David MD, Schubert P, Kennedy D, Schrader JW.** 2007. Distinct structural features of caprin-1 mediate its interaction with G3BP-1 and its induction of phosphorylation of eukaryotic translation initiation factor 2alpha, entry to cytoplasmic stress granules, and selective interaction with a subset of mRNAs. Mol Cell Biol 27:2324-42.

102. **Anderson P, Kedersha N.** 2009. RNA granules: post-transcriptional and epigenetic modulators of gene expression. Nat Rev Mol Cell Biol 10:430-6.

103. **Kedersha N, Anderson P.** 2009. Regulation of translation by stress granules and processing bodies. Prog Mol Biol Transl Sci 90:155-85.

104. **Thomas MG, Loschi M, Desbats MA, Boccaccio GL.** 2011. RNA granules: the good, the bad and the ugly. Cell Signal 23:324-34.

105. **Krysko DV, Vanden Berghe T, Parthoens E, D'Herde K, Vandenabeele P.** 2008. Methods for distinguishing apoptotic from necrotic cells and measuring their clearance. Methods Enzymol 442:307-41.

106. **D'Arcy MS.** 2019. Cell death: a review of the major forms of apoptosis, necrosis and autophagy. Cell Biol Int 43:582-592.

107. **Shi J, Gao W, Shao F.** 2017. Pyroptosis: Gasdermin-Mediated Programmed Necrotic Cell Death. Trends Biochem Sci 42:245-254.

108. **Vanden Berghe T, Linkermann A, Jouan-Lanhouet S, Walczak H, Vandenabeele P.** 2014. Regulated necrosis: the expanding network of non-apoptotic cell death pathways. Nat Rev Mol Cell Biol 15:135-47.

109. **Cho YS, Challa S, Moquin D, Genga R, Ray TD, Guildford M, Chan FK.** 2009. Phosphorylation-driven assembly of the RIP1-RIP3 complex regulates programmed necrosis and virus-induced inflammation. Cell 137:1112-23.

110. **He S, Wang L, Miao L, Wang T, Du F, Zhao L, Wang X.** 2009. Receptor interacting protein kinase-3 determines cellular necrotic response to TNF-alpha. Cell 137:1100-11.

111. **Holler N, Zaru R, Micheau O, Thome M, Attinger A, Valitutti S, Bodmer JL, Schneider P, Seed B, Tschopp J.** 2000. Fas triggers an alternative, caspase-8-independent cell death pathway using the kinase RIP as effector molecule. Nat Immunol 1:489-95.

112. **Vercammen D, Beyaert R, Denecker G, Goossens V, Van Loo G, Declercq W, Grooten J, Fiers W, Vandenabeele P.** 1998. Inhibition of caspases increases the sensitivity of L929 cells to necrosis mediated by tumor necrosis factor. J Exp Med 187:1477-85.

113. **Zhang DW, Shao J, Lin J, Zhang N, Lu BJ, Lin SC, Dong MQ, Han J.** 2009. RIP3, an energy metabolism regulator that switches TNF-induced cell death from apoptosis to necrosis. Science 325:332-6.

114. **Hsu H, Huang J, Shu HB, Baichwal V, Goeddel DV.** 1996. TNF-dependent recruitment of the protein kinase RIP to the TNF receptor-1 signaling complex. Immunity 4:387-96.

115. **Dhuriya YK, Sharma D.** 2018. Necroptosis: a regulated inflammatory mode of cell death. J Neuroinflammation 15:199.

116. **Yang D, Liang Y, Zhao S, Ding Y, Zhuang Q, Shi Q, Ai T, Wu SQ, Han J.** 2020. ZBP1 mediates interferon-induced necroptosis. Cell Mol Immunol 17:356-368.

117. **Rebsamen M, Heinz LX, Meylan E, Michallet MC, Schroder K, Hofmann K, Vazquez J, Benedict CA, Tschopp J.** 2009. DAI/ZBP1 recruits RIP1 and RIP3 through RIP homotypic interaction motifs to activate NF-kappaB. EMBO Rep 10:916-22.

118. **Ng SK, Weissbach R, Ronson GE, Scadden AD.** 2013. Proteins that contain a functional Z-DNA-binding domain localize to cytoplasmic stress granules. Nucleic Acids Res 41:9786-99.

119. **Ofengeim D, Ito Y, Najafov A, Zhang Y, Shan B, DeWitt JP, Ye J, Zhang X, Chang A, Vakifahmetoglu-Norberg H, Geng J, Py B, Zhou W, Amin P, Berlink Lima J, Qi C, Yu Q, Trapp B, Yuan J.** 2015. Activation of necroptosis in multiple sclerosis. Cell Rep 10:1836-49.

120. **Ash PE, Vanderweyde TE, Youmans KL, Apicco DJ, Wolozin B.** 2014. Pathological stress granules in Alzheimer's disease. Brain Res 1584:52-8.

121. **Wolozin B, Ivanov P.** 2019. Stress granules and neurodegeneration. Nat Rev Neurosci 20:649-666.

122. **Lutz MMt, Worth MP, Hinchman MM, Parker JSL, Ledgerwood ED.** 2019. Mammalian orthoreovirus Infection is Enhanced in Cells Pre-Treated with Sodium Arsenite. Viruses 11.

123. **Matsumoto M, Funami K, Tatematsu M, Azuma M, Seya T.** 2014. Assessment of the Toll-like receptor 3 pathway in endosomal signaling. Methods Enzymol 535:149-65.

124. **Vaure C, Liu Y.** 2014. A comparative review of toll-like receptor 4 expression and functionality in different animal species. Front Immunol 5:316.

125. **Zhang J, Yang Y, He W, Sun L.** 2016. Necrosome core machinery: MLKL. Cell Mol Life Sci 73:2153-63.

126. **Coupienne I, Fettweis G, Piette J.** 2011. RIP3 expression induces a death profile change in U2OS osteosarcoma cells after 5-ALA-PDT. Lasers Surg Med 43:557-64.

127. **Stöhr N, Lederer M, Reinke C, Meyer S, Hatzfeld M, Singer RH, Hüttelmaier S.** 2006. ZBP1 regulates mRNA stability during cellular stress. J Cell Biol 175:527-34.

128. **Davies KJ.** 1995. Oxidative stress: the paradox of aerobic life. Biochem Soc Symp 61:1-31.

129. **Fridovich I.** 1978. The biology of oxygen radicals. Science 201:875-80.

130. **Kerr ME, Bender CM, Monti EJ.** 1996. An introduction to oxygen free radicals. Heart Lung 25:200-9; quiz 210-1.

131. **Martinez-Cayuela M.** 1995. Oxygen free radicals and human disease. Biochimie 77:147-61.

132. **Di Meo S, Venditti P.** 2020. Evolution of the Knowledge of Free Radicals and Other Oxidants. Oxid Med Cell Longev 2020:9829176.

133. **Su Z, Yang Z, Xie L, DeWitt JP, Chen Y.** 2016. Cancer therapy in the necroptosis era. Cell Death Differ 23:748-56.

134. **Zhang T, Zhang Y, Cui M, Jin L, Wang Y, Lv F, Liu Y, Zheng W, Shang H, Zhang J, Zhang M, Wu H, Guo J, Zhang X, Hu X, Cao CM, Xiao RP.** 2016. CaMKII is a RIP3 substrate mediating ischemia- and oxidative stress-induced myocardial necroptosis. Nat Med 22:175-82.

135. **Zhe-Wei S, Li-Sha G, Yue-Chun L.** 2018. The Role of Necroptosis in Cardiovascular Disease. Front Pharmacol 9:721.

136. **Roychowdhury S, McMullen MR, Pisano SG, Liu X, Nagy LE.** 2013. Absence of receptor interacting protein kinase 3 prevents ethanol-induced liver injury. Hepatology 57:1773-83.

137. **Royce GH, Brown-Borg HM, Deepa SS.** 2019. The potential role of necroptosis in inflammaging and aging. Geroscience 41:795-811.

138. **Sridharan H, Upton JW.** 2014. Programmed necrosis in microbial pathogenesis. Trends Microbiol 22:199-207.

139. **Roy ER, Wang B, Wan YW, Chiu G, Cole A, Yin Z, Propson NE, Xu Y, Jankowsky JL, Liu Z, Lee VM, Trojanowski JQ, Ginsberg SD, Butovsky O, Zheng H, Cao W.** 2020. Type I interferon response drives neuroinflammation and synapse loss in Alzheimer disease. J Clin Invest 130:1912-1930.

140. **Li J, McQuade T, Siemer AB, Napetschnig J, Moriwaki K, Hsiao YS, Damko E, Moquin D, Walz T, McDermott A, Chan FK, Wu H.** 2012. The RIP1/RIP3 necrosome forms a functional amyloid signaling complex required for programmed necrosis. Cell 150:339-50.

141. **Gouras GK, Olsson TT, Hansson O.** 2015. beta-Amyloid peptides and amyloid plaques in Alzheimer's disease. Neurotherapeutics 12:3-11.

142. **Scheltens P, Blennow K, Breteler MM, de Strooper B, Frisoni GB, Salloway S, Van der Flier WM.** 2016. Alzheimer's disease. Lancet 388:505-17.

143. **Vanlangenakker N, Vanden Berghe T, Bogaert P, Laukens B, Zobel K, Deshayes K, Vucic D, Fulda S, Vandenabeele P, Bertrand MJ.** 2011. cIAP1 and TAK1 protect cells from TNF-induced necrosis by preventing RIP1/RIP3-dependent reactive oxygen species production. Cell Death Differ 18:656-65.

144. **Zhang Y, Su SS, Zhao S, Yang Z, Zhong CQ, Chen X, Cai Q, Yang ZH, Huang D, Wu R, Han J.** 2017. RIP1 autophosphorylation is promoted by mitochondrial ROS and is essential for RIP3 recruitment into necrosome. Nat Commun 8:14329.

145. **Kong Q, Lin CL.** 2010. Oxidative damage to RNA: mechanisms, consequences, and diseases. Cell Mol Life Sci 67:1817-29.

146. **Zhan Y, Dhaliwal JS, Adjibade P, Uniacke J, Mazroui R, Zerges W.** 2015. Localized control of oxidized RNA. J Cell Sci 128:4210-9.

147. **Nie B, Gan W, Shi F, Hu GX, Chen LG, Hayakawa H, Sekiguchi M, Cai JP.** 2013. Age-dependent accumulation of 8-oxoguanine in the DNA and RNA in various rat tissues. Oxid Med Cell Longev 2013:303181.

148. **Nunomura A, Hofer T, Moreira PI, Castellani RJ, Smith MA, Perry G.** 2009. RNA oxidation in Alzheimer disease and related neurodegenerative disorders. Acta Neuropathol 118:151-66.

149. **Chautan M, Chazal G, Cecconi F, Gruss P, Golstein P.** 1999. Interdigital cell death can occur through a necrotic and caspase-independent pathway. Curr Biol 9:967-70.

150. **Simpson-Holley M, Kedersha N, Dower K, Rubins KH, Anderson P, Hensley LE, Connor JH.** 2011. Formation of antiviral cytoplasmic granules during orthopoxvirus infection. J Virol 85:1581-93.

151. **Langland JO, Jacobs BL.** 2004. Inhibition of PKR by vaccinia virus: role of the N- and C-terminal domains of E3L. Virology 324:419-29.

152. **Teoh ML, Turner PV, Evans DH.** 2005. Tumorigenic poxviruses up-regulate intracellular superoxide to inhibit apoptosis and promote cell proliferation. J Virol 79:5799-811.

153. **Bonnet MC, Preukschat D, Welz PS, van Loo G, Ermolaeva MA, Bloch W, Haase I, Pasparakis M.** 2011. The adaptor protein FADD protects epidermal keratinocytes from necroptosis in vivo and prevents skin inflammation. Immunity 35:572-82.

154. **Hanus J, Anderson C, Wang S.** 2015. RPE necroptosis in response to oxidative stress and in AMD. Ageing Res Rev 24:286-98.

155. **Zhang S, Tang MB, Luo HY, Shi CH, Xu YM.** 2017. Necroptosis in neurodegenerative diseases: a potential therapeutic target. Cell Death Dis 8:e2905.

156. **Oberst A, Dillon CP, Weinlich R, McCormick LL, Fitzgerald P, Pop C, Hakem R, Salvesen GS, Green DR.** 2011. Catalytic activity of the caspase-8-FLIP(L) complex inhibits RIPK3-dependent necrosis. Nature 471:363-7.

157. **de Almagro MC, Goncharov T, Izrael-Tomasevic A, Duttler S, Kist M, Varfolomeev E, Wu X, Lee WP, Murray J, Webster JD, Yu K, Kirkpatrick DS, Newton K, Vucic D.** 2017. Coordinated ubiquitination and phosphorylation of RIP1 regulates necroptotic cell death. Cell Death Differ 24:26-37.

158. **Baker M, Shanmugam N, Pham CLL, Strange M, Steain M, Sunde M.** 2020. RHIM-based protein:protein interactions in microbial defence against programmed cell death by necroptosis. Semin Cell Dev Biol 99:86-95.

159. **Jang TH, Zheng C, Li J, Richards C, Hsiao YS, Walz T, Wu H, Park HH.** 2014. Structural study of the RIPoptosome core reveals a helical assembly for kinase recruitment. Biochemistry 53:5424-31.

160. **Cotsmire SM, Szczerba M, Jacobs BL.** 2021. Detecting Necroptosis in Virus-Infected Cells. Methods Mol Biol 2225:199-216.

161. **Lin J, Kumari S, Kim C, Van TM, Wachsmuth L, Polykratis A, Pasparakis M.** 2016. RIPK1 counteracts ZBP1-mediated necroptosis to inhibit inflammation. Nature 540:124-128.

162. **Yu X, Li Y, Chen Q, Su C, Zhang Z, Yang C, Hu Z, Hou J, Zhou J, Gong L, Jiang X, Zheng C, He S.** 2016. Herpes Simplex Virus 1 (HSV-1) and HSV-2 Mediate Species-Specific Modulations of Programmed Necrosis through the Viral Ribonucleotide Reductase Large Subunit R1. J Virol 90:1088-95.

163. **Placido D, Brown BA, 2nd, Lowenhaupt K, Rich A, Athanasiadis A.** 2007. A left-handed RNA double helix bound by the Z alpha domain of the RNA-editing enzyme ADAR1. Structure 15:395-404.

164. **Rich A, Zhang S.** 2003. Timeline: Z-DNA: the long road to biological function. Nat Rev Genet 4:566-72.

165. **van der Lee R, Buljan M, Lang B, Weatheritt RJ, Daughdrill GW, Dunker AK, Fuxreiter M, Gough J, Gsponer J, Jones DT, Kim PM, Kriwacki RW, Oldfield CJ, Pappu RV, Tompa P, Uversky VN, Wright PE, Babu MM.** 2014. Classification of intrinsically disordered regions and proteins. Chem Rev 114:6589-631.

166. **Wright PE, Dyson HJ.** 2015. Intrinsically disordered proteins in cellular signalling and regulation. Nat Rev Mol Cell Biol 16:18-29.

167. **Protter DSW, Rao BS, Van Treeck B, Lin Y, Mizoue L, Rosen MK, Parker R.** 2018. Intrinsically Disordered Regions Can Contribute Promiscuous Interactions to RNP Granule Assembly. Cell Rep 22:1401-1412.

168. **Namkoong S, Ho A, Woo YM, Kwak H, Lee JH.** 2018. Systematic Characterization of Stress-Induced RNA Granulation. Mol Cell 70:175-187.e8.

169. **Meng Z, Limbach PA.** 2006. Mass spectrometry of RNA: linking the genome to the proteome. Brief Funct Genomic Proteomic 5:87-95.

170. **Khaperskyy DA, Hatchette TF, McCormick C.** 2012. Influenza A virus inhibits cytoplasmic stress granule formation. Faseb j 26:1629-39.

171. **Abbott A.** 2020. Are infections seeding some cases of Alzheimer's disease? Nature 587:22-25.

172. **Esiri MM.** 1982. Viruses and Alzheimer's disease. J Neurol Neurosurg Psychiatry 45:759-60.

173. **Wozniak MA, Mee AP, Itzhaki RF.** 2009. Herpes simplex virus type 1 DNA is located within Alzheimer's disease amyloid plaques. J Pathol 217:131-8.

APPENDIX A

STATISTICAL ANALYSIS OF VIABILITY ASSAYS PRESENTED IN FIGURES 6 AND 9

Table A1.

F test and Student's t-test p-values for the viability assay experimental data presented in Figure 6.

	Untreated vs. TNFα + zVAD			Untreated vs. Ars + IFNα			Ars + IFNα vs. Ars + IFNα + GSK872		
H.P.T.	F test	Student's t-test	S.S.	F test	Student's t-test	S.S.	F test	Student's t-test	S.S.
0.5	0.55	0.76	n.s.	0.44	0.7	n.s.	0.47	0.72	n.s.
1	0.55	0.76	n.s.	0.44	0.7	n.s.	0.47	0.72	n.s.
1.5	0.15	0.27	n.s.	0.44	0.7	n.s.	0.47	0.72	n.s.
2	0.064	0.29	n.s	0.44	0.7	n.s	0.47	0.72	n.s
2.5	0.045	0.074	n.s.	0.44	0.7	n.s.	0.47	0.72	n.s.
3	0.036	0.0057	**	0.44	0.7	n.s.	0.47	0.72	n.s.
3.5	0.0053	0.02	*	0.44	0.7	n.s.	0.68	0.78	n.s.
4	0.64	$3.4x10^{-8}$	***	0.53	0.33	n.s.	0.79	0.8	n.s.
4.5	0.041	$5.9x10^{-4}$	***	0.072	0.32	n.s.	0.24	0.58	n.s.
5	0.0083	0.0029	**	0.012	0.19	n.s.	0.089	0.23	n.s.
5.5	0.014	0.0015	**	0.003	0.2	n.s.	0.042	0.24	n.s.
6	0.011	0.0018	**	0.0034	0.087	n.s.	0.048	0.1	n.s.
6.5	0.014	0.0014	**	0.0039	0.05	*	0.042	0.068	n.s.
7	0.012	0.0016	**	0.0046	0.036	*	0.077	0.022	*
7.5	0.012	0.0016	**	0.0065	0.019	*	0.091	0.0078	**
8	0.021	$8.3x10^{-4}$	***	0.0063	0.016	*	0.13	0.0068	**
8.5	0.021	$8.3x10^{-4}$	***	0.0066	0.012	*	0.17	0.004	**
9	0.021	$8.3x10^{-4}$	***	0.017	0.0036	**	0.47	$7.1x10^{-4}$	***
9.5	0.021	$8.3x10^{-4}$	***	0.038	0.0011	**	0.74	$1.4x10^{-4}$	***
10	0.047	$3.0x10^{-4}$	***	0.23	$2.6x10^{-7}$	***	0.31	$5.5x10^{-5}$	***
10.5	0.046	$3.1x10^{-4}$	***	0.12	$7.5x10^{-7}$	***	0.29	$2.1x10^{-4}$	***
11	0.046	$3.1x10^{-4}$	***	0.072	$1.7x10^{-6}$	***	0.43	$2.4x10^{-4}$	***
11.5	0.08	$3.3x10^{-7}$	***	0.039	$7.5x10^{-4}$	***	0.47	$8.6x10^{-4}$	***
12	0.9	$2.5x10^{-9}$	***	0.1	$7.2x10^{-7}$	***	0.2	$7.7x10^{-4}$	***

H.P.T.: hours post infection; S.S.: statistical significance; n.s.: not significant; * < 0.05; ** < 0.01; *** < 0.001

Table A2.
F test and Student t-test p-values for the viability assay experimental data presented in Figure 9.

	TNFα + zVAD vs. Ars		
H.P.T.	F test	Student's t-test	S.S.
0.5	1	1	n.s.
1	1	1	n.s.
1.5	1	1	n.s.
2	1	1	n.s.
2.5	0.031	0.43	n.s.
3	0.0039	0.36	n.s.
3.5	0.0022	0.15	n.s.
4	0.0014	0.11	n.s.
4.5	0.017	0.078	n.s.
5	0.036	0.028	*
5.5	0.072	0.0052	**
6	0.22	0.0027	**
6.5	0.47	0.0018	**
7	0.76	6.0×10^{-4}	***
7.5	0.43	4.5×10^{-4}	***
8	0.38	1.8×10^{-4}	***
8.5	0.23	4.1×10^{-4}	***
9	0.48	7.9×10^{-5}	***
9.5	0.43	1.0×10^{-4}	***
10	0.34	1.5×10^{-4}	***
10.5	0.56	2.1×10^{-4}	***
11	0.66	1.5×10^{-4}	***
11.5	0.96	3.5×10^{-4}	***
12	0.63	1.8×10^{-4}	***

H.P.T.: hours post infection; S.S.: statistical significance; n.s.: not significant; * < 0.05; ** < 0.01; *** < 0.001